بسم الله الرحمن الرحيم

Sudan University for Science and Technology

College of Graduate Studies

Biomedical Engineering Department

A dissertation submitted in partial fulfillment of the requirements for the M.Sc. (Honors) Degree in

Biomedical Engineering

A Wavelet Decomposition Technique for Breast Abnormality Detection

تقنية تحليل الويفلت للكشف عن الخلايا غير الطبيعية في الثدي

Presented by:

Maha Abdelhady Almona Ali

Supervisor:

Dr. Magdy Baker M Amien

December - 2015

Dedication

To...

My husband, My parent and My family

The sources of my motivation and the driving forces behind my

success ….

And,

To all women suffer from breast abnormality.

Acknowledgement

Thank God, beginning and ending for guiding my direction throughout this dissertation, and for granting me more knowledge, more insight and more enlightenment.

I am deeply indebted to my supervisor **Dr. Megdi** for overwhelming me with his wisdom, and for providing me with his persistent and unrelenting efforts to instruct, lead and direct me to the right path.

I am deeply indebted to **Dr. Mohamed Al fadel** for his wisdom to move me forward and help me to reach this level.

Also, I can’t even begin to describe my gratitude to **Engineer _Osama Fuad** for all the hard work and solid advice he devoted to me. My thanks extend to **Ali Abdelwahab, Almona's family, Engineer_ Fatehia Garma, Dr./ Awad Wedaaa, Dr./ Ahmed A.Gader, and Engineer Mihad** for dedicating to me some of their time and experience.

I am extremely grateful to all of my friends for presenting me with their undying love and support.

Abstract

Breast Cancer is the most common and life threatening cancer among women. Mammography is an effective way for early detection of breast abnormality. Radiologists can miss the breast abnormality due to the textural variation of breast tissues intensity in mammogram. This dissertation developed an algorithm as a second opinion for radiologists, to explore the breast tissue types in order to detect the abnormal cells in mammogram. It proposed the use of the wavelet decomposition technique using symlet wavelet to find out this detection. Different sets of proposed combination techniques were used, in order to obtain the best accuracy in breast abnormality detection. Every technique algorithm was applied on 300 samples from the normal tissues of the breast, 100 for every tissue type (dense, glandular and connective, and fat tissue) and 100 abnormal ones, which are taken from Mini Mais Database. The dissertation showed that the combination between the un-decimated discrete wavelet decomposition technique and the Spatial Gray Level Dependency Matrix achieved the best result. It achieved 98.8% accuracy, 95.0% sensitivity. This accuracy has been verified with the ground truth given in the mini-MIAS database. This dissertation is an important step in the development of a Computer Aided Detection for development of mammogram analysis.

المستخلص

يعتبر سرطان الثدي هو السرطان الأكثر شيوعا بين النساء والمهدد لحياتهن. التصوير الشعاعي للثدي (الماموغرافي) هو وسيلة فعالة للكشف المبكر عن شذوذ الثدي. يمكن لأخصائي الاشعة ان يفقد كشف الشذوذ في الثدي بسبب الاختلاف التكويني لانسجة الثدي في صورة الماموغرام. هذه الأطروحة طورت خوارزمية بمثابة رأي ثان لأطباء الأشعة، لاستكشاف أنواع أنسجة الثدي من أجل الكشف عن الخلايا غير الطبيعية في صور الأشعة. اقترحت استخدام تقنية تحليل المويجات باستخدام ال symlet wavelet لايجاد هذا الكشف. استخدمت مجموعات مختلفة من التقنيات المركبة للحصول على اكبر دقة في الكشف عن الخلايا غير الطبيعية في الثدي. تم تطبيق كل خوارزمية على 300 عينة من الأنسجة الطبيعية للثدي، 100 لكل نوع منها (glandular and connective, dense, and fat tissue)، و 100 من غير الطبيعية، هذ العينات أخذت من قاعدة البيانات Mini Mais Database . اوضحت هذه الدراسة ان الجمع مابين تقنية تحليل المويجات the un-decimated discrete wavelet decomposition ومصفوفة ل SGLD حققت افضل نتيجة وهي 98,8% دقة و حساسية 95,0% . تم التحقق من هذه الدقة بمقارنتها بالتشخيص المعتمد من قاعدة البيانات Mini Mais Database . وتعتبر هذه الدراسة خطوة مهمة في تطوير نظام التشخيص باستخدام الكمبيوتر لتطوير تحليل صور الماموغرام.

Contents

List of Figures

List of Tables

Abbreviations

Abbreviation	Stand for
ROI	Regions of Interest
LDA	Linear Discriminant Analysis
ANN	Artificial Neural Network
CAD	Computer Aided Diagnosis / Detection

DCIS	Ductal Carcinoma In Situ
LCIS	Lobular Carcinoma In Situ
IDC	Invasive Ductal Carcinoma
ILC	Invasive Lobular Carcinoma
CC	Cranio Caudal
MLO	Mediolateral Oblique
TP	True Positive
FP	False Positive
TN	True Negative
FN	False Negative
DB	Daubechies Wavelets
SYM	Symlet Wavelets
FT	Fourier Transform
STFT	Short-Time Fourier analysis
WT	Wavelet Transform
MRA	Multiresolution Analysis
CWT	Continuous Wavelet Transform
DWT	Discrete Wavelet Transform
RWT	Redundant Wavelet Transform
GLCM	Gray Level Co-occurrence Matrix
SGLD	Spatial Gray Level Dependency
EN	Entropy
EG	Energy
IN	Inertia
IDM	inverse different moment
CO	Correlation

VA	Variance
SA	Sum Average
SE	Sum Entropy
SV	Sum Variance
DA	Difference Average
DE	Difference Entropy
DV	Difference Variance
SPSS	Statistical Package for the Social Science
CPU	Central Processing Unit
RAM	Random Access Memory
DDWD	Decimated Discrete Wavelet Decomposition
UDDWD	Un-Decimated Discrete Wavelet Decomposition
L	Level
D	Dense tissue
G	Glandular and connective tissue
F	Fat tissue
MIAS	Mammographic Image Analysis Society

Chapter One

Introduction

1.1 General view

Breast Cancer is the most common and life threatening cancer among women [1]. Mammography is the process of using low-dose amplitude-X-rays to examine the human breast, so it is a key screening tool for breast abnormalities detection. It is an effective way that has demonstrated the ability to detect breast cancer at early stages, because it allows identification of tumor before being palpable [2, 3]. Sometimes due to small masses or breast density, radiologists may miss the suspicious regions, so the diagnosis can fail [1]. Therefore, a computer aided detection system has used to help the radiologists to give them opportunity to improve their image interpretation.

The mammogram analysis is the need to identify specific description of Regions of Interest (ROI). One way to achieve this is to develop features of the image which can be used to classify the image data [4]. A wavelet transform is a powerful tool to analyze and identify strong variations contained within the original data, since in each level of the transform data is divided into different scaling components [5].

Classification involves sorting objects in an image into separate classes. These features are then passed to a classifier that evaluates the evidence presented and makes a decision as to the class each object should be assigned. This is often the final step in a general diagnostic process [6].

Classifier can be designed to classify breast lesions once a comprehensive set of significant features is obtained. Common Classifiers are linear discriminant analysis (LDA) and artificial neural network (ANN) [7].

1.2 Significance of the study

This study provided an algorithm for mammogram image analysis, which assists the radiologists in image interpretation and improve the diagnosis of breast cancer. Therefore, it will minimize the miss detection rate, so early detection and following treatment can significantly improve the chance of survival for patients with breast cancer. Currently there are no methods to prevent breast cancer that is why early detection is very important in cancer treatment and allows reaching a high survival rate.

1.3 Problem Statement

Abnormal cells appear in mammogram as a brightest area, in the same time breast has different types of tissues, so they have textural variation in intensity. This makes diagnosis difficult or radiologists will not detect all breast abnormality on mammograms. Therefore, to reduce the high miss detection rate and assist radiologists, an objective method to identify and classify mammograms is need.

1.4 Objectives

The objectives of this research are:

1.4.1 General objective:

The main purpose of this research is to develop an algorithm as a second opinion for radiologists, to explore the breast tissue types in order to detect the abnormal cells in mammogram.

1.4.2 Specific objectives:

1. To classify normal tissue of the breast into glandular, fat, and dense tissue.
2. To detect abnormality in mammogram.
3. To examine wavelets as a tool for classifying mammogram.
4. To choose the features that produces the best results.

1.6 Thesis layouts

This dissertation consists of five chapters, chapter one is an introduction. Chapter two gives theoretical background and the literature reviews. The research methodology was described in chapter three. The result obtained and discussion of these results given in chapter four. Finally, chapter five is devoted for conclusion and recommendation.

Chapter Two

Theoretical Background and Reviews

This chapter aims to give a description of the theories leading to the detection of breast abnormality. It divides into two parts, part one is the theoretical background which aims to represent the importance of breast cancer study and gives some essential information on the breast anatomical structure and diseases. Demonstration of different types of breast cancer was shown. There is also a depiction of mammography equipment and computer aided diagnosis (CAD) idea. Ways which lead to do detection such as image feature extraction, texture analysis, and classification of texture, were depicted here. Part two is some reviews of the available literature.

2.1.1 The Female Breast

The breasts are specialized accessory glands of the skin that are capable of secreting milk [8]. They are the tissue overlying the chest (pectoral) muscles [9]. Located in left and right sides of the upper ventral region of the trunk and each extends from the second rib above to the sixth rib below, and from the side of the sternum to near the midaxillary line [10]. An overall view of breast is given in Fig 2.1.

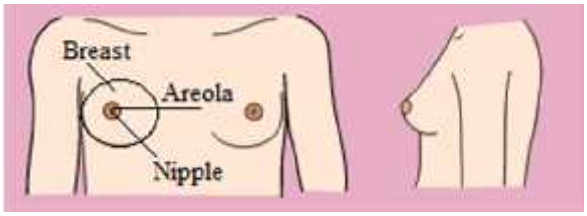

Fig 2.1: Morphology of breasts with the areola and nipple [11].

2.1.1.1 Female Breast Anatomy

The female breasts correspond to two large hemispherical eminences, which contain the mammary gland which secretes milk, when stimulated.

The surface of the breast is convex and has, just below the center, a small conical prominence, called papilla or nipple. It is located about the level of the fourth intercostal space. The base of the papilla is surrounded by dark area of skin called the areola [9, 10], which has a slightly rough surface due to the presence of rudimentary mammary glands, areolar glands, just below the surface [12].

The breast consists of gland tissue, fibrous tissue, fatty tissue, blood vessels, nerves and ducts. Connective tissue and ligaments provide support to the breast and give it its shape. Nerves provide sensation to the breast. The breast also contains lymph vessels and lymph nodes [9, 12].

The milk-producing part of the breast is organized into 15 to 20 sections, called lobes; within each lobe are smaller structures, called lobules, where milk is produced; lobules end in dozens of tiny bulbs that can produce milk [9, 12, 13]. Those lobules consist of alveoli and lactiferous ducts. These lactiferous ducts are network of tiny tubes; link all the lobes, lobules, and bulbs; which the milk travels through. They enlarge to form a small lactiferous sinus, which accumulates milk during lactation. The ducts connect and come together into larger ducts, which eventually exit the skin in the nipple. The milk leaves the breast trough some holes in the nipple. The fibrous tissue lays at the entire surface of the breast and connects the lobes together. The fatty tissue covers the surface of the gland, except for the areola, and is located between the lobes. Usually, this tissue is abundant and determines the form and size of the gland [9, 10, 12, 13].

The breast is hold in place as a result of the Cooper's ligaments support, which extends from fascia over the pectorals major muscles to the skin over the mammary glands [12].

There are no muscles in the breast, but they lie under each breast and cover the ribs [13]. Fig 2.2 shows structure of female breast.

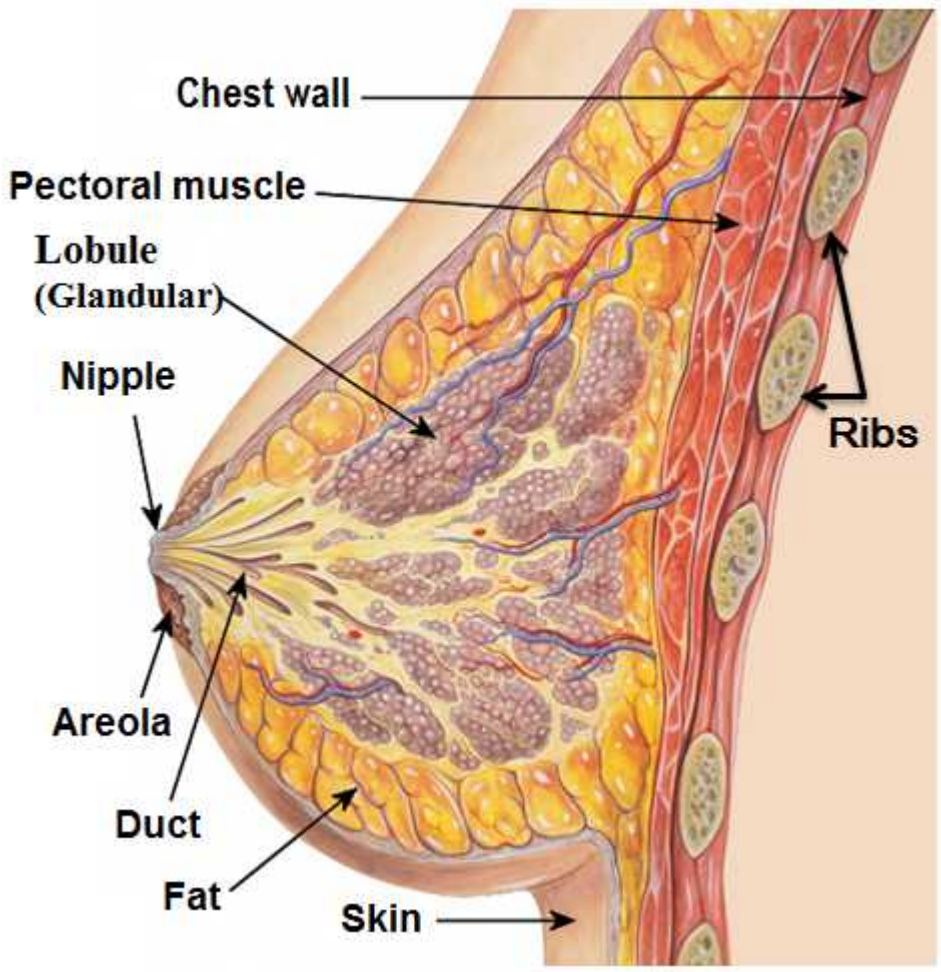

Fig 2.2: The structure of female breast [14].

2.1.1.2 Female breast and developments

The breasts weight and dimension differ between individuals and at different periods of life [10]. They begin to develop at puberty. This development is stimulated by the

hormones estrogens and progesterone of the monthly female sexual cycle; estrogens stimulate growth of the breasts' mammary glands plus the deposition of fat to give the breasts mass. Higher growth and glands development occurs during pregnancy, when the estrogens levels rise as they are secreted by the placenta and increase even more after delivery, when they are secreting milk to feed the baby. The breasts become atrophied in old age [12, 15].

A children breast consists principally of ducts with dispersed alveoli. A teenage breast mostly consists on fibrous and gland tissue. When adult, the fatty tissue substituted some of the fibrous and gland tissue. During menopause, the breast is mainly adipose tissue [16].

The breast is intensely influenced by some hormones. Estrogens stimulate the breast adipose deposition and the growth of the mammary glands, as well as the initial development of lobules and alveoli of the breast. Progesterone and prolactin cause the final growth and are responsible for the function of these structures, and cause the external appearance of the mature female breast [15].

During pregnancy, the concentration of estrogens and progesterone increases. This events cause expansion and branching of the breast gland ducts and deposition of additional adipose tissue. Prolactin is responsible for the milk production [17, 12].

2.1.2 Breast cancer

Breast cancer, is the Cancer that forms in the cells of breast tissues. It is an uncontrolled growth and multiplication of breast cells, which produces a tumor or a neoplasm [18, 20].

The cell division cycle is controlled and ordered in normal situations, allowing the formation, growth and tissue regeneration. When this does not occur and there is no reparation of the eventual mutations, there is tumor formation, as shown in Fig 2.3.

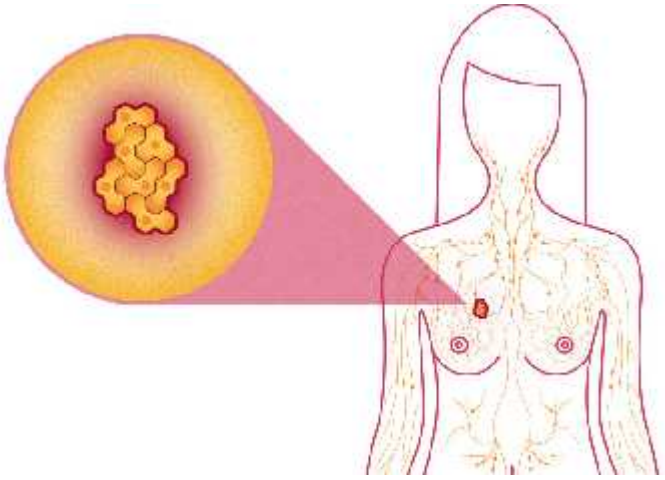

Fig 2.3: The female breast with mutated cells [19].

Cancer occurs as a result of mutations, or abnormal changes, in the genes responsible for regulating the growth of cells and keeping them healthy. The genes are in each cell's nucleus, which acts as the control room of each cell. Normally, the cells in our bodies replace themselves through an orderly process of cell growth: healthy new cells take over as old ones die out. But over time, mutations can turn on certain genes and turn off others in a cell. That changed cell gains the ability to keep dividing without control or order, producing more cells just like it and forming a tumor, as shown in Fig 2.4 [18].

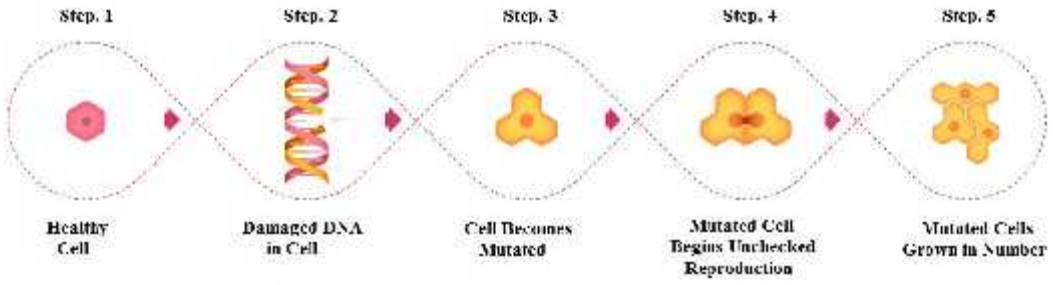

Fig 2.4:

The cancer cell reproduction [19]

After its formation, the evolution depends on the patient. However, an early detection and treatment is essential to stop the cancer evolution and to minimize the damages. The breast cancer, as the majority of other cancers, can have the ability to spread to other tissues, metastasizing, allowing the dissemination of cancer. When the breast cancer is early detected, this phenomenon does not occur, which provides a better prognosis for the patient [16].

A tumor is a mass of abnormal tissue. It can be benign (non-cancerous), or malignant (cancerous) [19]. Benign tumors are not considered cancerous: their cells are close to normal in appearance, they grow slowly, and they do not invade nearby tissues or spread to other parts of the body. Malignant tumors are cancerous. Left unchecked, malignant cells eventually attack nearby tissues and travel through the bloodstream or lymphatic system to other parts of the body, spreading a cancer by a process known as metastasis [18, 21].

2.1.2.1 Breast cancer lesions

Breast cancer has some characteristic lesions such as microcalcifications, masses, architectural distortions. Asymmetry between breasts can also be a breast cancer indicator.

2.1.2.1.1 Microcalcifications

They are small size lesions, are tiny specks of calcium in the breast, typically in the range 0.05 to 1 mm and are slightly brighter than surrounding tissues. These lesions with these dimensions are difficult to detect in mammography, because they are bright, have various sizes, shapes and distributions, in some cases low contrast due to a reduced intensity difference between the suspicious areas and the surroundings and it is proximal to the surrounding tissues. In dense tissues, suspicious areas are almost invisible as a result of the tissue superimposition. Some anatomic structures such as fibrous strands, breast borders or hypertrophied lobules are similar to microcalcifications in the mammographic image. They appear with low contrast due to their small size, although have high inherent attenuation properties [22, 23, 24, 25].

An accurate detection of microcalcifications is primary to the early detection of the majority of breast cancers because of the high correlation between the presence of them and breast cancer [26].

Generally, larger, round and oval shaped calcifications with uniform size have higher probability of being benign, while smaller, irregular, polymorphic and branching calcifications, with heterogeneous size and morphology have higher probability of being malignant (Fig 2.5) [27].

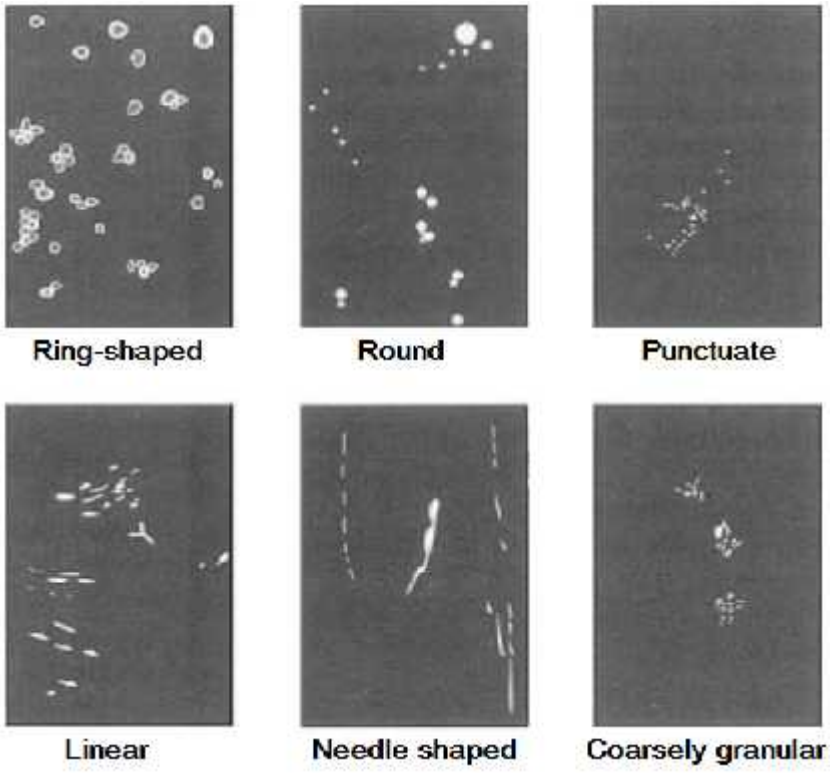

Fig 2.5: Microcalcifications types commonly seen on mammogram [17].

2.1.2.1.2 Masses

Masses appear as dense regions of different sizes and properties. They can be circular, oval, lobular or irregular/speculated, (Fig 2.6), and their margins can be (Fig 2.7) [27]:

- circumscribed, which are well-defined and distinctly demarcated borders;

- obscured, which are hidden by superimposed or adjacent tissue;

- Micro-lobulated, which have undulating circular borders;

- Ill-defined, which are poorly defined scattered borders;

- Spiculated, which are radiating thin lines.

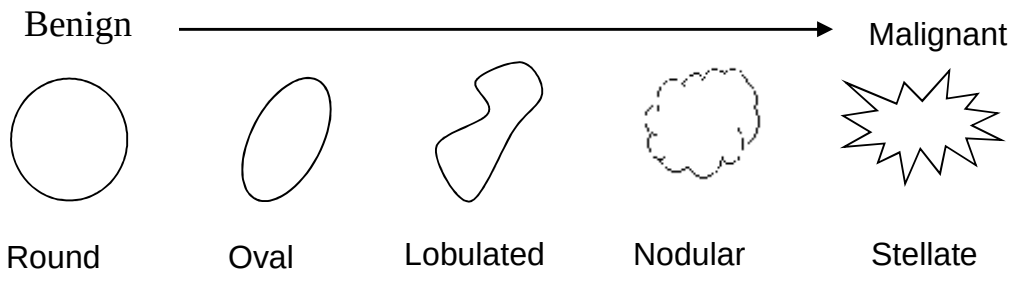

Fig 2.6: The morphologic spectrum of mammographic masses [28].

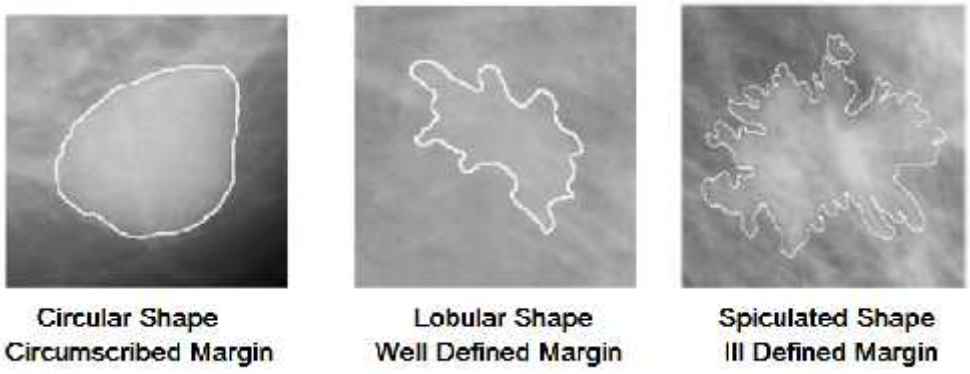

Fig 2.7: Mass examples with different shapes and borders [27].

The masses have different malignant probability depending on the morphology. The ill-defined and spiculated borders have higher probability of malignancy [27]. A benign process is usually associated with the presence of circular or oval masses. However, the great variability of the mass appearance is an obstacle to a correct mammography analysis [29].

2.1.2.1.3 Architectural Distortions

The anatomy of the breast included several linear structures that cause directionally oriented texture in mammograms, so a way to detect architectural distortions is the change of normal texture of the breast [20].

Architectural distortions refer to the derangement of the normal disposition of the parenchyma in a radiating or arbitrary pattern, without a visible center or mass. They are very variable and, consequently, very difficult to detect [29].

2.1.2.1.4 Bilateral Asymmetry

Bilateral asymmetry of breast means a difference between corresponding regions in left and right breast and can be classified into global asymmetry and focal asymmetry. The first, happens when a greater volume of fibroglandular tissue is present in one breast compared to another in the same region. The latter, corresponds to a circumscribed area of asymmetry seen on two views, and usually is an island of healthy fibroglandular tissue that is superimposed with surrounding fatty tissue [30, 31].

2.1.2.2 Breast Cancer Types

Breast cancer can be classified according to the breast tissue where the cancer was originated (glands, ducts, fat tissue or connective tissue) and according to the extent of the cancer spread (non-invasive/in situ or invasive/infiltrating). Both in situ and infiltrating cancers can be ductal and lobular, depending on the breast cancer location [17, 32].

2.1.2.2.1 Noninvasive (in situ) Breast Cancer

Sometimes it called carcinoma in situ (in the same place) or pre-cancers. In it the abnormal cells stay within the milk ducts or lobules in the breast and do not grow or spread into the surrounding breast tissue [33, 34].

2.1.2.2.1.1 Types of the noninvasive breast cancer

a) **Ductal Carcinoma In Situ (DCIS)**

It called stage 0. It arises from ducts. With it, the abnormal cells are contained in the milk ducts of the breast and haven't spread into the surrounding breast tissue (Fig 2.8). It considered a precancerous lesion, but if it is left un-treated or un-detected, it can spread into the surrounding breast tissue, so eventually it developed into an invasive cancer [32, 33].

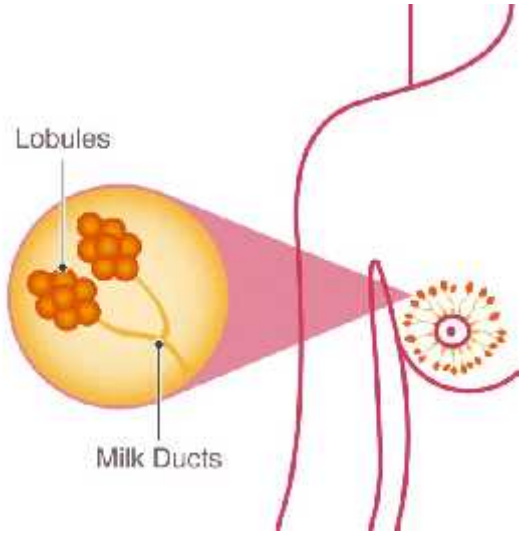

Fig 2.8: Ductal carcinoma in situ (non-invasive).

b) Lobular Carcinoma In Situ (LCIS)

It arises from lobules. It isn't considered precancerous because it won't eventually evolve into invasive cancer [32].

2.1.2.2.2 Invasive Breast Cancer

It has spread from the original site (either the milk ducts or the lobules) into the surrounding breast tissue. It may have spread to the lymph nodes and/or other parts of the body. If breast cancer is stage I, II, III or IV, it must have invasive breast cancer [33, 35].

2.1.2.2.2.1 Types of Invasive Breast Cancer [35, 36]

a) Invasive Ductal Carcinoma (IDC)

The abnormal cancer cells began growing in the milk ducts and invading the surrounding breast tissue. It has the ability to move to other parts of the body either through the bloodstream or the lymphatic system. It develops as a hard lump with irregular borders that usually shows on a mammogram as a spiked mass.

b) Invasive Lobular Carcinoma (ILC)

It develops in the lobules of the breast. It has the ability to spread to other parts of the body. It is less likely to show up on a mammogram.

- **The difference between DCIS and IDC**

DCIS means the cancer is still contained in the milk duct and has not invaded any other area. IDC is cancer that began growing in the duct and is invading the surrounding tissue (Fig 2.9).

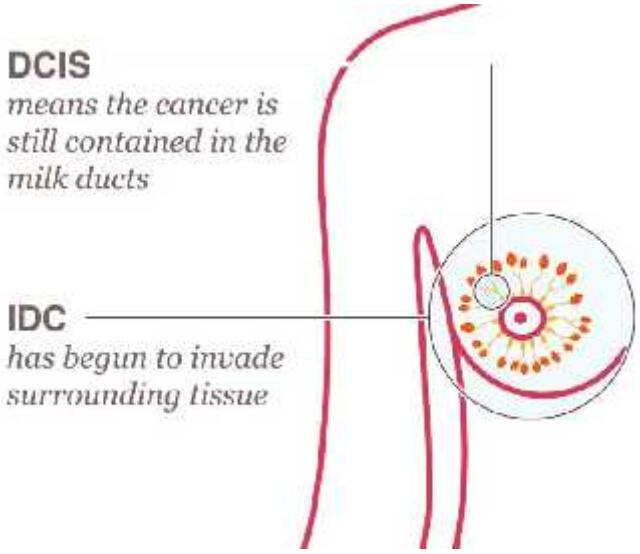

Fig 2.9: The difference between DCIS and IDC

2.1.2.3 Breast Cancer Risk Factors

The personal history of previous breast cancer is the single strongest risk factor. The breast cancer risk is increased with the age, where the majority of patients are over 50 years, age at menarche and menopause, age at first pregnancy. Also a first degree relative with the disease, nulliparity or late parity, early menarche, late menopause, obesity, mutations in the genes needed to correct errors in DNA and exposure to large amounts of ionizing radiation; however, 70% of women diagnosed with breast cancer have no significant risk factors [12, 13, 17, 37].

2.1.2.4 Diagnosis

Breast cancers are diagnosed with a clinical breast exam, mammography, ultrasonography, and biopsy. The clinical exam is used to locate obvious lumps in the breast. It is often possible to tell if a lump is benign or malignant by the way it feels, how easily it moves, and its texture [13].

2.1.2.5 Prevention of Breast Cancer

Advances in treatment and better delivery of care can reduce mortality. Also screening programs, where women over 40 or with higher risk of developing breast cancer perform mammographic exams in a periodic interval. So detecting breast cancer early and treating it when it is small and before it has had the chance to spread reduce morbidity and mortality from it [16, 37].

2.1.3 Mammography

Mammography is a specific type of imaging procedure; similar to the other X-Rays, however, it uses a low-dose x-ray system imaging, for examination of the breast, presenting a high quality that leads to high contrast and resolution and low noise. It gives information about breast morphology, anatomy and pathologies, also for pre surgical localization of suspicious areas and in the guidance of needle biopsies. It detects lumps that are often too small or too deep to feel. It is used for detection and diagnosis of breast cancer at a pre-symptomatic phase with high sensitivity and specificity, as well as evaluates mass lesions in breast [1, 38, 39, 40, 41, 42].

Mammography is considered the most effective, low cost, and reliable technique in early detection of breast cancer [43]. It is more sensitive and specific in assessing fatty than dense breasts. Dense breast tissue is particularly difficult to assess in young women. So the performance of the mammography decreases as the density of the breast increases [20, 42].

Mammography exam produce a black and white x-ray image of the breast tissue. Depending on the type of machine, the image is either on a large sheet of film or digital image that can be displayed on a computer monitor. The differences between these two techniques are in the way the picture is recorded, looked at by the doctor, and stored [44].

2.1.3.1 Image formation

Image formation is depending on the structures' densities absorption when penetrated with the X-rays. The image must have high spatial resolution to delineate the edges of structures of reduced dimension such as microcalcifications [45].

Mammogram is the resulted image of mammography exam. In a mammogram, breast regions can be divided into background, fat tissue, dense, glandular tissues and tumors with increasing intensity levels. Tumors are radiolucent and appear

bright in the image [2]. Fig 2.10 illustrates the anatomy of the breast and its associated mammogram. Typical it is soft tissue structures of a pre-menopausal breast. The glandular tissue is interspersed with fat and there are relatively regular bands of suspensory ligaments known as Cooper's ligaments [45].

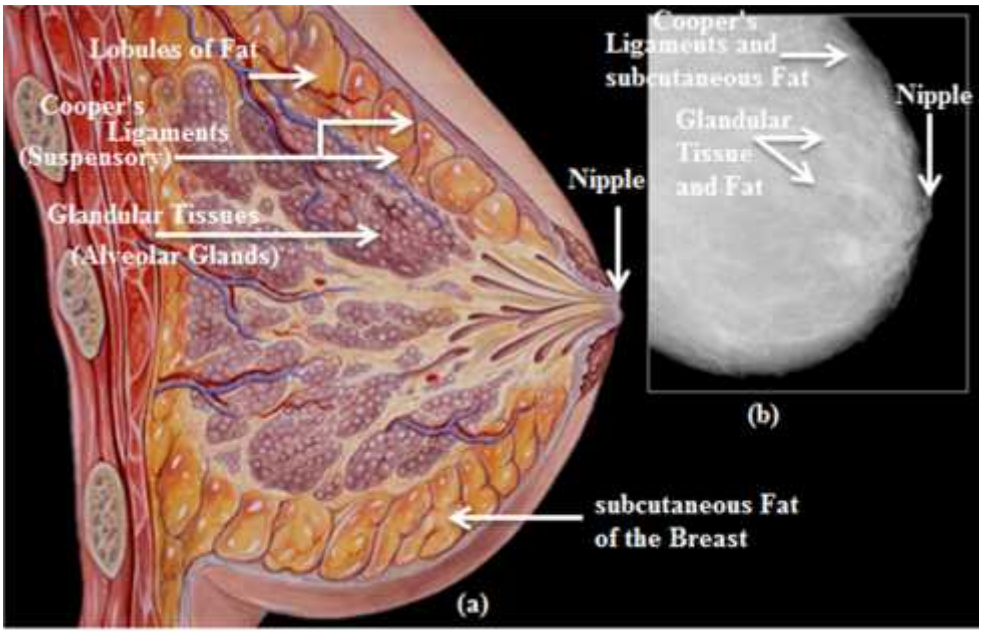

Fig 2.10: (a) the anatomy of the breast, (b) its associated mammogram.

2.1.3.2 Image projections

In order to assess differences in density between the breast tissue, image acquisition is done using two views, so usually there are two standard image projections [20]

a- Cranio-Caudal (CC), which is a view from top, allowing a better imaging of the central and inner breast sectors, Fig 2.11 a.
b- Mediolateral Oblique (MLO), which is a lateral view from a certain angle, having a better perspective of the glands, Fig 2.11 b.

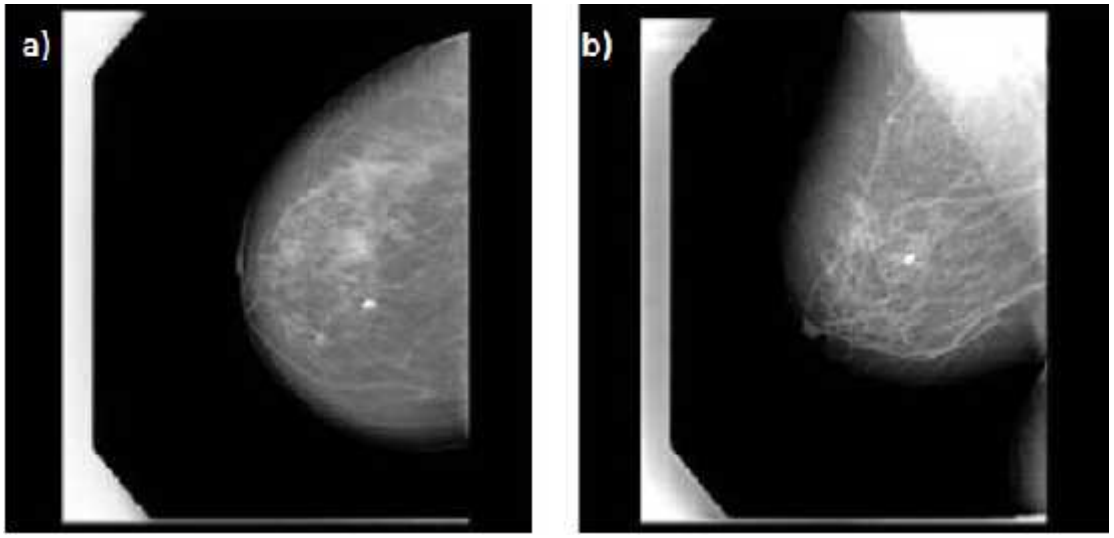

Fig 2.11: Two distinct mammography projections (a) cranio-caudal view, (b) mediolateral oblique view

More breast tissue can be projected on MLO view because of the slope and curve of the chest wall. On CC projection, must be included all breast tissue with the exception of the axillaries portion [20].

2.1.3.3 What does the doctor look for on a mammogram?

Radiologists are reading Mammogram to find evidence of abnormality. When possible, they compare it to the same person previous mammograms. This helps them find small changes that could be signs of cancer. Any abnormalities or changes over time are considered suspicious. The doctor reading mammogram will look for different types of changes or lesions, such as breast density, calcification, a mass, and architectural distortion [22, 46].

2.1.4 Computer Aided Detection

Computed aided detection and computer aided diagnosis, both commonly abbreviated as CAD, can be defined as the detection and/or diagnosis made by the

radiologist considering the results of a computed algorithm which characterize lesions through automatic image analysis [16].

Radiologists may double read the exams to properly detect mammogram lesions [48]. However, less costly in man terms, software may be an important assistance as a second opinion to improve the performance of individual readers. This allows the reduction of variability in the radiologists' reading and the frequency of errors by assuring that suspicious regions are revised and increasing the influence of subtle signs, which may be dismissed otherwise. So the CAD systems aim to improve the correct detection of abnormalities in the breast [48, 49].

CAD systems read images faster. They generally perform automatic assessments of patient images and present to radiologist areas that they have determined as having the appearance of an abnormality because the variability between radiologists can be very large [20].

2.1.4.1 Steps that the use of CAD supposed to follow them [16]:

- Initial radiologist mammography reading, marking suspicious areas;

- A CAD system scanning to detect suspicious features.

The most CAD algorithms (Fig 2.12) in mammogram analysis consist of the following typical steps: segmentation, feature extraction, feature selection and classification. Segmentation step aims to extract regions of interest (ROIs) containing breast abnormalities from the normal breast tissue and to locate the suspicious lesion candidates from the region of interest. The feature extraction consists in determine the characteristics of the ROI. The input of this stage is a set of lesion candidate regions that are characterized by a number of features extracted from those regions. The best set of features chosen for eliminating false positives

and for classifying lesion types which are selected in the feature selection step. Then the features extracted and selected are used to classify them into lesion non-lesion state aiming at substantially reduction of the false positives [20].

Computer-aided detection systems use a digitized mammographic image that can be obtained from either a conventional film mammogram or a digitally acquired mammogram. The computer software then searches for abnormal areas of density, mass, or calcification that may indicate the presence of cancer. The CAD system highlights these areas on the images, alerting the radiologist to the need for further analysis [39].

CAD has become a part of clinical work because it is a computational tool that radiologists can use, which aims to improve the correct detection of abnormalities in the breast, but is still in the infancy of its full potential for applications to many different types of lesions obtained with various modalities. CAD results of a computed algorithm which characterizes lesions through automatic image analysis, this tool, when correctly used, improves the correct detection of microcalcification and masses and consequently the presence of a breast tumor [16, 20].

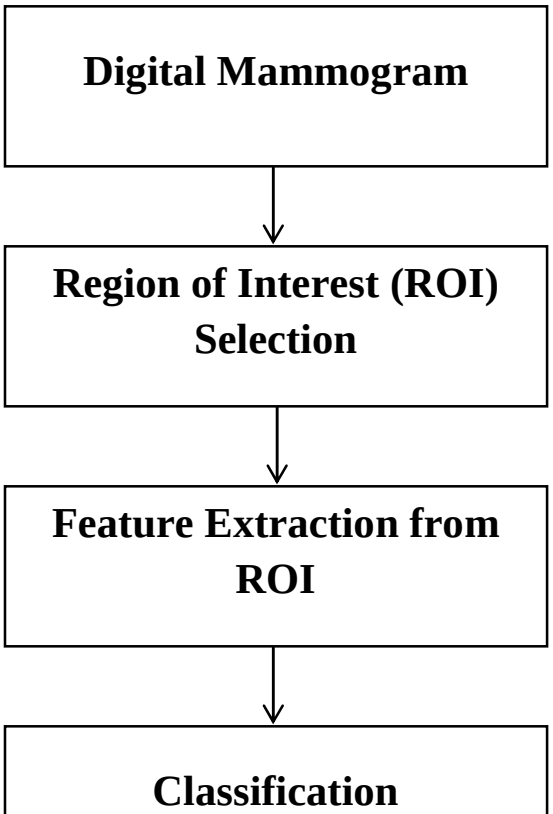

Fig 2.12: A schematic diagram for CAD system

2.1.4.2 CAD Evaluation

The performance of CAD systems is variable and depends on the organ, disease, type of image finding, and so on. In general, CAD systems tend to err on the side of caution, presenting images with a large number of false positive (FP) marks. The efficiency of CAD systems can be classified as true positive (TP), false positive (FP), true negative (TN) and false negative (FN) in the context of detecting the presence or absence of abnormality. In this classification, positive/negative refers to the decision made by the algorithm and true/false refers to how the decision agrees with the actual clinical state [16].

- True Positive (TP), when the suspected abnormality is in fact malignant;
- True negative (TN), when there is no detection of abnormality in a healthy person;
- False positive (FP), when occurs detection of abnormality in a healthy person;
- False negative (FN), when there is no detection of a malignant lesion.

The result false positive may put the patient in delicate and fragile position but, with the help of complementary exams, this result can be excluded. However, when in the results are a false negative, is a more worrying situation once the person has the lesion but the algorithm does not detect [20].

2.1.5 Image Feature Extraction

It is how to extract ideal features that can reflect the intrinsic content of the image [50]. It consists in transforming arbitrary data, such images, into numerical features usable for machine learning [51].

Feature extraction is methods of constructing combinations of the variables to describe the data with sufficient accuracy. It starts from an initial set of measured data and builds derived values (features) intended to be informative. Feature extraction is related to dimensionality reduction. It involves reducing the amount of resources required to describe a large set of data [52].

2.1.6 Texture Analysis

Texture is observed in structural patterns of surfaces of objects. It is one of the important characteristics for identifying objects and Region of Interest (ROI) of various kinds of images. The visual texture is something that everyone understands it, but is difficult to define. Texture generally refers to repetition of primitive texture elements called texels, the texels describe the spatial relations between them. Texture may be lightness, uniformity, density, roughness, regularity, linearity, frequency, phase, directionality, coarseness, randomness, fineness, smoothness, granulation, etc. of the texture as a whole [44, 53].

2.1.6.1 Classification of texture

Approaches to texture in image analysis are usually categorized into

2.1.6.1.1 Structural approaches

These approaches are to detect texture elements. Then try to find a compact description of their distribution.

Structural approaches represent texture by well-defined primitives (micro-texture) and a hierarchy of spatial arrangements (macro-texture) of those primitives. To describe the texture, one must define the primitives and the placement rules. The choice of a primitive (from a set of primitives) and the probability of the chosen primitive to be placed at a particular location can be a function of location or the primitives near the location. The advantage of the structural approach is that it provides a good symbolic description of the image; however, this feature is more useful for synthesis than analysis tasks. The abstract descriptions can be ill defined for natural textures because of the variability of both micro- and macrostructure and no clear distinction between them [44].

2.1.6.1.2 Statistical approaches

These methods are used pixels values as the texture elements and then try to characterize the texture of an image region using statistical measures.

Statistical approaches do not attempt to understand clearly the hierarchical structure of the texture. Instead, they represent the texture indirectly by the non-deterministic properties that govern the distributions and relationships between the grey levels of an image [44].

2.1.6.1.2.1 First-order statistics

First-order statistics measure the likelihood of observing a gray value at a randomly-chosen location in the image. First-order statistics can be computed from the histogram of pixel intensities in the image. These depend only on individual pixel values and not on the interaction or co-occurrence of neighboring pixel values. The average intensity in an image is an example of the first-order statistic [44].

2.1.6.1.2.2 Second-order statistics

Second-order statistics are defined as the likelihood of observing a pair of gray values occurring at the endpoints of a dipole (or needle) of random length placed in the image at a random location and orientation. These are properties of pairs of pixel values.

Methods based on second-order statistics (i.e. statistics given by pairs of pixels) have been shown to achieve higher discrimination rates than the power spectrum (transform-based) and structural methods. The most common second-order statistical features for texture analysis are derived from the so-called co-occurrence matrix [54]. They were demonstrated to feature a potential for effective texture discrimination in biomedical-images. The approach based on multidimensional co-occurrence matrices was recently shown to outperform wavelet packets (a transform-based technique) when applied to texture classification [44].

2.1.6.1.3 Model based approaches

A method that combines the statistical and structural approaches is based on what have been called mosaic models. These models represent random geometric all processes.

Model based texture analysis using fractal and stochastic models, attempt to interpret an image texture by use of, respectively, generative image model and stochastic

model. The parameters of the model are estimated and then used for image analysis. In practice, the computational complexity arising in the estimation of stochastic model parameters is the primary problem. The fractal model has been shown to be useful for modeling some natural textures. It can be used also for texture analysis and discrimination however; it lacks orientation selectivity and is not suitable for describing local image structures [44].

2.1.6.1.4 Transform approaches

Transform methods of texture analysis, such as Fourier and wavelet transforms represent an image in a space whose co-ordinate system has an interpretation that is closely related to the characteristics of a texture (such as frequency or size). The wavelet transforms feature several advantages:

- Varying the spatial resolution allows it to represent textures at the most suitable scale,
- There is a wide range of choices for the wavelet function, so one is able to choose wavelets best suited for texture analysis in a specific application.

They make the wavelet transform attractive for texture segmentation. The problem with wavelet transform is that it is not translation-invariant [26].

Texture is a very useful characterization for a wide range of image. It is generally believed that human visual systems use texture for recognition and interpretation. In general, color is usually a pixel property while texture can only be measured from a group of pixels. A large number of techniques have been proposed to extract texture features. Based on the domain from which the texture feature is extracted, they can be broadly classified into spatial texture feature extraction methods and spectral texture feature extraction methods. For the former approach, texture features are extracted by computing the pixel statistics or finding the local pixel structures in

original image domain, whereas the latter transforms an image into frequency domain and then calculates feature from the transformed image [50].

2.1.7 Wavelet Approach

2.1.7.1 Wavelets

A wavelet is a waveform of limited duration that has an average value of zero. Wavelets have a beginning and an end. They are irregular and often non symmetrical. They are better at describing anomalies, pulses, and other events that start and stop within the signal [55].

Some wavelets which called crude wavelets are defined by a mathematical expression and are drawn as continuous and infinite. To use them with digital signal, they must be converted to wavelet filters having a finite number of discrete points, by evaluating their equation at desired points in time. Others wavelets start out as filters having two points as little, then estimation built from the original filter points by interpolating and extrapolating more points [55].

Wavelets are mathematical functions that cut up data into different frequency components, and then study each component with a resolution matched to its scale [56].

2.1.7.1.1 Wavelet Families

There are several types of wavelets. They used in the different Wavelet Transforms, to achieve some practical applications, due to their specific properties.

2.1.7.1.1.1 Haar Wavelets

They are the simplest, shortest and the first wavelet to be used. Haar wavelet is discontinuous, and resembles a step function. A continuous Haar wavelet (Figure

2.13) is multiple point estimation produced by up sampling and low pass filtering (interpolating) the simple High pass filter ([1-1]) [55, 57].

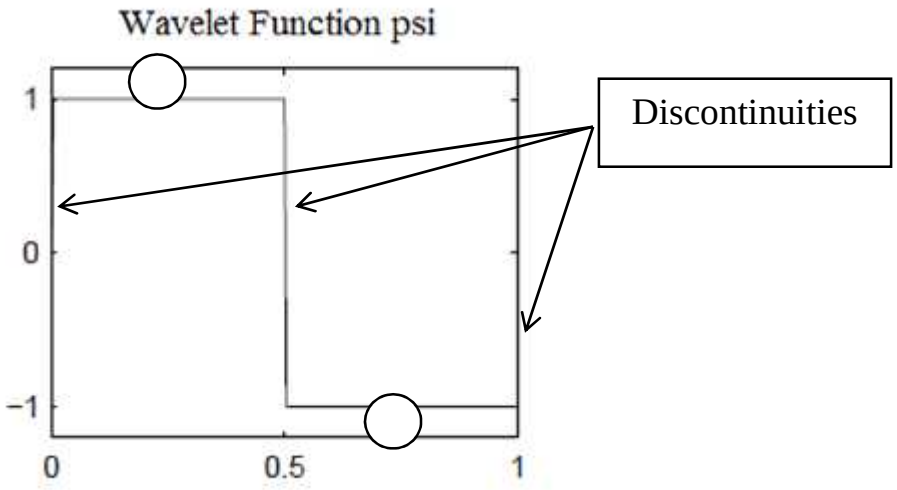

Fig 2.13: The Haar wavelet

Haar wavelets are not smooth or regular. They are anti-symmetric and have linear phase. They are excellent for time resolution but poor in frequency resolution. They are good for edge detection, matching binary pulses, and for very short phenomenon [55].

2.1.7.1.1.2 Daubechies Wavelets

It is name is dbN, where N is the order. The db1 wavelet is the same as Haar wavelet. In Fig 2.14 the wavelet functions (psi) of the next nine members of the family. They don't have linear phase. The four daubechies wavelets filters are robust, fast, and adaptable [55].

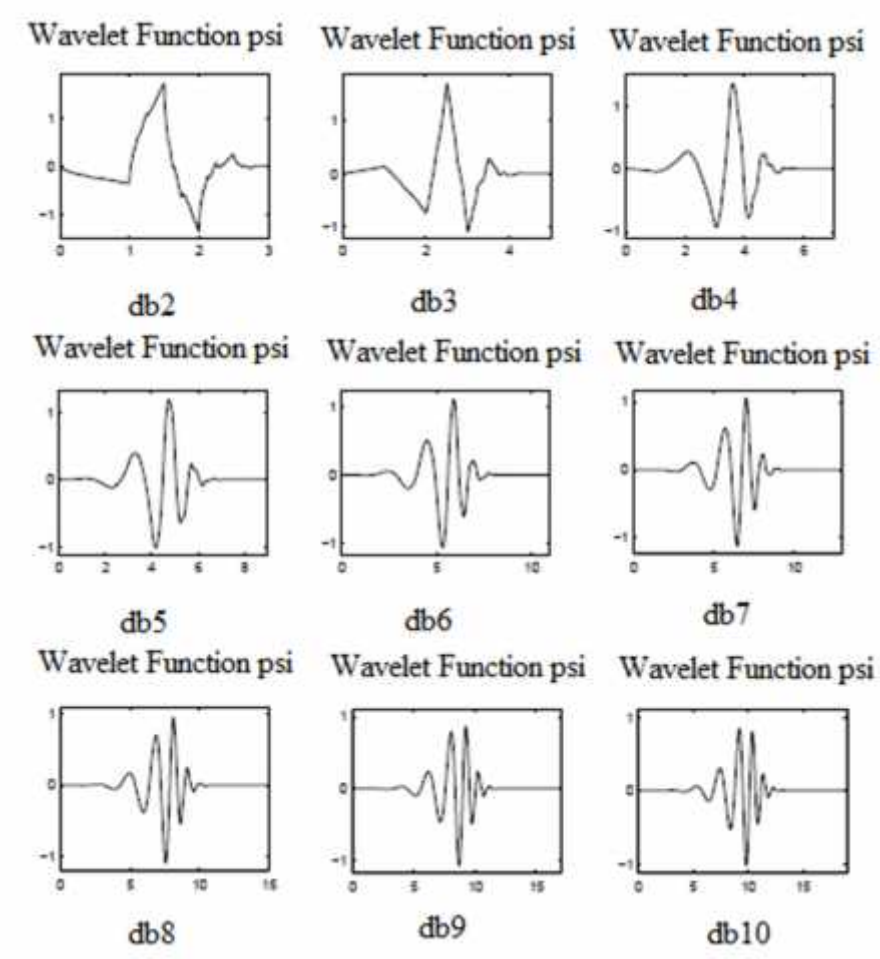

Fig 2.14: Daubechies wavelets (db2 to db10).

2.1.7.1.1.3 Symlet Wavelets

They are more symmetrical than the Daubechies wavelets. They proposed by Daubechies as modifications to the db family. The properties of the two wavelet families are similar. Fig 2.15 shows the wavelet functions (psi). They are nearly symmetrical, the larger Symlets (sym12, Sym16, etc.) have nearly linear phase. Symlets share the same properties as the Daubechies wavelets. They become more regular with larger N (SymN). They have the same compact support for a given N, and the same number of vanishing moments as DbN family. They have the perfect reconstruction and alias cancellation capability that allows them to be used in both the CWT and the DWT [55].

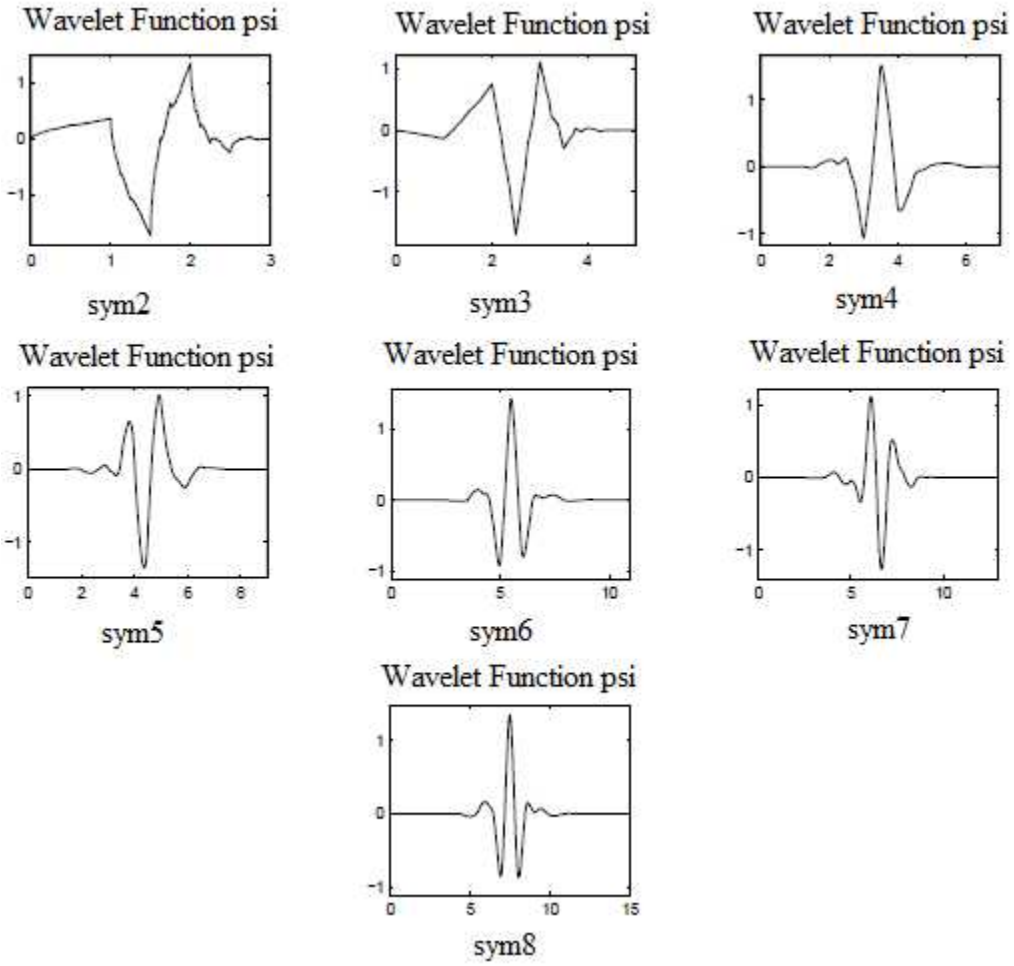

Fig 2.15: Symlet Wavelets (sym2 to sym8)

2.1.7.1.1.4 Coiflets Wavelets

They were developed to invent an orthogonal wavelet (filter set) that had vanishing moment capabilities for both the highpass and lowpass filters (Fig 2.16). The wavelet function has 2N moments equal to 0 and the scaling function has 2N-1 moments equal to 0. The two functions have a support of length 6N-1 [55].

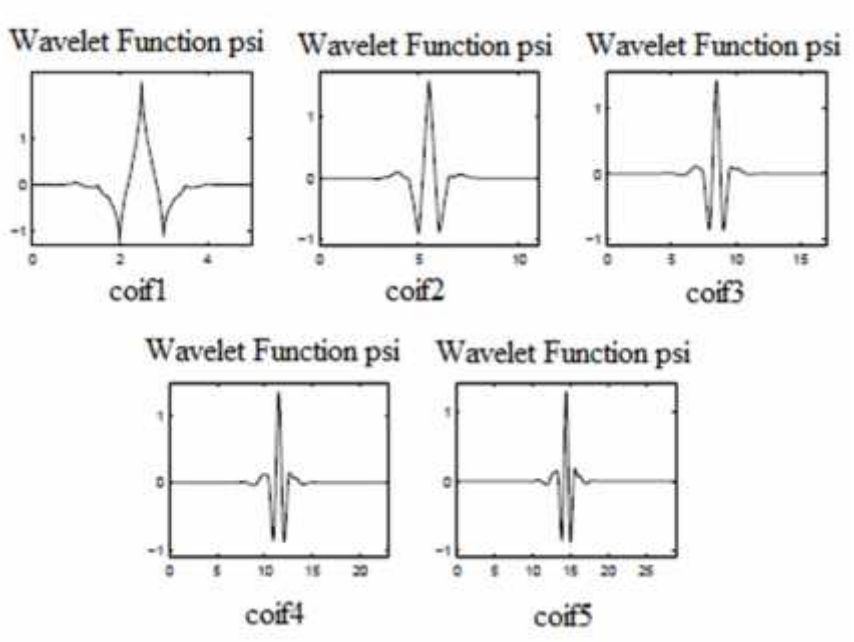

Fig 2.16: The Coiflets Wavelets (coif1 to coif5)

Coiflets are used in many of the same applications as the Daubechies and Symlets [55].

2.1.7.1.1.5 Morlet Wavelet

It has no scaling function, but is explicit. It is symmetrical, infinitely regular, and has an effective support from -4 to +4 (Fig 2.17). It is good for periodic data due to their smoothness and periodicity [55].

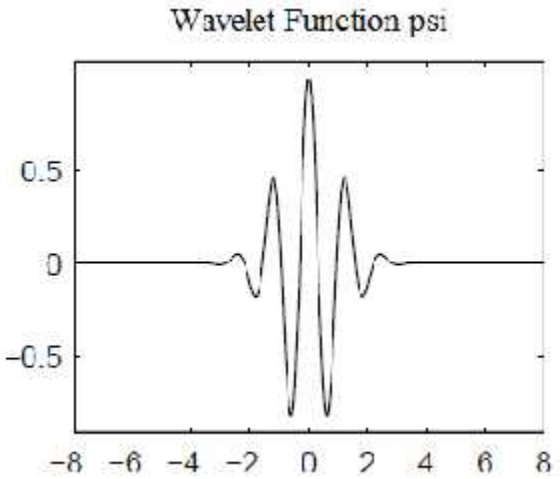

Fig 2.17: The Morlet Wavelet

2.1.7.1.1.6 Mexican Hat Wavelet

It looks like the side view of a sombrero (Fig 2.18). It has no scaling function and is derived from a function that is proportional to the second derivative function of the Gaussian probability density function, thus the symmetry [55].

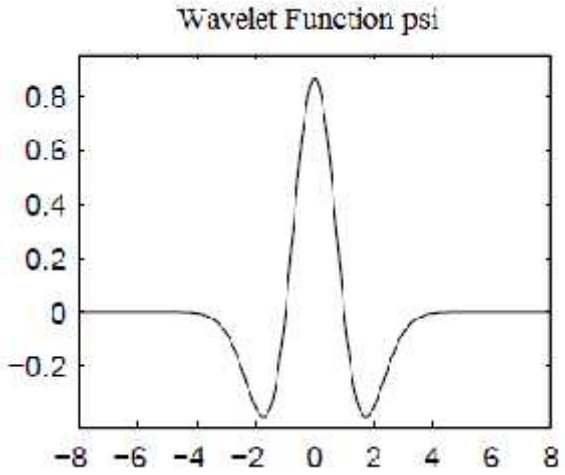

Fig 2.18: The Mexican Hat Wavelet

2.1.7.1.1.7 Meyer Wavelet

They are defined in the frequency domain rather than by the time domain equations. Theoretically infinite in the time domain, an effective support from -8 to +8 is used [55] (Fig 2.19).

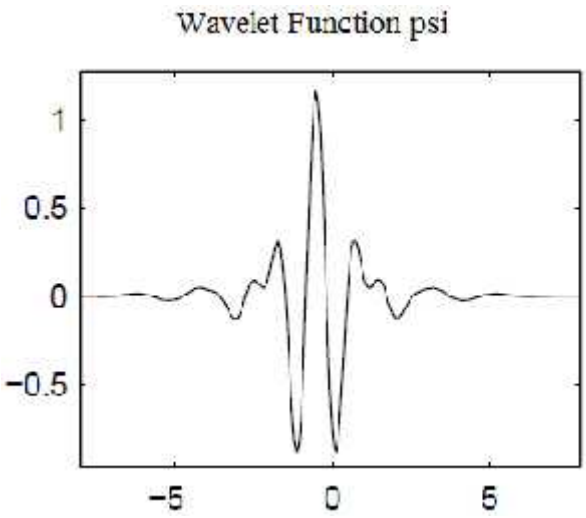

Fig 2.19: The Meyer Wavelet

So wavelets come in various shapes and sizes. By stretching and shifting the wavelet, it can match to the hidden event and thus discover its frequency and location in time. In addition, a particular wavelet shape may match the event unusually well, when stretched and shifted appropriately. This tells about the shape of the event; it probably looks like the wavelet to obtain such a good match or correlation [55].

2.1.7.2 Fourier Transform (FT)

It breaks down a signal into constituent sinusoids of different frequencies, using a mathematical formula for transforming the signal from time domain to frequency domain (Fig 2.20) [57].

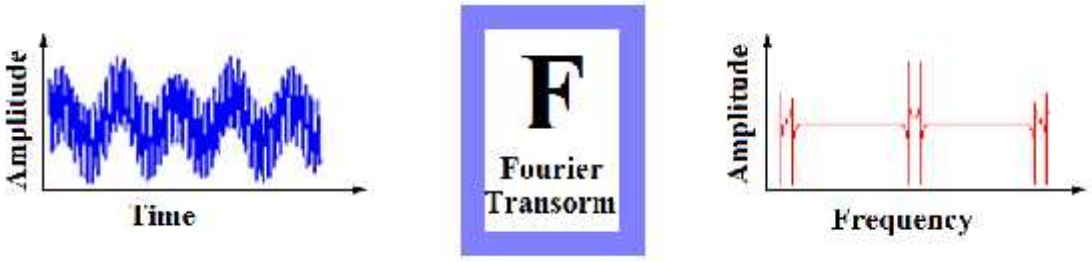

Fig 2.20: Fourier Transform

When the signal is transformed with Fourier analysis, time information is lost. It is impossible to tell when a particular event took place. So FT is not suited to detecting drift, trends, abrupt changes, and beginnings and ends of events which contained in most interesting signals [58].

2.1.7.3 Short-Time Fourier analysis (STFT)

It is providing both time and frequency information about an embedded event. Windowing the signal is divided the total time interval into several shorter time intervals then the FFT took for each interval (Fig 2.21) [58].

Fig 2.21: Short-Time Fourier Transform

The STFT provides some information about both when and at what frequencies a signal event occurs. This information can only obtained with limited precision, and that precision is determined by the size of the window. The STFT drawback is in choosing the size for the time window; it is the same for all frequencies. If the chosen window is narrow it results in good time resolution but poor frequency resolution. Conversely, a wide window causes good frequency resolution but poor time resolution. Many signals require changing the window size to determine more accurately either time or frequency [57, 58].

2.1.7.4 Wavelet Transform (WT)

It is developed to overcome the resolution problem, it allows variable size window, so it results in varying resolution (Fig 2.22). Wavelet analysis windowing technique with variable sized regions allows the use of long time intervals where more precise low frequency information is needed, and shorter regions where high frequency information is needed [55, 57].

Fig 2.22: Wavelet Transform

The wavelet transform is a method to decompose an input signal into a set of wavelets and provides a way to analyze the signal by examining the coefficients of these wavelets. So it relates the signal to wavelets, by multiplying it with a function (wavelet), and the transform is computed separately for different portions of the time domain signal to obtain information that is not readily available in the raw signal [56, 78].

Wavelet analysis is capable of revealing aspects of data such as trends, breakdown points, discontinuities in higher derivatives, and self-similarity. Furthermore, it affords a different view of data than those presented by traditional techniques [57].

Wavelet analysis has a significant impact on the science of medical imaging and the diagnosis of disease and screening protocols, because it is a powerful underlying mathematical theory. It offers exciting opportunities for the design of new multiresolution image processing algorithms [59].

2.1.7.5 Wavelet Transform and Multiresolution Analysis (MRA)

It analyzes the signal at different frequencies with different resolutions. It is designed to give good time resolution at high frequencies and good frequency resolution at low frequencies [58].

The wavelet transform provides a multiresolutional representation with dilated windows, which is achieved by dyadically changing the size of the window. So it decomposes the image using various scale frequency resolutions. The high frequency analysis is done using narrow windows and the low frequency analysis is done using wide windows [60, 61].

Most images correspond to signals which have high-frequency components of short duration (details) and low-frequency components of long duration (approximations). So the multiresolution analysis works best with this kind of signals [59].

2.1.7.5.1 1-D Wavelet analysis filter bank

The 1-D wavelet transform analysis is the first step in the multiresolution approach. The MRA decomposes the dataset into a hierarchy of several levels of approximation and detail maps by exposing it to a filter bank made up of a high pass and low pass filter, which result in giving detail and approximation maps. The approximation map contains the image's low frequency information and the detail map contains the high frequency information. To construct the next level, the approximation is decomposed into descendent detail and approximation by exposing it to a high pass filter and a low pass filter. Iteratively exposing the approximation creates the next level of the hierarchy. The decomposition can proceed until the individual details consist of a single observation. In the hierarchical model, the resolution is the highest at the lowest level. As the levels increase, details are removed, and the approximations are at increasingly lower resolutions. Fig 2.23 illustrates the MRA hierarchical model with j levels. Each level contains an approximation A_j and

details D_j. A_0 is the original image. Approximation A_1 is the low frequency components of A_0, and D_1 is the high frequency components of A_0 [60, 62].

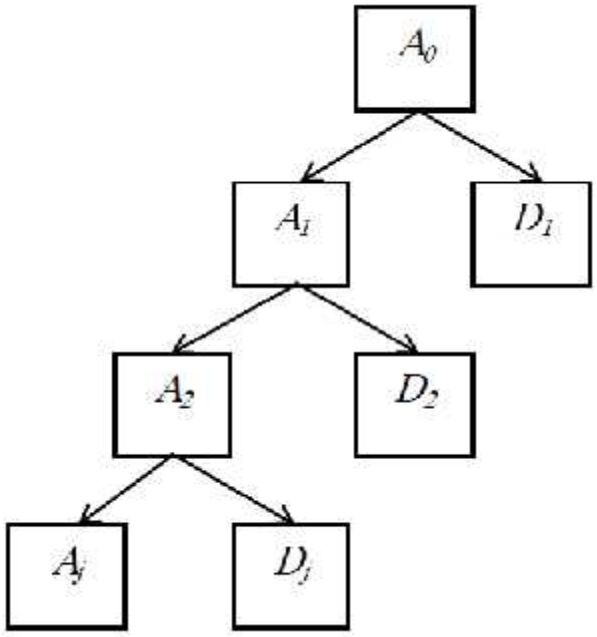

Fig 2.23: Multiresolution Hierarchical Model

The mathematical description of the MR hierarchy as in equations (2.1 and 2.2)

$$a_0(t) = a_j(t) + \sum_{k=1}^{j} d_k(t) \qquad (2.1)$$

$$a_j(t) = a_{j+1}(t) + d_{j+1} \qquad (2.2)$$

Where: $a_0(t)$ is the original signal, $a_j(t)$ is the approximation, d(t) is the detail, and j is the level.

The dyadic nature of multiresolution decomposition is closely related to implementing the DWT using filter bank (Fig 2.24) made up of a high pass component (g) called the wavelet function, and a low pass component (h) called the

scaling function. At every decomposition level, the filtering and subsampling will result in half the number of samples [59, 62].

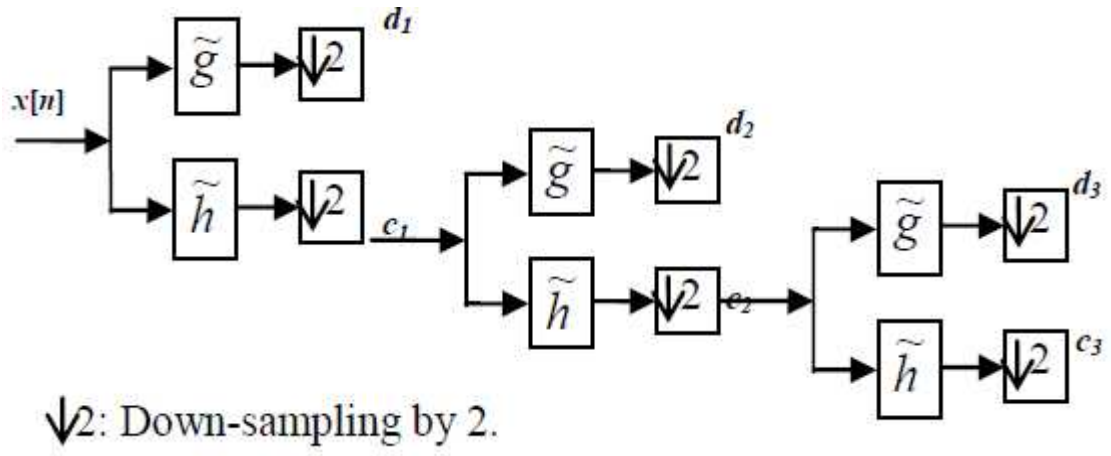

Fig 2.24: 1-D DWT filter bank implementation

2.1.7.6 To understand WT, some concepts must know first

2.1.7.6.1 Scaling Wavelet

It is stretching or shrinking the wavelet in time. The scale factor is often denoted by the letter (a), the smaller a, the more compressed the wavelet (Fig 2.25). Dilation is also used to describe either stretching or shrinking the wavelet in time [55].

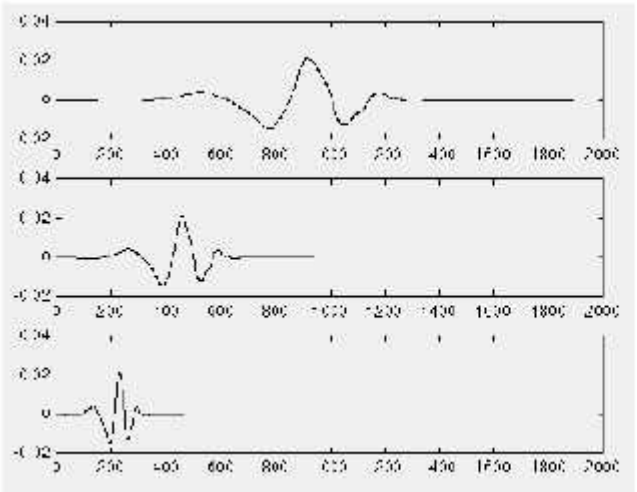

$$f(t) - \psi(t) \quad ; \quad a - 1$$

$$f(t) - \psi(2t) \quad ; \quad a - \frac{1}{2}$$

$$f(t) - \psi(4t) \quad ; \quad a - \frac{1}{4}$$

Fig 2.25: The effect of the scale factor (a) on wavelets.

2.1.7.6.2 Shifting Wavelet

It is delaying or hastening its onset. Mathematically, delaying a function f(t) by k is represented by f(t - k) (Fig 2.26) [55].

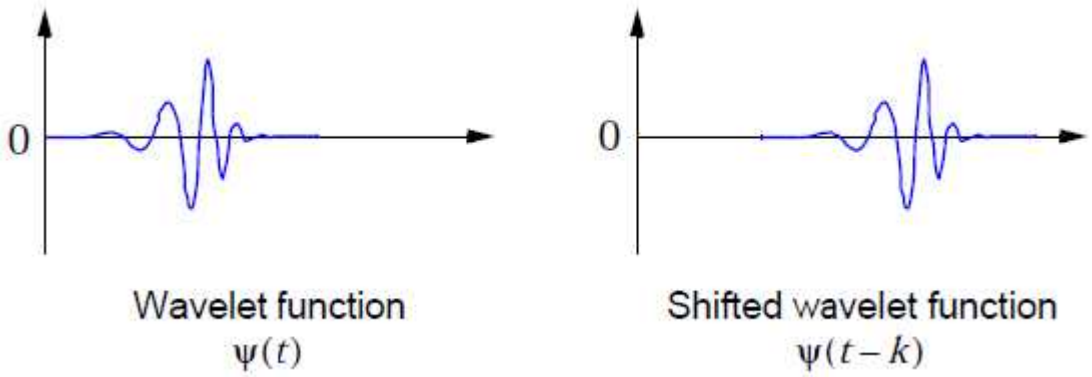

Fig 2.26: The wavelet and its shifted wavelet

2.1.7.6.3 Scaling function

It makes up the low pass component of the wavelet decomposition filter bank. It generates the basic functions for the approximation [44].

Set of scaling functions in terms of integer translates of the basic scaling function is defined as

$$\ddot{}_{k} = \ddot{}(t-k) \qquad (2.3)$$

A two-dimensional family of functions is generated from the basic scaling function by scaling and translation as

$$¨_{j,k}(t) = 2^{j/2} ¨ (2^j t - k) \qquad (2.4)$$

The decomposition level is j, k represents the dilation, and t is time. The scale index j indicates the wavelet's width and the location index k gives its location or (translation). The scaling function coefficients $¨_{j,k}$ are the coefficients used to make the approximation maps [44].

2.1.7.6.4 Wavelet Function

It is the basis function for the detail in the wavelet decomposition. The wavelet function is defined as equation (2.5)

$$·_{j,k}(t) = 2^{j/2} · (2^j t - k) \qquad 2.5$$

The scale is represented by j, translation by k, time by t, and $·_{j,k}$ is the coefficients for the detail. The wavelet function can be expressed in terms of the scaling function at equation (2.6) which shows the relationship between the mother wavelet, $·(t)$ and the scaling function $¨(t)$ at the next scale. The coefficients g_k, h_k, make up the high pass filter that is used with the wavelet coefficients, $·_{j,k}$ to reconstruct the detail in the wavelet decomposition [44].

$$·_{j,k}(t) = \sum_k g_k ¨_{1,k}(t) = \sqrt{2} \sum_k g_k ¨ (2t - k) \qquad 2.6$$

$$g_k = (-1)^i h_{L-I-1} \qquad 2.7$$

The Wavelet function $·(t)$ and the Scaling function $¨(t)$ are needed for the multiresolution formulation. All other wavelets are obtained by simple scaling and translating of $·(t)$ [59].

2.1.7.7 Types of Wavelet Transform

2.1.7.7.1 Continuous Wavelet Transform (CWT)

It is the sum over all time of the signal multiplied by scaled, shifted versions of the wavelet function or correlating with various stretched, wavelets [44, 55].

2.1.7.7.2 Discrete Wavelet Transform (DWT)

The DWT minimizes the highly redundant number of continuous wavelet transform's coefficients by restricting the variation in translation and scale, usually to powers of two. DWT will produce a non-redundant, bilateral transform [44].

The DWT analyzes the signal at different frequency bands with different resolutions by decomposing the signal into a coarse approximation and detail information, as shown in equations (2.8, 2.9) where equation (2.8) is the approximation coefficients and (2.9) is the detailed coefficients [44].

$$W_{\cdot\cdot}(j_0,k) = \frac{1}{\sqrt{M}} \sum_n x(n)^{\cdot\cdot}{}_{j_0,k}(n) \qquad 2.8$$

$$W_{\cdot}(j,k) = \frac{1}{\sqrt{M}} \sum_n x(n) \cdot {}_{j,k}(n) \qquad 2.9$$

x(n), $^{\cdot\cdot}{}_{j_0,k}(n)$ and $\cdot\,{}_{j,k}(n)$ are discrete functions defined in [0, M − 1], totally M points.

2.1.7.7.3 The Redundant Wavelet Transform (RWT)

In the RWT there is no decimation as in the usual implementation of the DWT. Instead of signal downsampling, the filter responses themselves are upsampled by inserting appropriate number of zeros between filter taps [63].

The RWT splits the input image into the detail coefficient, and the approximation coefficient which serve as input for the next decomposition level (Fig 2.27).

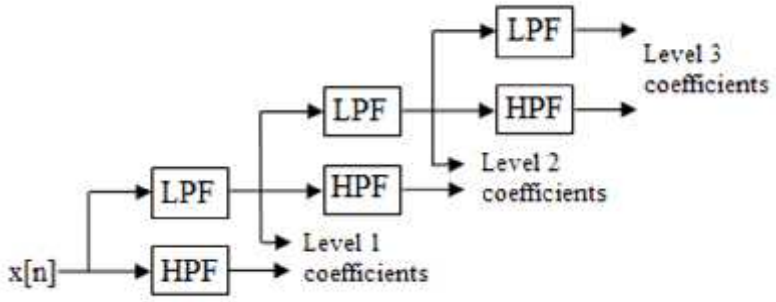

Fig 2.27: The RWT decomposition to three levels

2.1.7.8 Wavelet Transform on Images

For images the 1D DWT become 2D DWT. The transformed coefficient becomes two variable functions. The scaling and wavelet function are two variable functions, denoted $\ddot{}(x,y)$ and $\cdot(x,y)$. The scaled and translated basis functions are defined as [44]:

$$\ddot{}_{j,m,n}(x,y) = 2^{j/2}\ddot{}(2^j x - m, 2^j x - n) \qquad 2.10$$

$$\cdot^{i}_{j,m,n}(x,y) = 2^{j/2}\cdot(2^j x - m, 2^j x - n)\ ,\ i = \{H,V,D\} \qquad 2.11$$

Wavelet functions measure intensity or gray level variations for image along different directions. $\cdot^{H}(x,y)$ respond to variation along columns (horizontal edge), $\cdot^{V}(x,y)$ respond to variation along rows (vertical edges) and $\cdot^{D}(x,y)$ measures variations along diagonals [44].

The discrete wavelet transform of image f(x, y) of size M×N is computed as given in equations (2.12) and (2.13):

$$W_{\cdot\cdot}(j_0,m,n)=\frac{1}{\sqrt{MN}}\sum_{x=0}^{M-1}\sum_{y=0}^{n-1}f(x,y)^{\cdot\cdot}{}_{j_0,m,n}(x,y) \qquad 2.12$$

$$W^{i}(j_0,m,n)=\frac{1}{\sqrt{MN}}\sum_{x=0}^{M-1}\sum_{y=0}^{N-1}f(x,y)\cdot{}^{i}_{j_0,m,n}(x,y)\ ,\ i=\{H,V,D\} \qquad 2.13$$

Where: j_0 starting scale normally let it equal to zero, $w_{\cdot\cdot}(j_0,m,n)$ is define an approximation of f(x,y) at the scale and normally obtained by convolving signal with the low pass filter and $w^{i}_{\cdot}(j_0,m,n)$ is define horizontal, vertical and diagonal details normally obtained using high - pass filter [44].

So for the processing of images, the 1-D DWT decomposition is extended to 2-D DWT. So at each level, implement the 1D DWT on each row signal. Then, apply the 1D DWT to each column of the preceding output. Fig 2.28 shows how the transform matrix is applied to an image to achieve a wavelet transform. A total of four subband images HH, HL, LH and LL are generated (L= Low, H = High). The LL subband contains an approximation of the original image while the other subbands contain the missing detail. The LL subband output from any stage can be decomposed further [59, 64].

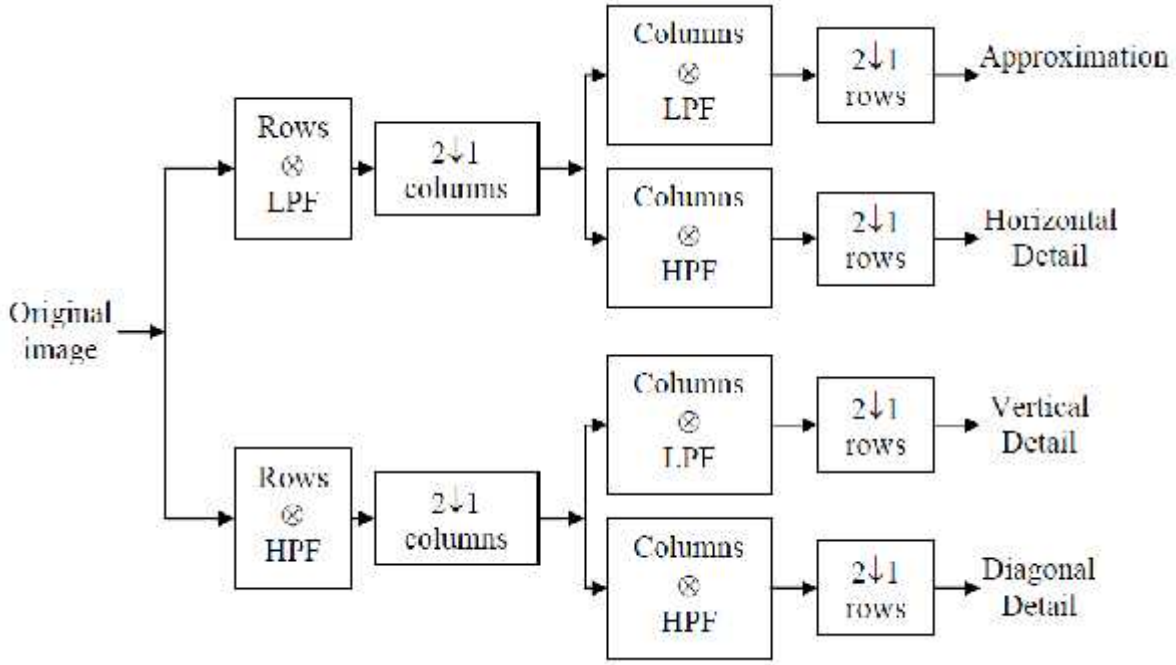

Fig 2.28: Block diagram of Two Dimensional Wavelet transform. ⊗ represents convolution and 2↓1 represents dyadic decimation [65].

The different subband images (Fig2.29) contain different information and they may be processed individually using different algorithms. The subband image LL corresponds to the lowest frequencies. It contains the smooth information and the background intensity of the image. HL, LH, and HH contain the detail information of the image. HL gives the vertical high frequencies (horizontal edges), LH gives the horizontal high frequencies (vertical edges) and HH gives the high frequencies in both directions (corners and diagonal edges) [59].

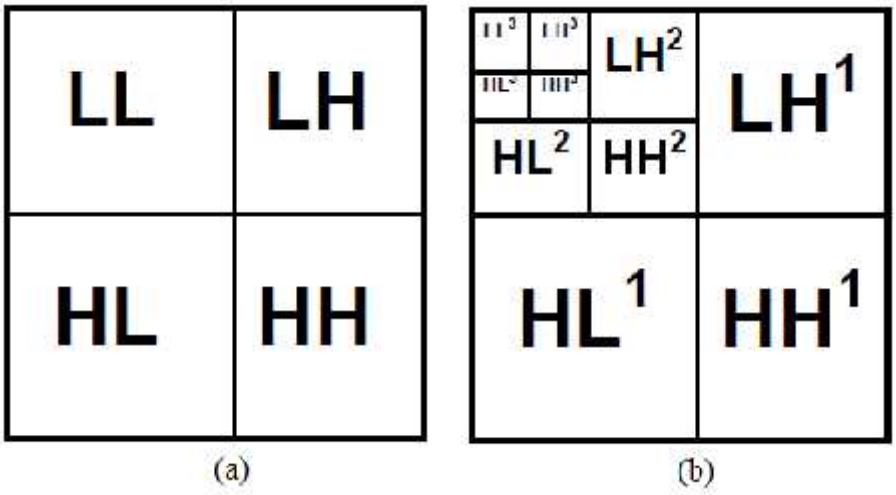

Fig 2.29: The wavelet transform decomposition subband images: (a) Decomposition level 1 and (b) Decomposition level 2.

2.1.8 The Gray Level Co-occurrence Matrix (GLCM)

It is also named the Spatial Gray Level Dependency (SGLD) Matrix. It is one of the most widely used statistical texture measures. It is used to describe the patterns of neighboring pixels in an image at a given distance, d. It displays the gray level spatial-dependency along different angular relationships, horizontal, vertical, right diagonal and left diagonal directions (0°, 90°, 45° and 135° respectively) and a distance d of one pixel on an image, to calculate textural measures. Fig 2.30 illustrates the geometrical relationships of GLCM measurements made for four distances d and angles of $\theta = 0, \pi/4, \pi/2$ and $3\pi/4$ radians under the assumption of angular symmetry.

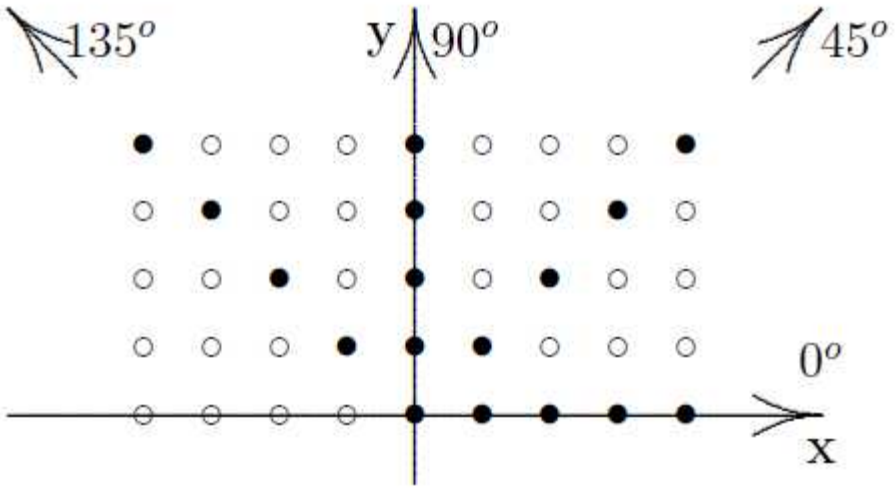

Fig 2.30: Geometry for measurement of gray level co-occurrence matrix for 4 distances d and 4 angles θ.

The GLCM counts the number of two-pixel combinations and normalized them so that the matrix may be treated as a probability density function (PDF). The idea of the method is to consider the relative frequencies for which two neighboring pixels are separated by a distance on the image. Since the GLCM collects information about pixel pairs instead of single pixels, it is called a second-order statistic. GLCM is a way of extracting second order statistical texture features. Texture measures, such as homogeneity, contrast, and entropy are derived from the co-occurrence matrix. In the calculation of the texture features, four such matrices are needed to describe different orientations. More specifically, one SGLD matrix describes pixels that are adjacent one to another horizontal, vertical direction and diagonally in both directions [44, 60, 66, 67].

The matrix element P(i, j, d, θ) is the relative occurrence frequency of which two pixels, separated by a pixel distance (d), along the direction of angle θ, occur within a given neighborhood, one with intensity i and the other with intensity j. One may also say that the matrix element P(i, j, d, θ) contains the second order statistical

probability values for changes between gray levels i and j at a particular displacement distance d and angle (θ).

In order to obtain a statistically estimate of the joint probability distribution, the matrix must contain a reasonably large average occupancy level. This can be achieved by using a relatively large window. It causes uncertainty and error if the texture changes over the large window. A typical compromise is to use a window of about 30 to 50 pixels on each side [67].

The non-normalized frequencies P(i, j, d, θ) of SGLD matrices for a defined window M×N neighborhood of an input image containing G gray levels from 0 to G − 1, with distance d and angles of 0°, 90°, 45° and 135° are defined by [44]:

$$p(i,j,d,0^\circ) = \#\{((k,l),(m,n)) \in (M\times N)\times(M\times N) : k-m=0, |n-l| = d, I(k,l)=i, I(m,n)=j\} \quad (2.14)$$

$$p(i,j,d,90^\circ) = \#\{((k,l),(m,n)) \in (M\times N)\times(M\times N) : |k-m|=0, n-l=d, I(k,l)=i, I(m,n)=j\} \quad (2.15)$$

$$p(i,j,d,45^\circ) = \#\{((k,l),(m,n)) \in (M\times N)\times(M\times N) : (k-m=d, |n-l|=-d) or (k-m=-d), I(k,l)=i, I(m,n)=j\} \quad (2.16)$$

$$p(i,j,d,135^\circ) = \#\{((k,l),(m,n)) \in (M\times N)\times(M\times N) : (k-m=d, n-l=d) or (k-m=-d, n-l=-d, I(k,l)=i, I(m,n)=j\} \quad (2.17)$$

Where: # denotes the number of elements. It is observed that SGLD matrix is symmetrical because p (i, j, d, θ) = p (j, i, d, θ).

2.1.9 Haralick Texture Features

Haralick has made a series of contributions in the field of computer vision. He has worked in image texture analysis using spatial gray frequency co-occurrence texture features. These features have been used with success on biological cell images, x--ray images, satellite images, aerial images and many other kinds of images [68].

There are a set of 12 texture features which can be extracted from each of the gray level spatial dependence matrix or the wavelet coefficients [69]. They are the Entropy (EN), Energy (EG), Inertia (IN), inverse different moment (IDM), Correlation (CO), Variance (VA), Sum Average (SA), Sum Entropy (SE), Sum Variance (SV), Difference Average (DA), Difference Entropy (DE) and Difference Variance (DV). The following equations shown in table (2.1) define these features. Each cell will be denote by p(i, j) where i, j are the intensities or the relative frequency of the pixel.

Table (2.1): The Twelve Haralick's Texture Features

No	Texture feature	Equation
1	Energy (EG)	$EG = \sum_{i=0}^{n=1}\sum_{j=0}^{n=1} p^2(i,j)$
2	Correlation (CO)	$CO = \frac{\sum_{i=0}^{n-1}\sum_{j=0}^{n-1}(i-«_x)(j-«_y)p(i,j)}{±_x ±_y}$
3	Entropy (EN)	$EN = \sum_{i=0}^{n-1}\sum_{j=0}^{n-1} p(i,j)\log_2 p(i,j)$
4	Inertia (IN)	$IN = -\sum_{i=0}^{n-1}\sum_{j=0}^{n-1}(i-j)^2 p(i,j)$
5	Inverse Difference Moment (IDM)	$IDM = \sum_{i=0}^{n-1}\sum_{j=0}^{n-1}\frac{1}{1+(i-j)^2}p(i,j)$

6	Sum Average (SA)	$SA = \sum_{k=0}^{2n-2} k p_{x+y}(k)$
7	Sum Entropy (SE)	$SE = -\sum_{k=0}^{2n-2} p_{x+y}(k) \log_2 p_{x+y}(k)$
8	Difference Entropy (DE)	$DE = -\sum_{k=0}^{n-1} p_{x-y}(k) \log_2 p_{x-y}(k)$
9	Sum Variance (SV)	$SV = \sum_{k=0}^{2n-2} (k - SA)^2 p_{x+y}(k)$
10	Difference Average (DA)	$DA = \sum_{k=0}^{n-1} k p_{x-y}(k)$
11	Difference Variance (DV)	$DV = \sum_{k=0}^{n-1} (k - DA)^2 p_{x-y}(k)$
12	Variance (VA)	$VA = \sum_{i=0}^{n-1} (i - «)^2 p_x(i)$

Where

n ≡ the number of grey level in the image

$$«_x = \sum_{i=0}^{n-1} i p_x(i) \qquad ±_x^2 = \sum_{i=0}^{n-1} (i - «_x)^2 p_x(i)$$

$$«_y = \sum_{j=0}^{n-1} j p_y(j) \qquad ±_y^2 = \sum_{j=0}^{n-1} (i - «_x)^2 p_y(j)$$

$$p_x(i) = \sum_{j=0}^{n-1} p(i, j) \qquad p_y(j) = \sum_{j=0}^{n-1} p(i, j)$$

Are the mean and variance of the marginal distribution $p_x(i)$ and $p_y(j)$

$$p_{x+y}(k) = \sum_{i=0}^{n-1} \sum_{j=0}^{n-1} p(i, j)$$

$$i + j = k \qquad k = 0,...,2n-2$$

$$p_{x-y}(k) = \sum_{i=0}^{n-1} \sum_{i=j}^{n-1} p(i, j)$$

$$|i - j| = k \qquad k = 0,..., n-1$$

2.1.9.1 Definitions to some of these features [44]

2.1.9.1.1 The Entropy (EN)

The Entropy coefficient (EN) is a descriptor of randomness produces a low value for an irregular SGLD matrix. It achieves its highest value when all elements of the SGLD matrix are equal for an irregular image.

2.1.9.1.2 The Energy (EG):

It returns the sum of squared elements. It measures the homogeneity.

2.1.9.1.3 The Inertia (IN)

It called Contrast feature, it is a measure of image intensity contrast or the local variations present in an image to show the texture fineness.

2.1.9.1.4 Correlation (CO)

The descriptor Correlation (CO) measures the linear dependence of gray level values or describes the correlations between the rows and columns.

2.1.9.1.5 Variance (VA)

It is a measure of variation. A variance of zero indicates that all the values are identical. A non-zero variance is always positive: A small variance indicates that the data points tend to be very close to the mean and hence to each other, while a high variance indicates that the data points are very spread out from the mean and from each other.

2.1.10 Linear Discriminant Analysis (LDA)

It is a technique for data classification, looks for linear combinations of the input variables that can provide an adequate separation for a given class. It uses an empirical approach to define linear decision plans in the attribute space, by trying to find a mapping from the high-dimensional space to a low-dimensional space in which the most discriminant features are preserved, to provide maximum class separability and draw a decision region between the given classes, by minimizing the variation within the same class and maximizing the variation between classes [70, 71, 72].

The discriminant functions used by LDA are built up as a linear combination of the feature variables that seek to maximize the differences between the classes [71]; mathematically it can be express as

$$y = b + \sum_{i=1}^{n} a_i x_i \qquad 2.25$$

Where: n is the number of feature variables, x are the values of the feature variables, a_i are coefficients (eigenvector), and b is constant a_i and b estimated from the input data during training, so that the separation between the distributions of the discriminant scores y is a maximum of groups.

Then the problem is to find a suitable vector. One of the most successful rules is the Fisher Linear Discriminant Rule.

Fisher's Rule is considered a sensible classification, in the sense that it is intuitively attractive. It makes use of the fact that distributions that have a greater variance between their classes than within each class should be easier to separate. Therefore, it searches for a linear function in the attribute space that maximizes the ratio of the between-group sum-of-squares B to the within group sum of squares W_{LDA}. This can be achieved by maximizing the ratio

$$\frac{a_i B a}{a_i W_{LDA} a} \qquad 2.18$$

And it turns out that the vector that maximizes this ratio a_i is the eigenvector corresponding to the largest eigenvalue of W_{LDA} B i.e. the LD function y is equivalent to the first canonical variate [71].

2.1.11 SPSS (Statistical Package for the Social Science)

It is a good first statistical package to perform quantitative research in social science because it is easy to use and it can be a good starting point to learn more advanced statistical packages. Many of the widely used social science data sets come with an easy method to translate them into SPSS; this significantly reduces the preliminary work needed to explore new data [73].

3.13.1 SPSS is used for

- conducting statistical analyses
- Manipulating data
- Generating tables and graphs that summarize data

3.13.2 Goods about SPSS

- Easy-to-use pull-down menus, like Microsoft XP/Office
- Users do not need to know complex statistical equations to use it

- SPSS is like a calculator: users enter the numbers and select the tasks, and the software does the rest
- Results are clearly presented
- Tables and graphs can be copied directly into Word files [74].

2.2 Literature Reviews

Reviews are the basis for discovery of which is the end of the first effort and at the same time the beginning of the recent discoveries. So Literature reviews were done to know the recent theories leading to the detection of breast cancer with good results, in order to do new method in order to achieve best result.

Several types of wavelet transforms were employed in algorithms to achieve automated or semi-automated detection of breast cancer. Many researchers have conducted research on the segmentation of breast, enhancement mammogram images, and also on feature extraction and classification of breast tissues. In this section, a few most important techniques for breast cancer detection are reviewed.

(Pelin Gorgel, et al. 2013) developed a system to diagnose the breast cancer, using Fast Wavelet Transform and feature extraction for pre-processing, Adaptive Neuro-Fuzzy Inference System (ANFIS) based Fuzzy subtractive clustering and Support Vector Machines (SVM) methods for the classification as malignant or benign. ANFIS based subtractive clustering produced 92% while SVM produced 88% accuracy in malignant-benign classification [1].

(Nizar Ben Hamad, et al. 2013) developed computer aided detection of microcalcifications algorithm using multiresolution analysis based on 2-D discrete wavelet transform in analysis and synthesis on screening mammograms in order to detect the microcalcifications. The positive predictive value (PPV) of the system

which calculated for the technique of thresholding is 97.5% and the specificity (S) is 55.6% [59].

(Juuso Olkkonen 2011) developed a generalized computer-aided diagnosis system that is based on the Discrete Wavelet Transform (DWT). Applied on three image databases, small bowel, mammogram and retinal images. He proposed a texture analysis scheme based on human texture perception to quantify differences between textures in normal and abnormal images, using a shift-invariant DWT to extract features. At various levels of decomposition, wavelet-domain graylevel cooccurrence matrices were implemented in a variety of directions over all subbands to capture the orientation of such texture elements. Texture features were extracted from each of the wavelet subbands to quantify the randomness of the coefficients and they are classified using a linear classifier. Bowel images were correctly classified at an average rate of 85%, retinal images had an average classification accuracy of 82.2% and the mammogram lesions were classified correctly 69% on average [60].

(Shruti Dalmiya, et al. 2012) presented a research on mammography images using wavelet transformation and K – means clustering for cancer tumor mass segmentation. Discrete wavelet transform (DWT) is used to extract high level details from MRI images. K-means algorithm is applied to the sharpened image in which the tumor region can be located using the thresholding method. The combination of noise-robust nature of and the simple K-means algorithm gives better results [76].

(Ms. S. M. Salve and V. A. Chakkarwar 2013) proposed a system to classify mammographic images using Histogram equalization and median filter for images enhancement, Gabor Wavelet and Discrete Wavelet Transform (DWT) for feature extraction, Principal Component Analysis (PCA) for dimensionality reduction, and support vector machine for classifies the images into normal or abnormal (benign or

malignant) images, achieving that the recognition rate of DWT is 89% and Gabor Wavelet is 86% [76].

(Pelin Gorgel et al. 2013) classified the cropped region of interests (ROI's) as benign or malignant, they applied Spherical Wavelet Transform (SWT) to the original ROI matrix prior to feature extraction, and then extract some predetermined pixel and shape features both from wavelet and scaling coefficients. Finally they classified using Artificial Neural Networks (ANN) and K-Nearest Neighbour (KNN) systems. They achieved 87% classification accuracy for SWT-ANN method [77].

(R.Ramani, et al. 2013) presented a survey of recent clustering techniques for detection of breast cancer. They used K –means clustering segmentation, Adaptive K-means Clustering Algorithm, Fuzzy C-means Algorithm, Kernelized Fuzzy C-means Algorithm, Multiple kernel fuzzy c-means (MKFC), Hierarchical Clustering, Wavelet based K-means Algorithm and Fuzzy k-c-means Clustering Algorithm for image segmentation. They found that Clustering techniques may help to enhance the efficiency of the image recovery process. All the clustering techniques may obtain satisfaction results but not able to produce 100 % of accuracy [78].

(Rajashekar K.R Mtech 2012) presented a novel approach for classifying mammograms by computer aided design using image processing and data mining techniques. In preprocessing the breast image is standardized. Then suspicious regions of cancer are acquired from mammogram by K-means clustering technique. Features are extracted from these regions and are given as input to the pre-trained decision tree based classifier, which in turn classifies the mammogram into normal, benign and malignant. The system has very high accuracy. The false negative rate was as very low compared to the other existing methods. It was found that out of 90 images, 83 images were rightly classified and remaining 7 were misclassified to other categories [2].

(S. Mohan Kumar and G. Balakrishnan 2013) developed a system to classify the mammogram images into normal or abnormal, and the abnormal severity into benign or malignant; the classification is achieved by using Stochastic Neighbor Embedding (SNE) for reducing high dimensionality data into relatively low dimensional data and K-Nearest Neighbor (KNN) Classifier. Results show that the proposed system achieves 100% classification rate for normal and malignant cases and over 80% classification rate for benign and abnormal cases [79].

(Seyyid Ahmed Medjahed et al. 2013) studied and evaluated the performance of different distances that can be used in the K-NN algorithm. Also they analyzed this distance by using different values of the parameter k and by using several rules of classification. The results advocate the use of the k-nn algorithm with both types of Euclidean distance and Manhattan. These distances are effective in terms of classification and performance but are consuming much time. Nevertheless, they remain two types of distance that give the best results (98; 70% for Euclidean distance and 98; 48% for Manhattan whith k = 1) [80].

(B. N. Prathibha 2013) proposed CAD system to discriminate the abnormal severity of mammograms into normal-benign (non-cancerous, non-spreadable), normal-malign (cancerous) and benign-malign, using wavelet features combined with spectral domain. He classified using Kernel Discriminant Analysis (KDA). The study revealed that the optimal smoothing parameters are increasing functions of the sample size of the complementary classes, features used to classify and value of the bandwidth.

(Carissa Erickson 2005) improved breast cancer screening protocols first by collecting small angle x-ray scattering (SAXS) images from breast biopsy tissue, and second, by applying pattern recognition techniques as a semi-automatic screen. He used Wavelet Transform as a feature extraction. 100% classification rate was achieved for distinguishing between normal and tumor samples [65].

(Jihene Malek, et al. 2008) proposed a design of automated detection, segmentation, and classification of breast cancer nuclei using a fuzzy logic. He did segmentation using an active contour for cell tracking and isolating of the nucleus in the cytological image. Wavelet transforms was used for feature extraction. A fuzzy C-means (FCM) clustering algorithm was used to classify the images into malign and benign ones, achieving classification rate of 95% of the testing data [82].

(Fatehia Garma et al. 2013) proposed an algorithm to detect cancer in mammogram, using Haralick texture features derived from spatial grey level dependence (SGLD) matrix as a feature extraction, and linear dsciminant analysis for features classification into normal or abnormal tissue. The algorithm achieved 92.7% classification accuracy [83].

(Fatehia Garma 2014) developed an algorithm to explore the breast tissue type in order to detect the cancer cells in mammogram, firstly using the spatial gray level dependence (SGLD) matrix then Haralick features as a feature extraction, secondly using discrete wavelet transform as a feature extraction. And linear discriminant analysis as a classifier, achieving 95.7% as a result of SGLD matrix of original grouped cases correctly classified and 61.7% at the wavelet transform [44].

2.2.1 Summary of literature reviews

In the literature reviews, it was observed that wavelet transform is extremely used to enhance mammogram images and extract features of abnormal breast tissues (benign, micro-calcifications and malignant).

In this study, wavelet transform has been used as feature extraction to characterize the tissues in digitized mammograms as normal (fat, glandular + connective tissues, and dense) or abnormal.

Chapter Three
Material and Methodology

This chapter presents a description about the different methods implemented. The techniques have been programmed in Matlab (R2010a) then the classification has done using the SPSS (version 20) in a computer with CPU Pentium (R) Dual Core T4500, with 2.30 GHz and 2GB RAM memory.

The appearance of masses is one of the important symptoms of breast abnormality in the mammograms. They have a higher X-ray attenuation than the normal breast tissue and appear as brighter area. In order to recognize with exactitude mass regions on mammograms, the expert radiologist was asked, and he marked manually the position of the pixels corresponding to the mass. The knowledge of the breast tissue type makes it possible to detect the abnormal tissue. This study proposed the use of the wavelet decomposition technique to find out this detection. Symlet wavelet families were used for the detection of abnormality.

This work includes mainly three stages as shown in Fig 3.1. Firstly the feature extraction, where several combination techniques were used to extracted features. Secondly the feature optimization, Haralick's features were used to optimize the features of each technique. Finally the classification, the Linear Discriminant Analysis (LDA) was used to classify the optimized features in each technique. Sensitivity and Specificity performance criterion have been calculated to assess the efficiency of CAD system used.

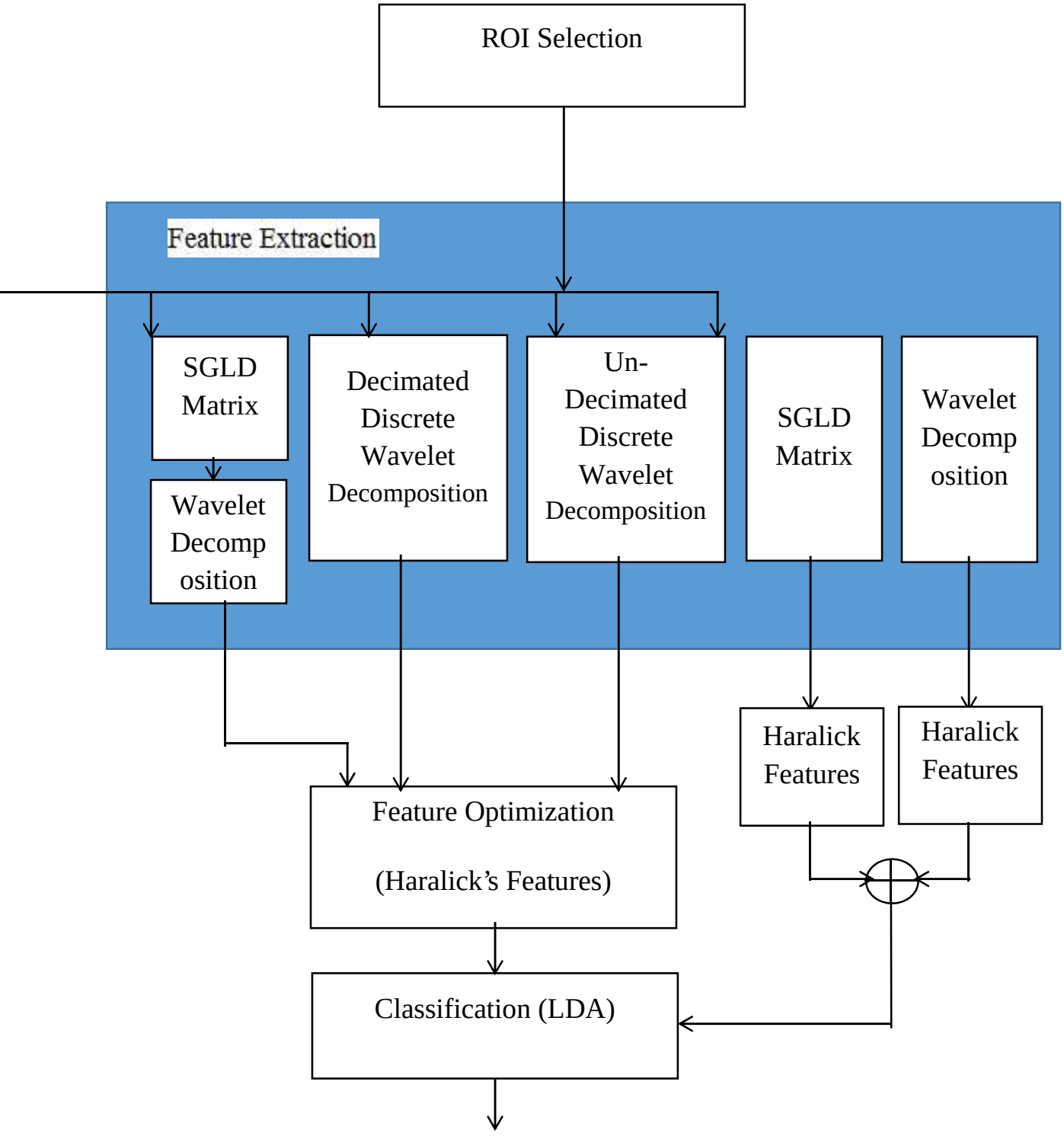

Fig 3.1: The proposed algorithms of breast tissues classification.

3.1 Mammogram Database

The mammographic images which were used in this dissertation correspond to real cases obtained from mini MIAS Database [84]. It contains mammograms of size 1024 × 1024 pixels at 256 gray levels, and in the gray scale file format (.pgm).

This database categorized the normal breast tissues into three tissue types, which they are the fatty, fatty-glandular, and dense glandular. Also it divided the abnormal classes into six kinds, which they are the calcifications, well-defined/circumscribed masses, spiculated masses, ill-defined masses, architectural distortion, and asymmetry. The file provided appropriate details about the abnormalities, i.e., type of cancer, severity of the diagnosis, center coordinates of location of the abnormality and radius (in pixel) of the circle enclosing the abnormality.

3.2 Region of Interest (ROI) Selection

Three regions containing the fatty, glandular and connective, and dense tissue were selected from the mammographic images. Extraction of these three types of normal tissues is included in order to identify the abnormal tissues. Every ROI is 40×40 pixels, because the tumor size range in this number of pixels, if it was increased or decreased more it will give an accurate result. Each of the pixels in the region are similar with respect to some characteristic or computed properly, such as color, intensity, or texture are significantly different with respect to the same characteristic. Fig 3.2 shows the ROIs that were selected from mammogram.

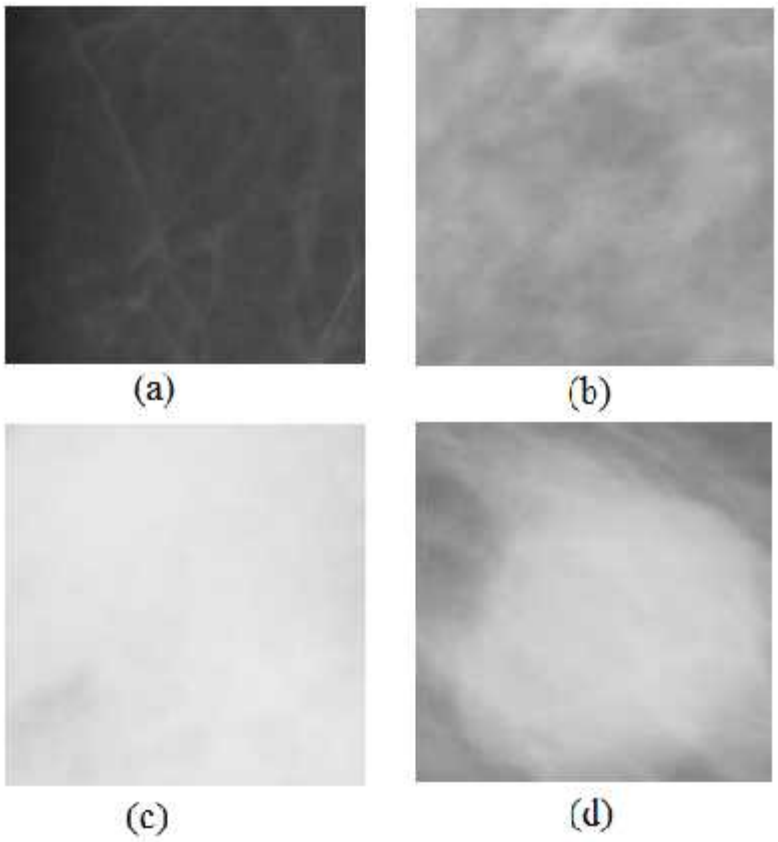

Fig 3.2: ROIs: (a) Fat, (b) Glandular and Connective, (c) Dense and (d) ROI with abnormal tissues.

3.3 Feature Extraction

It is the transforming of the input data into set of features that measure the difference characteristics of image segments. The definition of these features can describe the breast tissues by representing the texture of such region in order to distinct between different tissues.

In this dissertation various sets of features based on the wavelet decomposition technique were combined to obtain the best representation of the breast tissues:

- Texture descriptors from the Wavelet decomposition domain (from the decimated and the un-decimated discrete wavelet domain);

- Discrete wavelet decomposition on the co-occurrence matrix;
- Texture descriptors from the discrete wavelet decomposition combined with the Statistical texture descriptors from the co-occurrence matrix.

In this dissertation every technique algorithm was applied on 300 samples from the normal tissues of the breast, 100 for every tissue type (dense, glandular and connective, and fat tissue) and 100 abnormal ones, which are taken from Mini Mais Database.

3.3.1 The Wavelet Decomposition Techniques

The wavelet decomposition permits the decomposition of the image at different levels of resolution. It generates a total of four sub-band images HH, HL, LH and LL. The subband image LL is the approximation coefficient which corresponds to the lowest frequencies. HL, LH, HH contain the high level detail information of the image. These images contain different information and they may be processed individually using different algorithms.

In this dissertation two types of Wavelet Decomposition Techniques were used, the decimated discrete wavelets decomposition and the un-decimated discrete wavelet decomposition using the Symlet wavelet (sym2, sym4 and sym8) as a mother function. They decompose the ROIs into approximation and detail coefficients.

3.3.1.1 The Decimated Discrete Wavelet Decomposition (DDW) Technique

Firstly the decimated discrete wavelet decomposition using the sym2 level 3 was applied on the ROIs; it decomposed them into three levels. Every level produced approximation and detail coefficients. On the first algorithm the approximation coefficients of level one were extracted, the approximation coefficients of level two

were extracted in the second algorithm, and in the third one, the approximation coefficients of level three were extracted.

The fourth algorithm extracted the approximation coefficients of level three from the DDW decomposition using sym4 level 4. And the fifth one extracted the approximation coefficients of level four from the decimated discrete wavelet decomposition using sym4 level 4.

Another algorithm extracted the approximation coefficients of level three from the DDW decomposition using sym8 level 3.

3.3.1.2 The Un-Decimated Discrete Wavelet (UDDW) (Redundant Wavelet) Decomposition Technique

The un-decimated discrete wavelet decomposition was applied on the Region of Interests, using sym2 level three. It decomposed them into three levels. The approximation coefficients of level three were extracted.

Also the UDDW decomposition using sym8 level 3 was applied on the ROIs. It decomposed them into three levels. The approximation coefficients of level three were extracted.

Another algorithm using sym8 level four in the UDDW decomposition on the ROIs, it decomposes them into four levels. The approximation coefficients of level four were extracted.

3.3.2 The Spatial Gray Level Dependency (SGLD) Matrix Followed By the Un-Decimated Discrete Wavelet Decomposition Technique

On an independent algorithm the SGLD matrix with distance 1 and angles of 0°, was applied on the Region of Interests (ROIs). Then the un-decimated discrete wavelet

decomposition using symlet4 wavelet as a mother wavelet function level three was applied on the resultant matrix. It decomposed it into three levels. The approximation coefficients of level three were extracted.

3.3.3 Combination between the un-decimated discrete wavelet decomposition technique and the SGLD Matrix

This algorithm is a combination with two algorithms of the SGLD matrix and the un-decimated discrete wavelet decomposition (sym8 level three) algorithm. In the SGLD matrix algorithm, the SGLD matrix with distance 1 and angles of 0°, was applied on the ROIs. Then the Haralicks features were extracted from the resultant matrix. In the UDDW the ROIs were decomposed into three levels using sym8. Then the approximation coefficients of level three were extracted. Then the Haralick features were used to optimize them. The optimized features were combined with the optimized extracted features from SGLD matrix of the same ROI.

3.4 Feature Selection (Feature Optimization)

Feature selection is the process of selecting a subset of relevant features to use them in the classification. It chooses discriminating and independent features. It leads to the dimensionality reduction.

In this dissertation Haralick’s features were used to optimize or select the extracted features that were extracted in all algorithms.

3.5 Classification

In this dissertation the LDA was used to classify the three normal tissues and the abnormal one into four distinctive classes. It performed in two stages. Firstly; a stepwise procedure is performed to identify the suitable feature variables from all

the input features for the formulation of the discriminant function. It selects the features from the twelve Haralick's features (Entropy (EN), Energy (EG), Inertia (IN), inverse different moment (IDM), Correlation (CO), Variance (VA), Sum Average (SA), Sum Entropy (SE), Sum Variance (SV), Difference Average (DA), Difference Entropy (DE) and Difference Variance (DV)) that provides the maximum separation between the distributions of the discriminant scores for the four classes (the Dense, Glandular and connective, Fat and the abnormal class). Secondly, these selected features of the input cases were used to determine the coefficients of each feature variable in the discriminant function to achieve the maximum separation.

3.6 CAD Evaluation

The performance criteria can be limited to the detection of obvious cancers with a moderate sensitivity and a relative good specificity. These metrics are based on true/false, positives/negatives metrics. The sensitivity refers to how often the algorithm used reports that an abnormality exists in the instances where it actually exists, and is also called true positive fraction (TPF) [20]

$$Sensitivity = \frac{TP}{(TP + FN)} \qquad (3.1)$$

High values of sensitivity imply minimal false negative detection.

On the other hand, specificity refers to how frequently the algorithm correctly reports normal when no abnormal exists, and False Positive Fraction (FPF) is the same as specificity. The specificity of the test is the fraction of the true negative cases over the real negative cases [20]

$$Specificity = \frac{TN}{(TN + FP)} \tag{3.2}$$

High values of specificity imply minimal false positive detection.

3.7 The Proposed Algorithm

The proposed algorithm was shown in Fig 3.3. Firstly input the mammogram image. Then select a ROI (40×40 pixels). Secondly extract the features from the ROI using the combination method. Lastly classify them into Dense, Glandular and connective, Fat, and abnormal tissue using the LDA. The coefficients of the selected features that have the maximum ability to discriminate between the classes were used in the proposed algorithm in order to detect the abnormality in the breast.

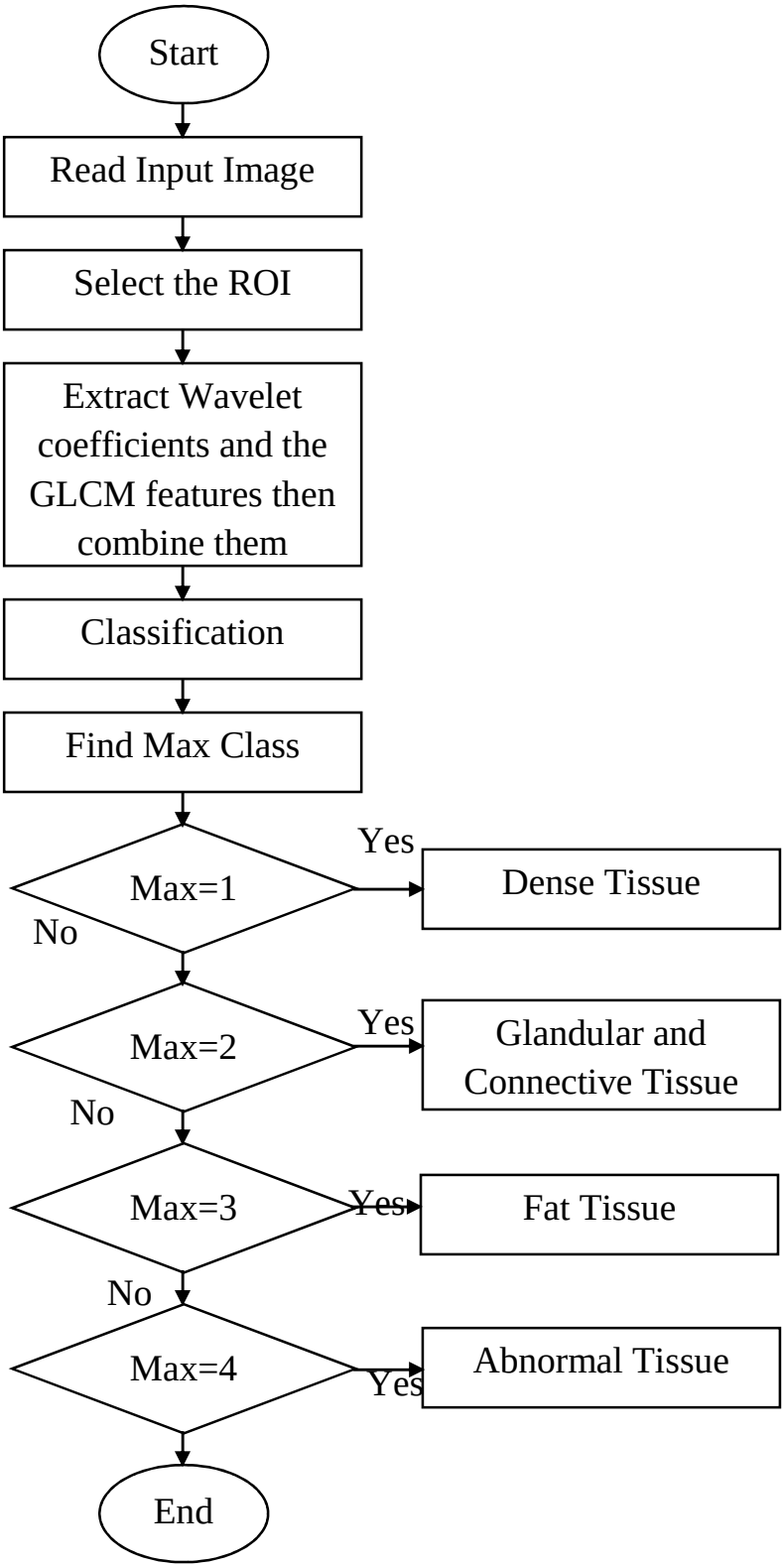

Fig 3.3: The proposed algorithm for detection of breast abnormality.

Chapter Four

Results and Discussion

4.1 Results

This Chapter presents the results which obtained from all steps that were explained in the methodology. The main objective of this dissertation is to detect the abnormal tissue in the breast. So firstly it is important to distinguish between the normal tissues (which they were classified into fat tissue, glandular and connective tissue, and dense tissue) and abnormal one. Different sets of proposed combination techniques were used, in order to obtain the best accuracy in breast abnormality detection. Every technique algorithm was applied on 300 samples from the normal tissues of the breast (100 for every tissue type) and 100 abnormal ones, which are taken from Mini Mais Database. Sensitivity and Specificity performance criterion have been calculated to assess the efficiency of CAD system used.

4.1.1 Wavelet Decomposition Technique

On investigation of the wavelet decomposition technique which achieved the best result in the classification, two types of wavelet decomposition techniques were used, the decimated discrete wavelet and the un-decimated discrete wavelet decomposition technique. On both techniques symlet wavelet was used as the mother wavelet function.

4.1.1.1 The Decimated Discrete Wavelet Decomposition Technique

The decimated discrete wavelet decomposition was applied on the Region of Interest (ROI) samples, using symlet wavelet as a mother wavelet function (sym2, sym4 and sym8) level four. It decomposed them into four levels. Every level produced approximation and detail coefficients. The approximation coefficients of each level were extracted. Then the Haralick features were used on the extracted coefficients at every time, to optimize them. Then the calculated features were used in the classification process.

4.1.1.1.1 Level one approximation coefficients extraction (sym2)

Table 4.1 illustrates the classification accuracy of the proposed algorithm which extracted Level one approximation coefficients, to use them in the classification of the four classes (Fat, Glandular, Dense and abnormal tissue). The diagonal elements denote the correct classifications and the off-diagonal elements show the misclassification made by the classifier. The accuracies for classifying the dense, fat, glandular and abnormal tissues are 95.0%, 76.0%, 57.0%, and 85% respectively. The overall classification accuracy for detecting these tissues is 78.3% of original grouped cases correctly classified. The scatter plot of the four classes was shown on Fig 4.1.

Table 4.1: The classification results of the discrete wavelet decomposition level1

Class		Predicted Group Membership				Total
		Fat	Glandular	Dense	Abnormal	
%	Fat	76.0	19.0	5.0	.0	100.0
	Glandular	37.0	57.0	.0	6.0	100.0
	Dense	5.0	.0	95.0	.0	100.0
	Abnormal	.0	15.0	.0	85.0	100.0

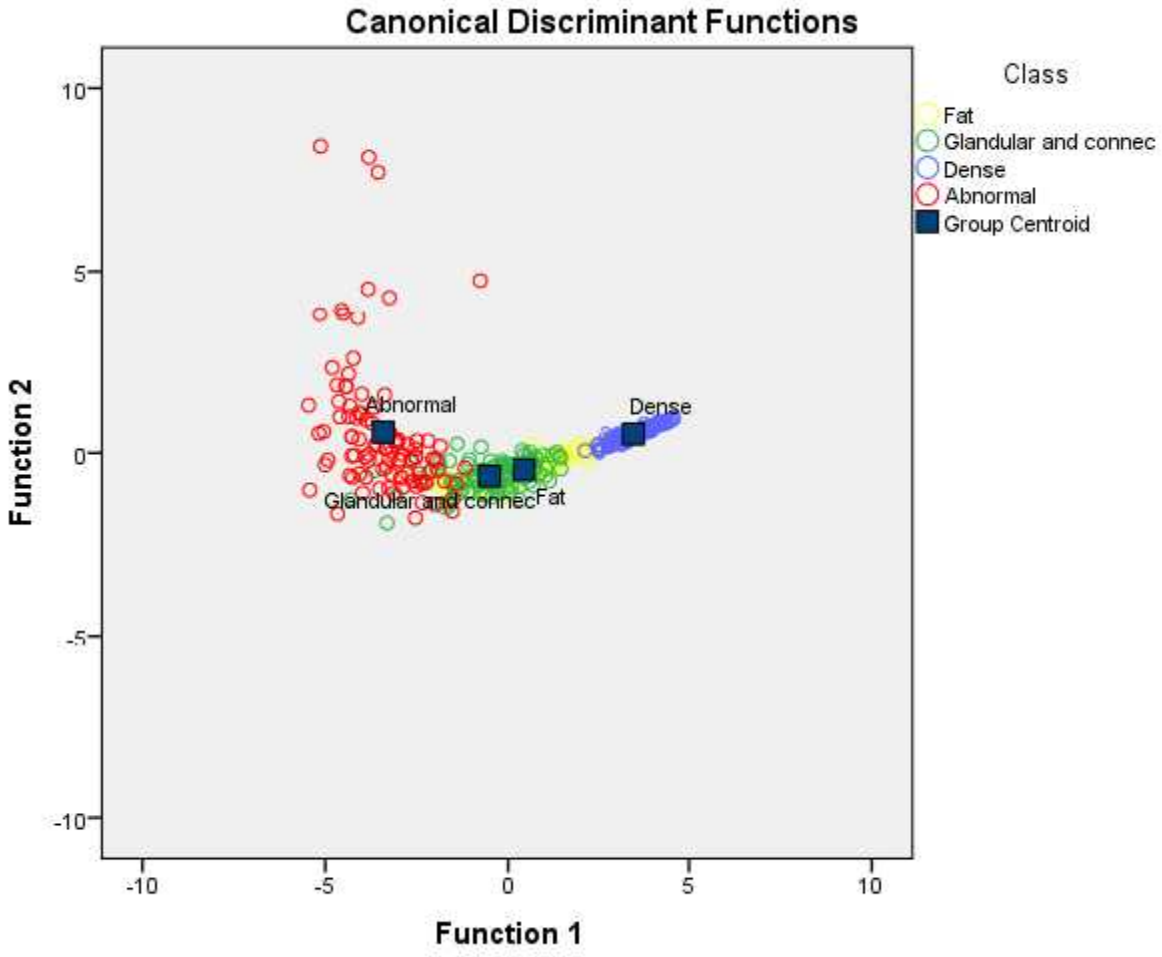

Fig 4.1: The scatter plot of the four classes which classified using discrete wavelet decomposition level 1 approximation coefficients (sym2).

4.1.1.1.2 Level two approximation coefficients extraction (sym2)

Table 4.2 illustrates the classification accuracy of the proposed algorithm which extracted Level two approximation coefficients, to use them in the classification of the four classes. This method achieved 78.3% of original grouped cases correctly classified. The scatter plot of the four classes was shown on Fig 4.2.

Table 4.2: The classification results of the discrete wavelet decomposition level2

Class		Predicted Group Membership				Total
		Fat	Glandular	Dense	Abnormal	
%	Fat	76.0	18.0	6.0	.0	100.0
	Glandular	39.0	58.0	.0	3.0	100.0
	Dense	5.0	.0	95.0	.0	100.0
	Abnormal	1.0	15.0	.0	84.0	100.0

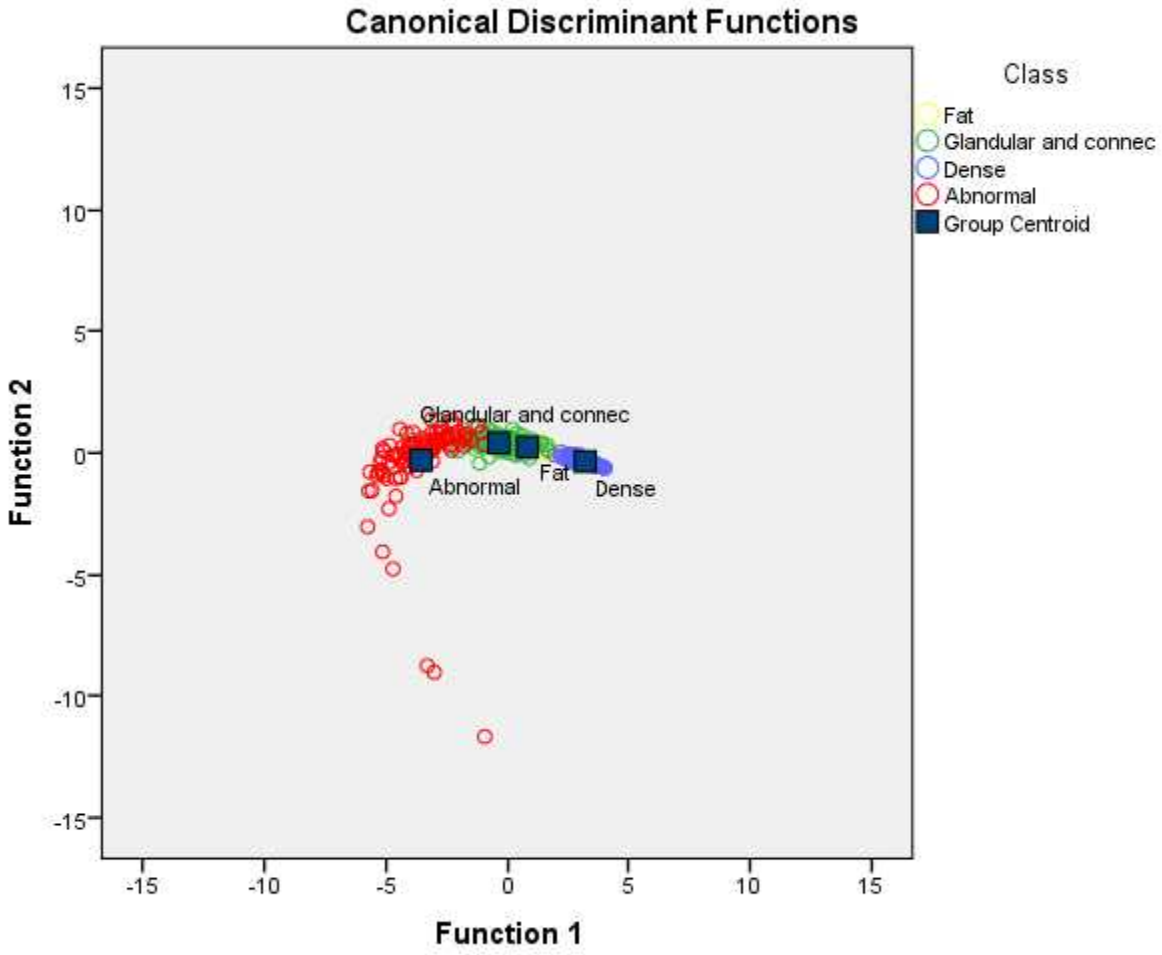

Fig 4.2: The scatter plot of the four classes which classified using discrete wavelet decomposition level 2 approximation coefficients (sym2).

4.1.1.1.3 Level three approximation coefficients extraction (sym2)

Table 4.3 illustrates the classification accuracy of the proposed algorithm which extracted Level three approximation coefficients, to use them in the classification of the four classes. This method achieved 76.8% of original grouped cases correctly classified. The scatter plot of the four classes was shown on Fig 4.3.

Table 4.3: The classification results of the discrete wavelet decomposition level3

	Class	Predicted Group Membership				Total
		Fat	Glandular	Dense	Abnormal	
%	Fat	67.0	21.0	12.0	.0	100.0
	Glandular	34.0	60.0	2.0	4.0	100.0
	Dense	7.0	.0	93.0	.0	100.0
	Abnormal	.0	13.0	.0	87.0	100.0

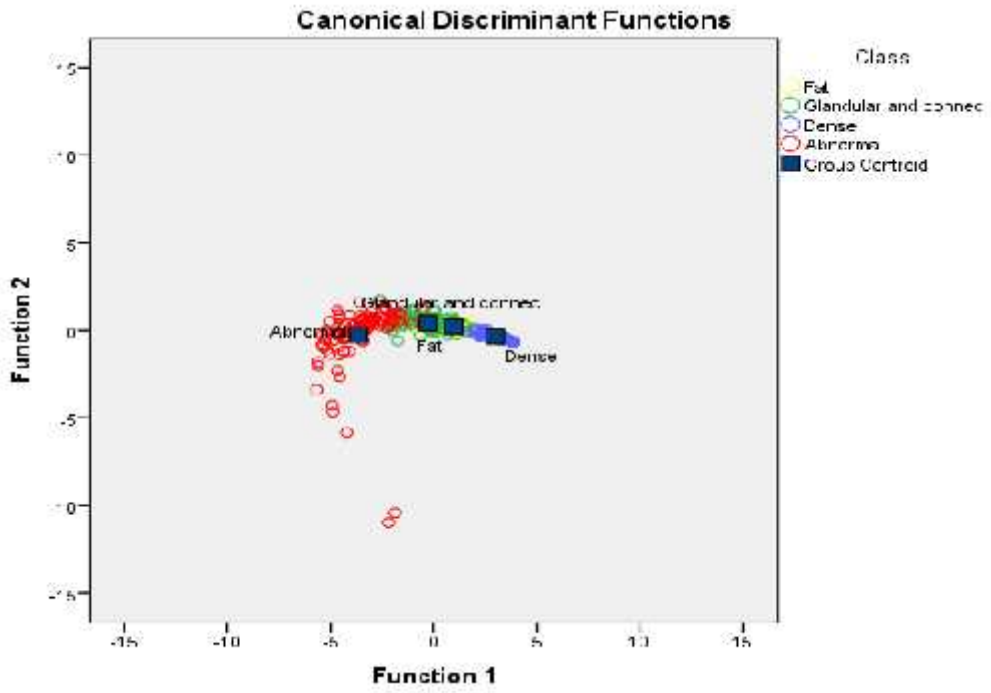

Fig 4.3: The scatter plot of the four classes which classified using discrete wavelet decomposition level 3 approximation coefficients (sym2).

4.1.1.1.4 Level three approximation coefficients extraction (sym4)

Table 4.4 illustrates the classification accuracy of the proposed algorithm which extracted Level three approximation coefficients, to use them in the classification of the four classes. This method achieved 96.8% of original grouped cases correctly classified.

Table 4.4: The classification results of the discrete wavelet decomposition level3

	Class	Predicted Group Membership				Total
		Dense	Glandular	Fat	Abnormal	
%	Dense	100.0	.0	.0	.0	100.0
	Glandular	.0	97.0	.0	3.0	100.0
	Fat	.0	.0	100.0	.0	100.0

	Abnormal	.0	10.0	.0	90.0	100.0

4.1.1.1.5 Level four approximation coefficients extraction (sym4)

Table 4.5 illustrates the classification accuracy of the proposed algorithm which extracted Level four approximation coefficients, to use them in the classification of the four classes. This method achieved 94.5% of original grouped cases correctly classified. The scatter plot of the four classes was shown on Fig 4.4.

Table 4.5: The classification results of the discrete wavelet decomposition level4

Class		Predicted Group Membership				Total
		Dense	Glandular	Fat	Abnormal	
%	Dense	98.0	.0	.0	2.0	100.0
	Glandular	.0	86.0	.0	14.0	100.0
	Fat	.0	.0	100.0	.0	100.0
	Abnormal	2.0	4.0	.0	94.0	100.0

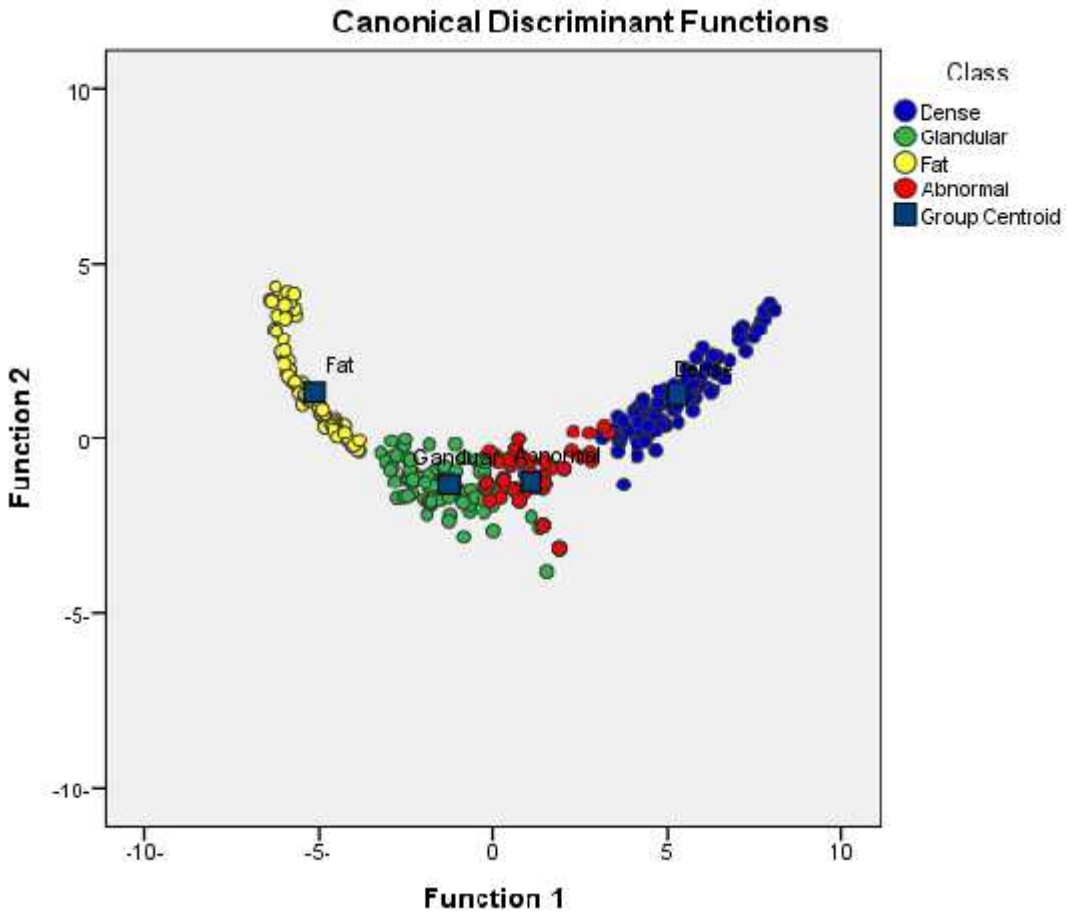

Fig 4.4: The scatter plot of the four classes which classified using discrete wavelet decomposition level 4 approximation coefficients (sym4).

4.1.1.1.6 Level three approximation coefficients extraction (sym8)

Table 4.6 illustrates the classification accuracy of the proposed algorithm which extracted Level three approximation coefficients, to use them in the classification of the four classes. This method achieved 82.5% of original grouped cases correctly classified. The scatter plot of the four classes was shown on Fig 4.5.

Table 4.6: The classification results of the discrete wavelet level 4

Class		Predicted Group Membership				Total
		Dense	Glandular	Fat	abnormal	
%	Dense	95.0	.0	.0	5.0	100.0
	Glandular	.0	73.0	.0	27.0	100.0
	Fat	.0	4.0	96.0	.0	100.0
	Abnormal	.0	33.0	1.0	66.0	100.0

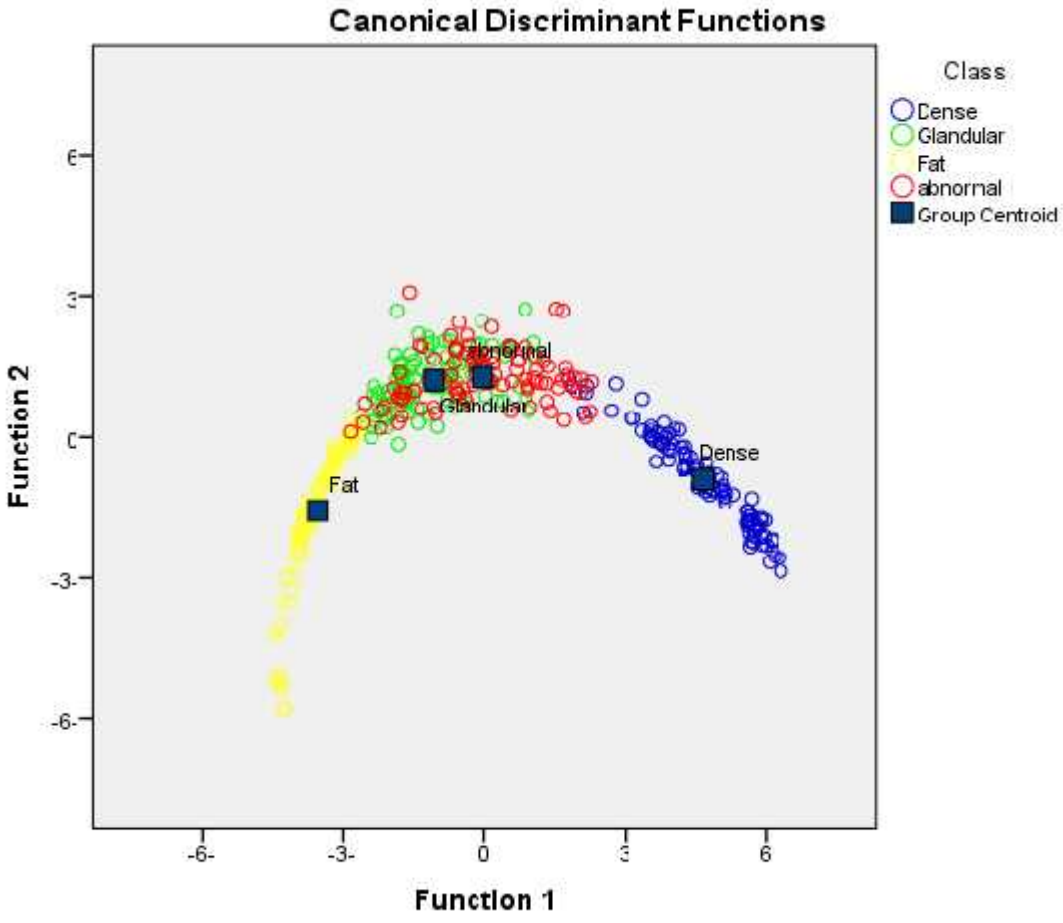

Fig 4.5: The scatter plot of the four classes which classified using discrete wavelet decomposition level 3 approximation coefficients (sym8).

4.1.1.2 The Un-Decimated Discrete Wavelet (Redundant Wavelet) Decomposition Technique

The un-decimated discrete wavelet decomposition was applied on the Region of Interest (ROI) samples, using symlet wavelet as a mother wavelet function. Every level produced approximation and detail coefficients. The approximation coefficients were extracted. Then the Haralick features were used on the extracted coefficients, to optimize them. Then the calculated features were used in the classification process.

4.1.1.2.1 The Un-Decimated Discrete Wavelet Decomposition using sym2

The un-decimated discrete wavelet decomposition was applied on the Region of Interests, using sym2 level three. It decomposed them into three levels. The approximation coefficients of level three were extracted. Then the Haralick features were used to optimize the extracted coefficients. Then the calculated features were used in the classification process. Table 4.7 illustrates the classification accuracy of the proposed algorithm. This method achieved 77.0% of original grouped cases correctly classified. The scatter plot of the four classes was shown on Fig 4.6.

Table 4.7: The classification results of the un-decimated discrete wavelet decomposition sym2 level 3.

Class		Predicted Group Membership				Total
		Fat	Glandular	Dense	Abnormal	
%	Fat	76.0	19.0	5.0	.0	100.0
	Glandular	42.0	54.0	.0	4.0	100.0
	Dense	3.0	.0	97.0	.0	100.0
	Abnormal	3.0	16.0	.0	81.0	100.0

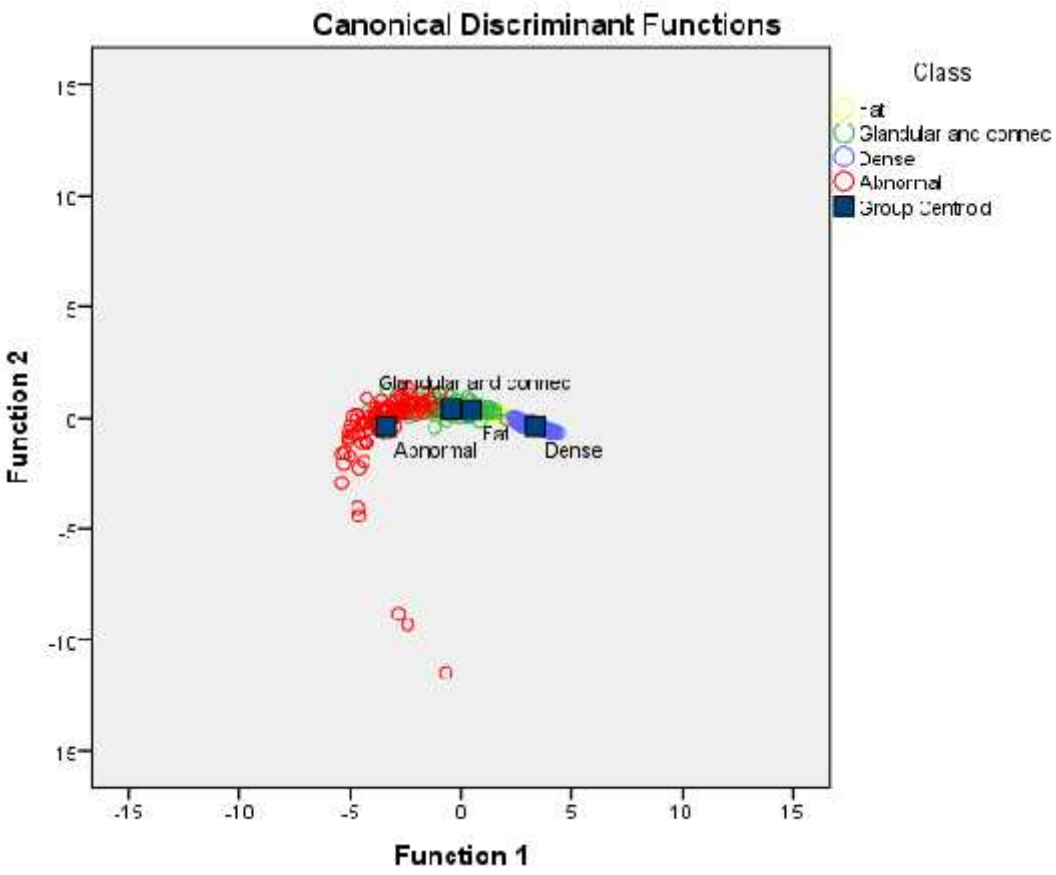

Fig 4.6: The scatter plot of the four classes which classified using the un-decimated discrete wavelet (sym2 level 3).

4.1.1.2.2 The Un-Decimated Discrete Wavelet Decomposition using sym8

The un-decimated discrete wavelet decomposition was applied on the Region of Interests, using sym8 level four. It decomposed them into four levels. The approximation coefficients of level four were extracted. Then the Haralick features were used to optimize the extracted coefficients. Then the calculated features were used in the classification process. Table 4.8 illustrates the classification accuracy of the proposed algorithm. This method achieved 91.8% of original grouped cases correctly classified. The scatter plot of the four classes was shown on Fig 4.7.

Table 4.8: The classification results of the un-decimated discrete wavelet decomposition sym8 level 3.

	class	Predicted Group Membership				Total
		Dense	Glandular	Fat	Abnormal	
%	Dense	100.0	.0	.0	.0	100.0
	Glandular	.0	90.0	.0	10.0	100.0
	Fat	.0	.0	100.0	.0	100.0
	Abnormal	4.0	16.0	3.0	77.0	100.0

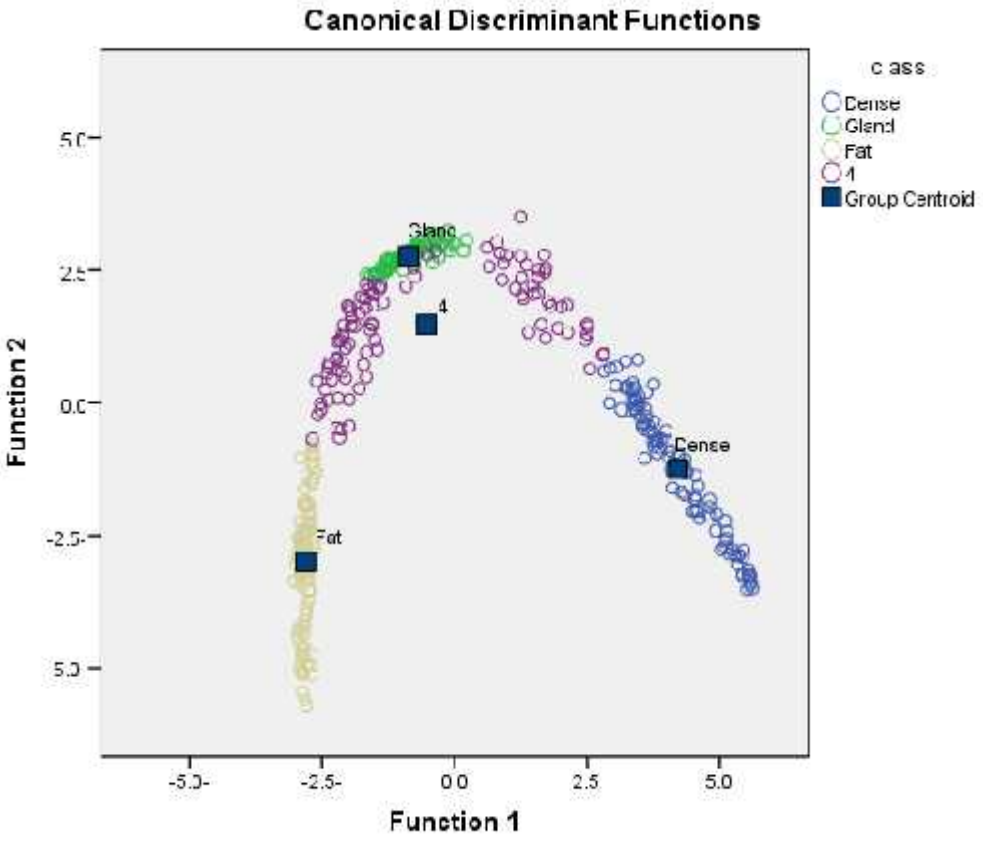

Fig 4.7: The scatter plot of the four classes which classified using the un-decimated discrete wavelet (sym8 level 3).

4.1.1.2.3 The Un-Decimated Discrete Wavelet Decomposition using sym8

The un-decimated discrete wavelet decomposition was applied on the Region of Interests, using sym8 level three. It decomposed them into three levels. The approximation coefficients of level three were extracted. Then the Haralick features were used to optimize the extracted coefficients. Then the calculated features were used in the classification process. Table 4.9 illustrates the classification accuracy of the proposed algorithm. This method achieved 91.0% of original grouped cases correctly classified. The scatter plot of the four classes was shown on Fig 4.8.

Table 4.9: The classification results of the un-decimated discrete wavelet decomposition sym8

class		Predicted Group Membership				Total
		Dense	Glandular	Fat	Abnormal	
%	Dense	100.0	.0	.0	.0	100.0
	Gland	.0	89.0	.0	11.0	100.0
	Fat	.0	.0	100.0	.0	100.0
	Abnormal	5.0	17.0	3.0	75.0	100.0

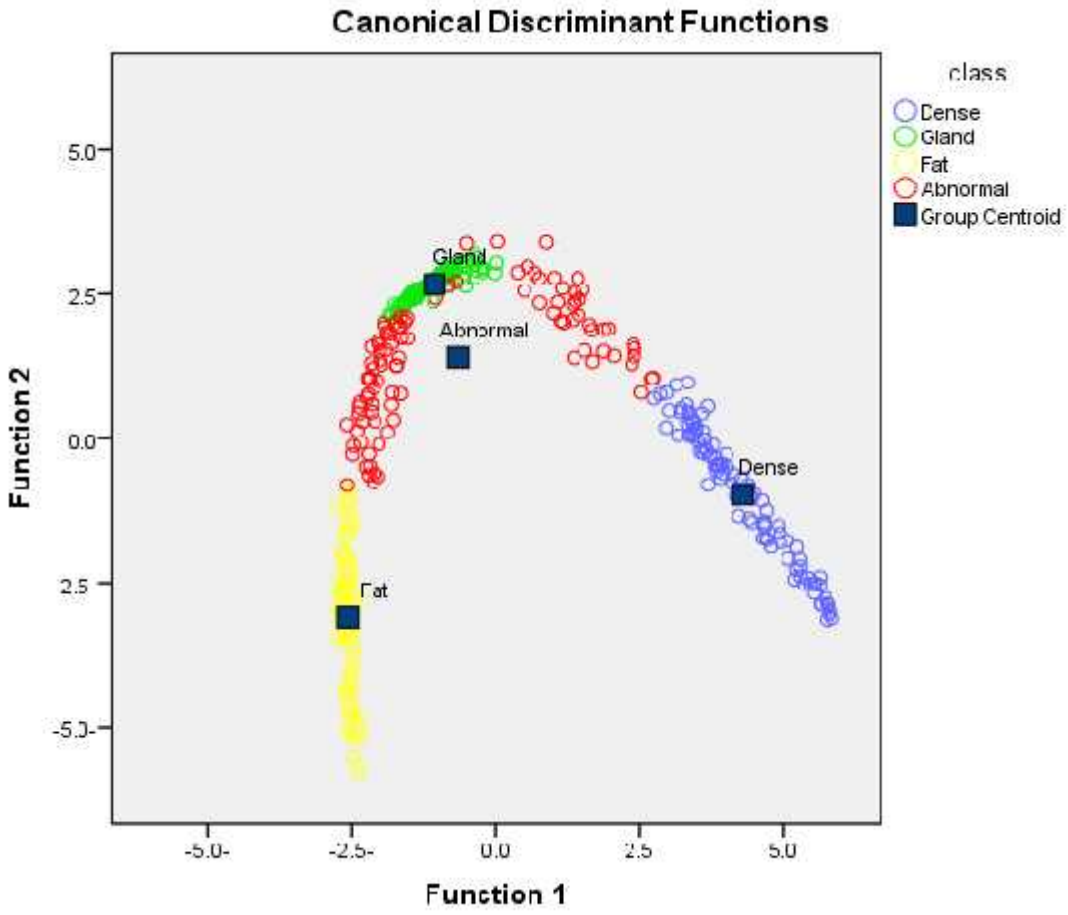

Fig 4.8: The scatter plot of the four classes which classified using the un-decimated discrete wavelet (sym8 level 4).

4.1.2.1 The Spatial Gray Level Dependency (SGLD) Matrix Followed By the Un-Decimated Discrete Wavelet Decomposition Technique

The SGLD matrix was applied on the Region of Interests (ROIs). Then the un-decimated discrete wavelet decomposition using sym4 wavelet as a mother wavelet function level three was applied on the resultant matrix. It decomposed it into three levels. The approximation coefficients of level three were extracted. Then the Haralick features were used on the extracted coefficients to optimize them. Then the calculated features were used in the classification process. Table 4.10 illustrates the

classification accuracy of the proposed algorithm. This method achieved 94.5% of original grouped cases correctly classified. The scatter plot of the four classes was shown on Fig 4.9.

Table 4.10: The classification results of the SGLD Matrix Followed By the Un-Decimated Discrete Wavelet Decomposition

Class		Predicted Group Membership				Total
		Dense	Glandular	Fat	Abnormal	
%	Dense	100.0	.0	.0	.0	100.0
	Glandular	.0	91.0	1.0	8.0	100.0
	Fat	.0	.0	100.0	.0	100.0
	Abnormal	3.0	10.0	.0	87.0	100.0

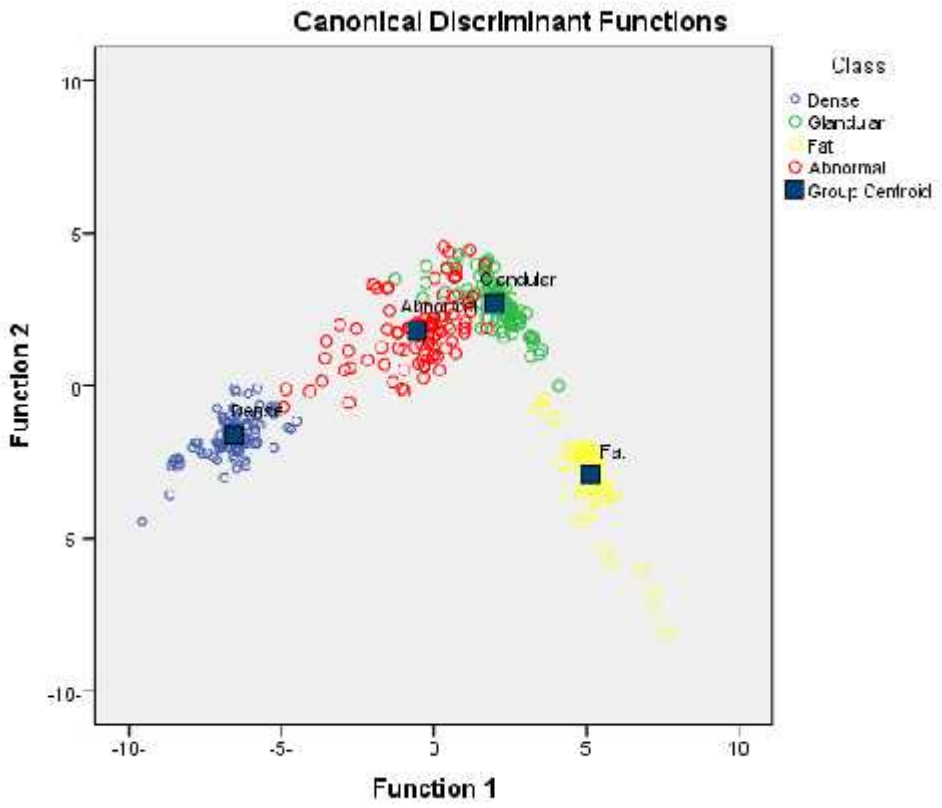

Fig 4.9: The scatter plot of the four classes which classified using the SGLD matrix followed by the un-decimated discrete wavelet Decomposition Technique (sym4 level 3).

4.1.2.2 The Spatial Gray Level Dependency (SGLD) Matrix Followed By the Decimated Discrete Wavelet Decomposition Technique

The SGLD matrix was applied on the Region of Interests (ROIs). Then the decimated discrete wavelet decomposition using sym4 wavelet as a mother wavelet function level three was applied on the resultant matrix. It decomposed it into three levels. The approximation coefficients of level three were extracted. Then the Haralick features were used on the extracted coefficients to optimize them. Then the calculated features were used in the classification process. This method achieved 87.5% of original grouped cases correctly classified.

4.1.3 Combination between the un-decimated discrete wavelet decomposition technique and the SGLD Matrix

In this steb the un-decimated discrete wavelet decomposition (sym8 level three) optimized features were combined with the optimized extracted features from SGLD matrix of the same ROI. Then the calculated features were used in the classification process. Table 4.11 illustrates the classification accuracy of the proposed algorithm. This method achieved 98.3% of original grouped cases correctly classified. The accuracies for detecting the dense, glandular, fat and abnormal tissues are 100%, 100%, 100% and 93% respectively. The scatter plot of the four classes was shown on Fig 4.10.

Table 4.11: The classification results of the Combination between the un-decimated discrete wavelet decomposition and the SGLD Matrix

Class		Predicted Group Membership				Total
		Dense	Glandular	Fat	Abnormal	
%	Dense	100.0	.0	.0	.0	100.0
	Glandular	.0	100.0	.0	.0	100.0
	Fat	.0	.0	100.0	.0	100.0
	Abnormal	1.0	4.0	.0	95.0	100.0

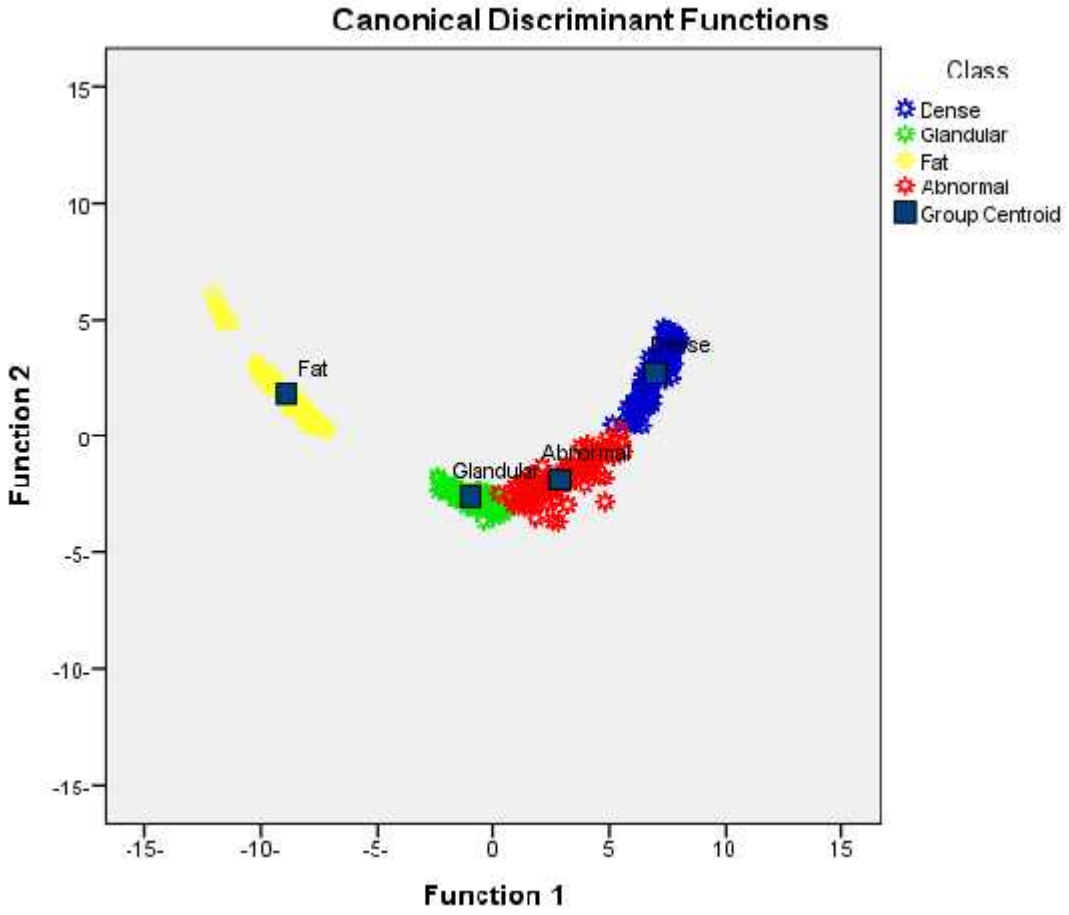

Fig 4.10: The scatter plot of the four classes (Dense, Glandular, Fat and abnormal) which classified using combination between the un-decimated discrete wavelet decomposition and the SGLD Matrix.

The comparison of the result accuracies of the breast tissues classification using different sets of proposed combination techniques were shown on table 4.12.

Table 4.12: The accuracies of the proposed combination techniques

No	The Proposed Combination Technique	Normal (%)			Abnormal (%)	Sensitivity (%)	Specificity (%)	Accuracy (%)
		D	G	F				
1	DDWD sym2 L1	95.0	57.0	76.0	85.0	85.0	76.0	78.3
2	DDWD sym2 L2	95.0	58.0	76.0	84.0	84.0	76.3	78.3
3	DDWD sym2 L3	93.0	60.0	67.0	87.0	87.0	73.3	76.8
4	DDWD sym4 L3	100.0	97.0	100.0	90.0	90.0	99.0	96.8
5	DDWD sym4 L4	98.0	86.0	100.0	94.0	94.0	94.6	94.5
6	DDWD sym8 L3	95.0	73.0	96.0	66.0	66.0	88.0	82.5
7	UDDWD sym2 L3	97.0	54.0	76.0	81.0	81.0	75.6	77.0
8	UDDWD sym8 L4	100.0	89.0	100.0	75.0	75.0	96.3	91.0
9	UDDWD sym8 L3	100.0	90.0	100.0	77.0	77.0	96.6	91.8
10	SGLD+DDWD sym4 L3	100.0	77.0	100.0	73.0	73.0	92.3	87.5
11	SGLD+UDDWD sym4 L3	100.0	91.0	100.0	87.0	87.0	97.0	94.5

12	Comb of UDDWD sym8 L3 + SGLD	100.0	100.0	100.0	95.0	95.0	100.0	98.8

Where: DDWD is the Decimated Discrete Wavelet Decomposition.

UDDWD is the Un-Decimated Discrete Wavelet Decomposition.

L is the Level. D is Dense. G is Glandular. F is Fat.

From table 4.12 the combination between the un-decimated discrete wavelet decomposition technique and the SGLD Matrix method achieved the best result, so it had been used to build the algorithm for the detection of breast abnormality. The twelve Haralick features that were used in the combination method to optimize the features in order to classify the breast tissues (dense, glandular, fat and abnormal) were shown independently on Figs (4.11 to 4.22) to see which one was able to discriminate between the four classes. As shown in Figs (4.11 to 4.14 and 4.16 to 4.22) eleven out of the twelve Haralick features were able to discriminate between these classes, which they are (Entropy (EN), Energy (EG), Inertia (IN), inverse different moment (IDM), Variance (VA), Sum Average (SA), Sum Entropy (SE), Sum Variance (SV), Difference Average (DA), Difference Entropy (DE) and Difference Variance (DV)), so the Correlation (CO) (Fig 4.15) was not able to discriminate between these classes.

The stepwise discriminant procedure was used to select the best features that can do this classification. The entire data set of 300 normal ROIs and 100 abnormal ROIs was used as input cases, so that the statistical properties of the feature variables could be more reliably determined.

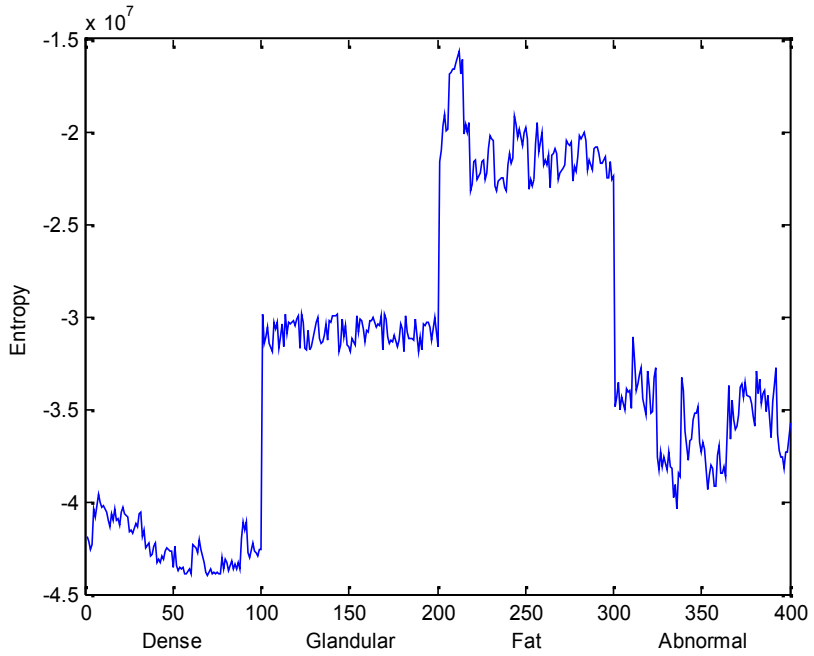

Fig 4.11: Entropy versus classes using the un-decimated discrete wavelet decomposition + the SGLD matrix.

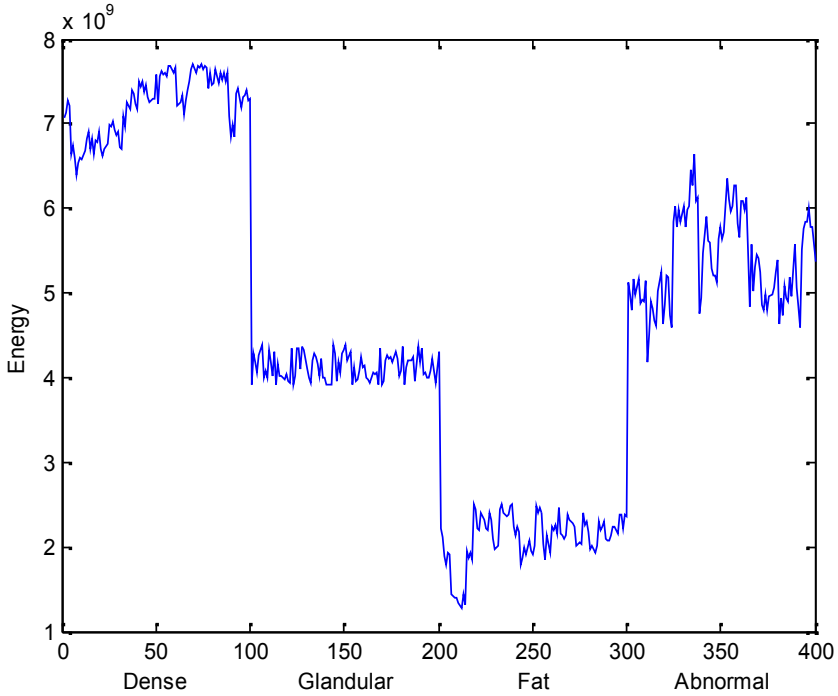

Fig 4.12: Energy versus classes using the un-decimated discrete wavelet decomposition + the SGLD matrix.

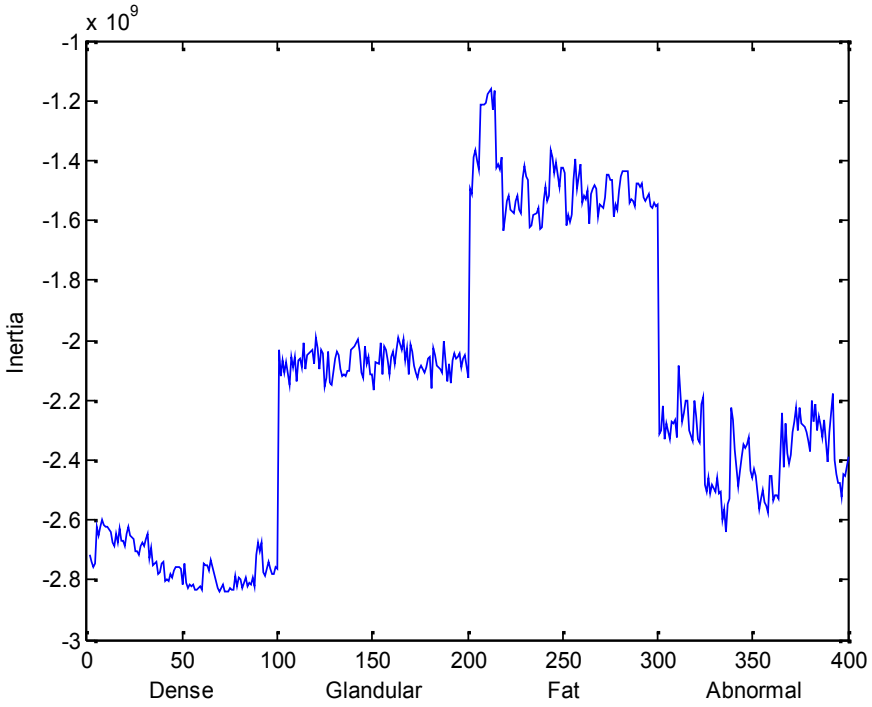

Fig 4.13: Inertia versus classes using the un-decimated discrete wavelet decomposition + the SGLD matrix.

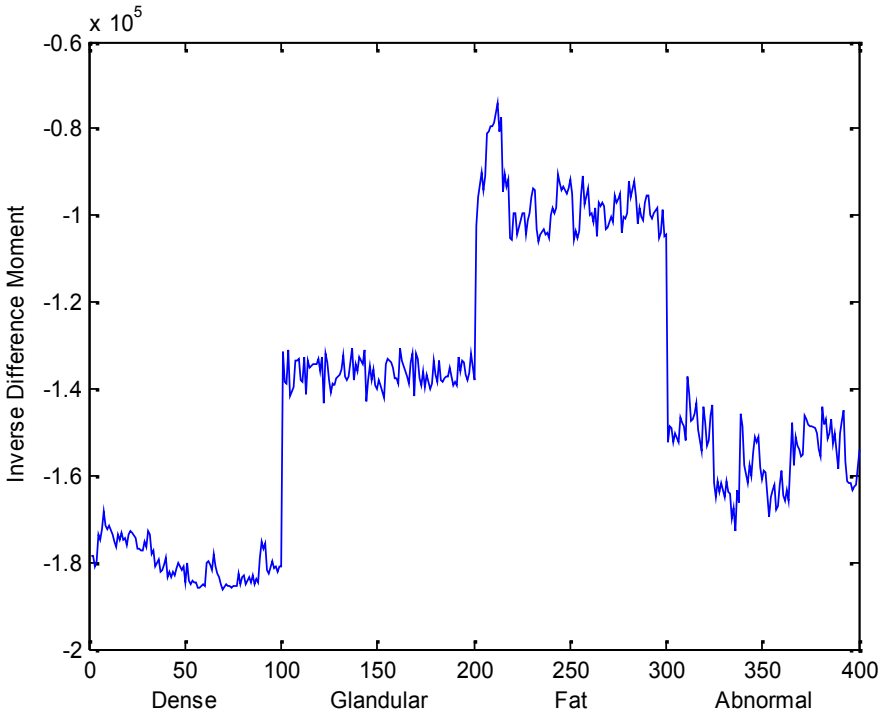

Fig 4.14: Inverse Difference Moment versus classes using the un-decimated discrete wavelet decomposition + the SGLD matrix.

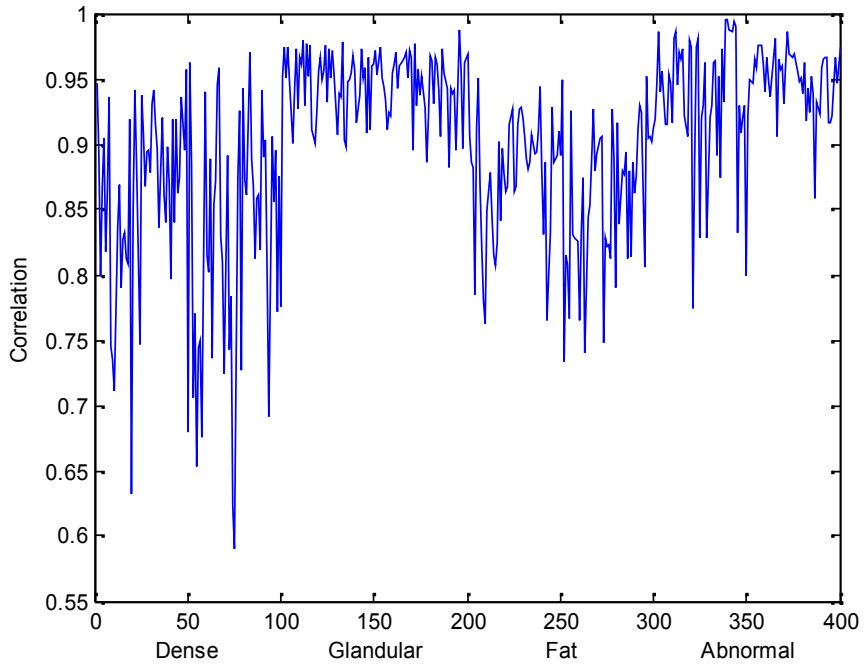

Fig 4.15: Correlation versus classes using the un-decimated discrete wavelet decomposition + the SGLD matrix.

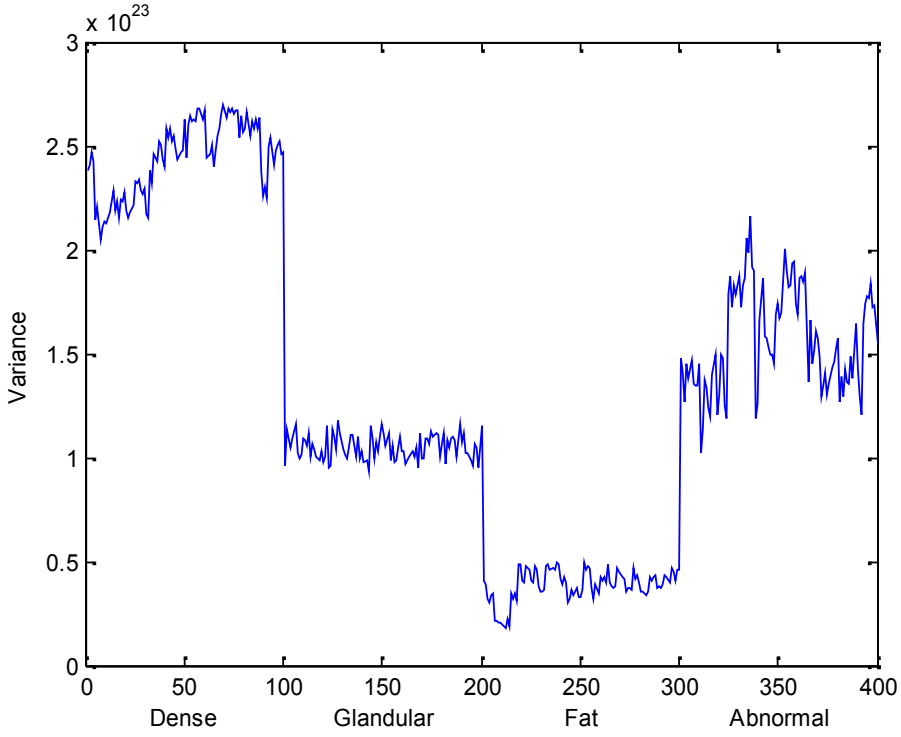

Fig 4.16: Variance versus classes using the un-decimated discrete wavelet decomposition + the SGLD matrix.

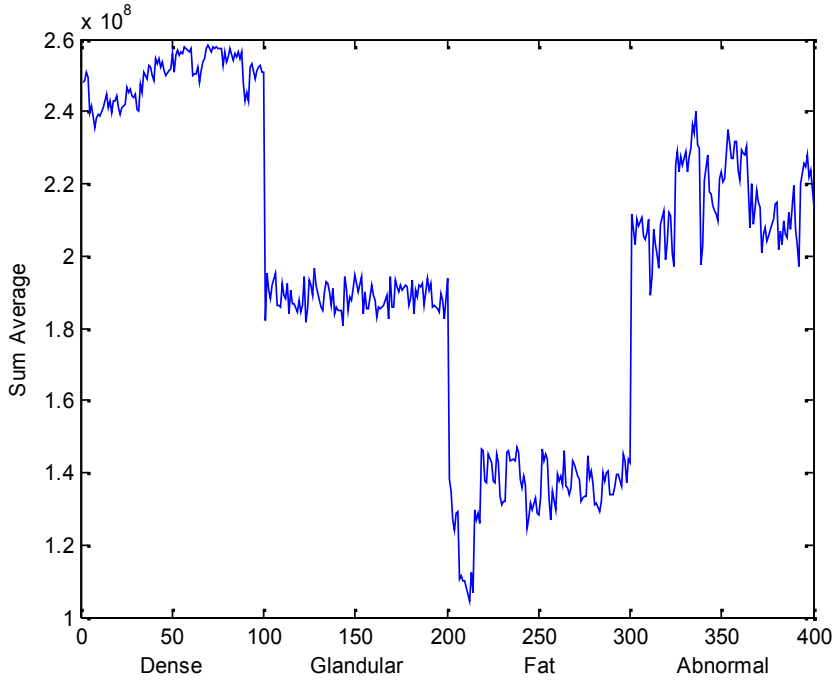

Fig 4.17: Sum Average versus classes using the un-decimated discrete wavelet decomposition + the SGLD matrix.

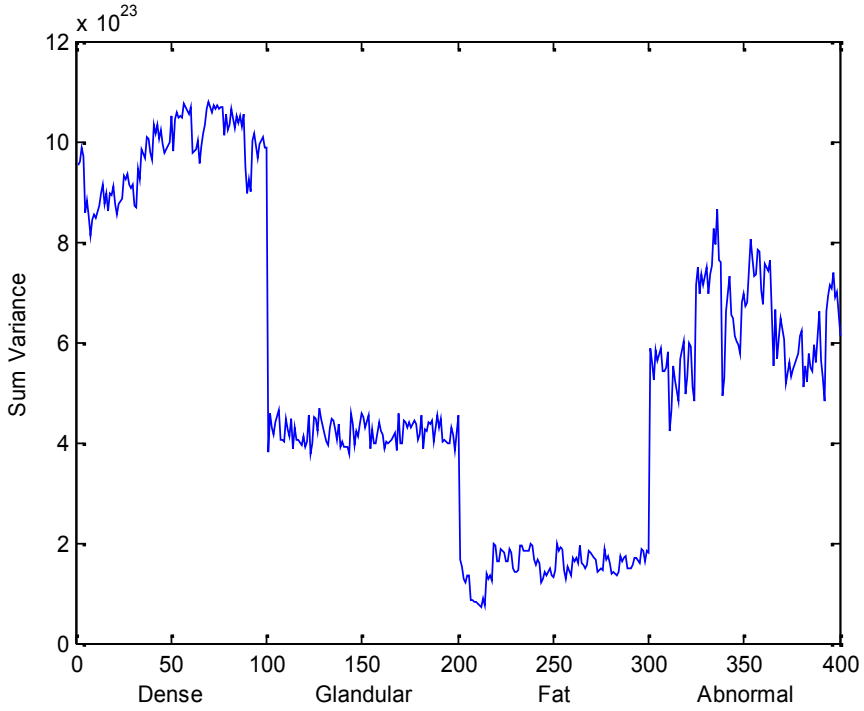

Fig 4.18: Sum Variance versus classes using the un-decimated discrete wavelet decomposition + the SGLD matrix.

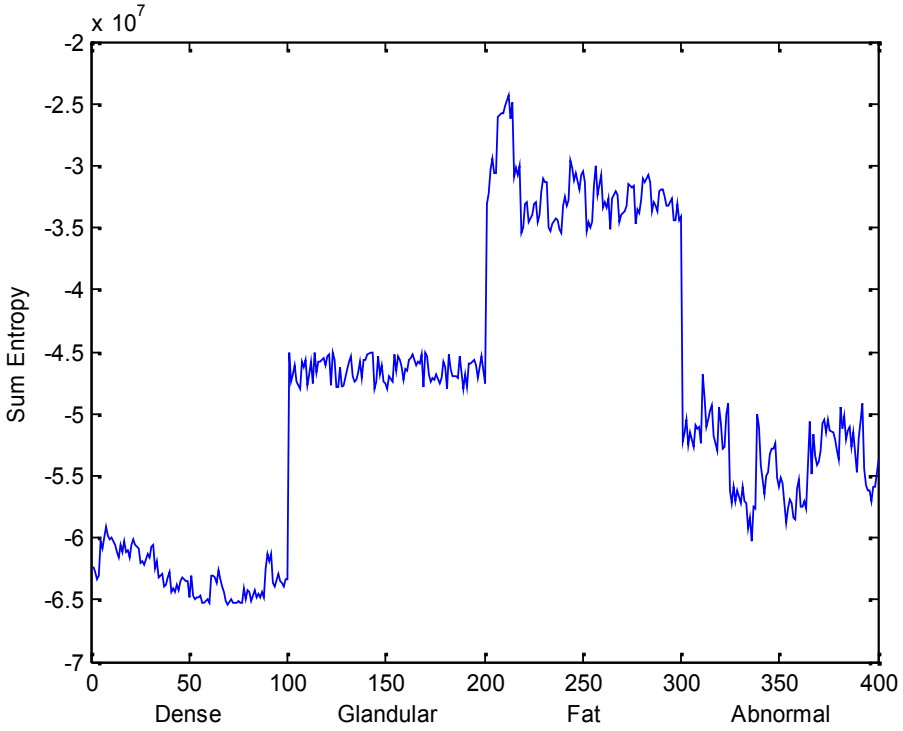

Fig 4.19: Sum Entropy versus classes using the un-decimated discrete wavelet decomposition + the SGLD matrix.

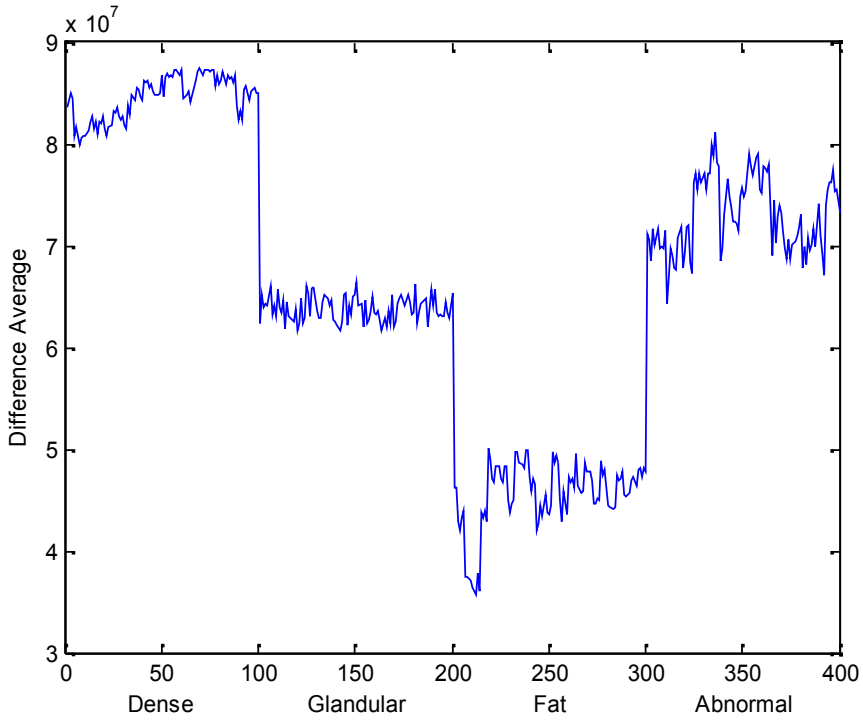

Fig 4.20: Difference Average versus classes using the un-decimated discrete wavelet decomposition + the SGLD matrix.

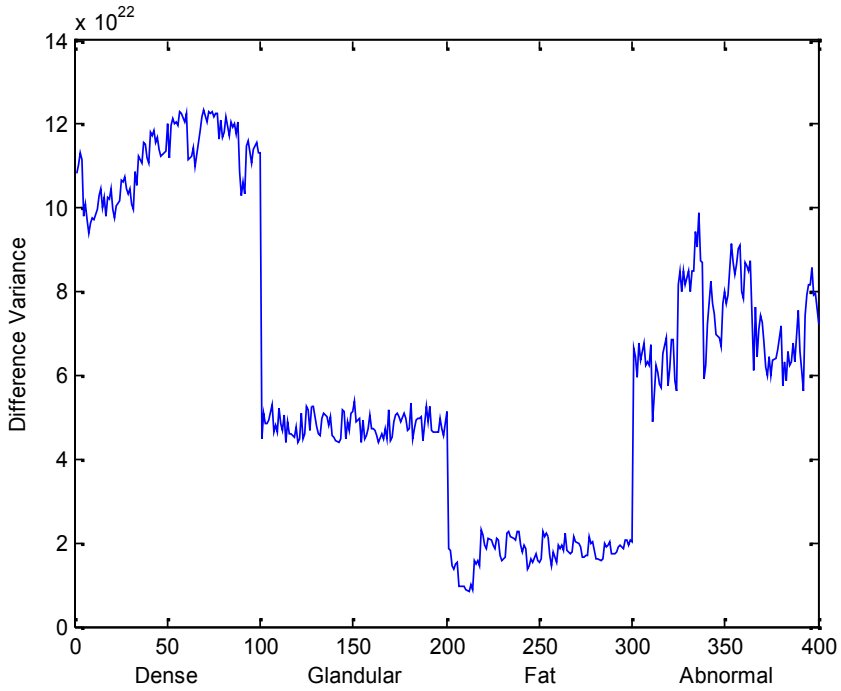

Fig 4.21: Difference Variance versus classes using the un-decimated discrete wavelet decomposition + the SGLD matrix.

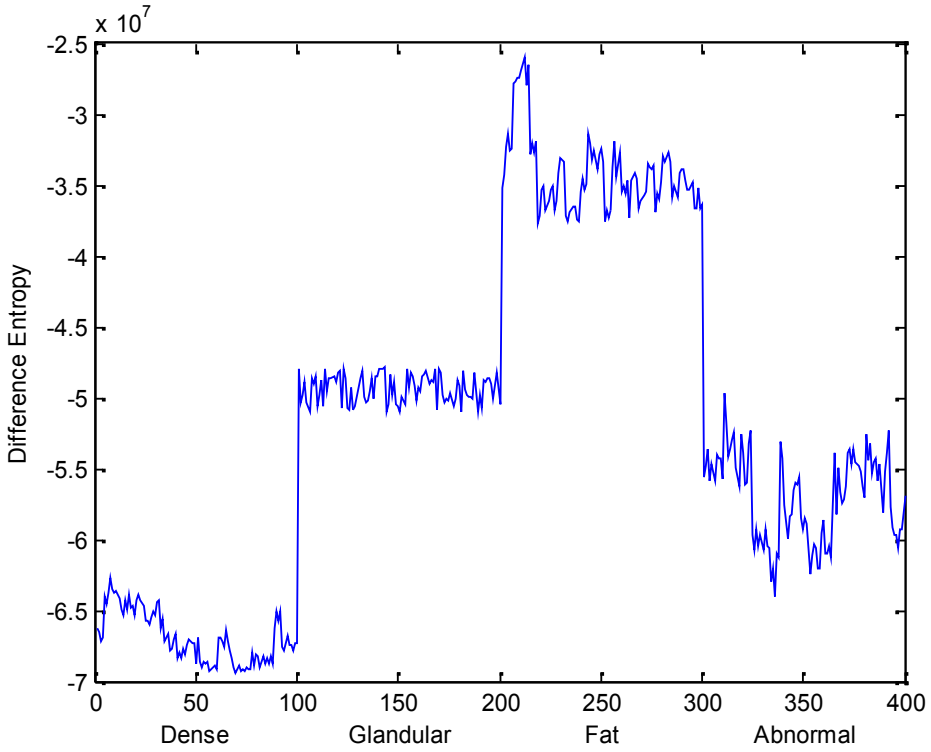

Fig 4.22: Difference Entropy versus classes using the un-decimated discrete wavelet decomposition + the SGLD matrix.

The stepwise discriminant analysis selected four features for the formulation of the discriminant function in order to discriminate between the classes. They are the Energy (EG), Variance (VA), Sum Variance (SV) and the Difference Variance (DV). It selected them because they achieved the best seperation between the classes. The selected features were used to determine the coefficients of each feature variable in the discriminant function to accomplish the maximum separation. The Classification function coefficients of these features illustrated in table 4.13. The detection is done based on this discriminant functions.

Table 4.13: The Classification Function Coefficients Generated by The Fisher's linear discriminant functions

Coefficients	Class			
	Dense	Glandular	Fat	Abnormal
EG	-1.955E-006	-2.059E-006	-2.259E-006	-1.975E-006
VA	-1.304E-020	-1.363E-020	-1.349E-020	-1.368E-020
SA	4.957E-005	5.200E-005	5.376E-005	5.058E-005
DV	7.581E-020	7.837E-020	8.544E-020	7.626E-020
(Constant)	-1784.197	-1829.454	-1734.770	-1812.309

4.2 Discussions

Based on the literature reviews (Pelin Gorgel, et al. 2013), (Nizar Ben Hamad, et al. 2013), (Ms. S. M. Salve and V. A. Chakkarwar 2013) and (Shruti Dalmiya, et al. 2012), the wavelet transform was considerably employed in algorithms as a feature extraction for the classification of mammographic images as malignant or benign. So it is extremely used to extract features of abnormal breast tissues (benign, micro-calcifications and malignant). In this dissertation several types of wavelet transforms with symlet wavelet family were employed in algorithms to characterize the breast tissues into dense, glandular, fat and abnormal, in order to achieve the detection of breast abnormality. Different sets of proposed combination techniques using the wavelet decomposition technique were implemented, in order to obtain the best accuracy in breast abnormality detection. As illustrated in table 4.12, the decimated discrete wavelet decomposition using sym2 as a mother function didn't provide high

accuracy as the using of sym4 and sym8. The decimated discerte wavelet decomposition with sym4 level 3 acheived 96.8% and with sym4 level 4 it achieved 94.5%, so it provided the highest accuracy with the sym4 level 3 than sym4 level 4, so in this dissertation the decimated discrete wavelet sym4 was able to discriminate between the breast tissues in level 3. The un-decimated discerte wavelet decomposition with sym8 level 3 acheived 91.0% and with sym8 level 4 it achieved 91.8%, so it provided the highest accuracy with the sym8 level 4 than sym8 level 3, so with the undecimated discrete wavelet sym8 was best able to discriminate between the breast tissues in level 4. Sym8 at level3 with the un-decimated discerte wavelet decomposition technique achieved 91.0%, while the using of it with the decimated discerte wavelet decomposition technique achieved 82.5%, so it provided highest accuracy with the un-decimated discerte wavelet decomposition technique. The SGLD matrix was applied before the un decimated wavelet decomposition technique with sym4 level 3, it achieved 94.5%, but when it was applied before the decimated wavelet decomposition technique with sym4 level 3, it achieved 87.5%. When the SGLD matrix was combined with the un-decimated discrete wavelet decomposition with sym8 level 3, it achieved 98.8%. So it was the best result. Also in this table observed that the highest accuracy in the normal tissues detection was achieved in the detection of the dense tissue, in all types of symlet wavelet orders, it was ranging from (93 to 100)%. The dense tissue is very smooth texture, so it is easy to detect because the values which extracted from it would be distinctive. The same in the fat tissue, it is rough texture, so the values extracted from it would be distinctive. The glandular tissue is between the dense and fat tissue, it is close to the abnormal tissue, for this reason its accuracy overlap with the abnormal tissue, and the classifier confuses in classification of it with the abnormal tissue.

Statistical and transformed features based on texture introduce frequency information in addition to intensity information in an image. Texture features are

suited to the analysis of mammograms because the different tissue structures in the mammogram display different statistical texture features.

To assess the performance of the proposed system, sensitivity and specificity performance criterion have been calculated and experiments with mini MIAS database images were performed. The performance of the proposed system is carried on 300 normal images and 100 abnormal one. The classification accuracy obtained using the combination method was shown in table 4.11. From the table 4.11, it is clearly found that all the normal images are classified with no error but the abnormal images classification accuracy is 95%. While the other methods, in a simillar way, available in the literature reviews achieved classification result bellow this accuracy. (Fatehia Garma 2014) achieved 61.7% at the wavelet transform; (Juuso Olkkonen 2011) achieved an average classification accuracy of 69% of the mammogram lesions and (Ms. S. M. Salve and V. A. Chakkarwar 2013) achieved accuracy of 89%.

The combination method achieved 98.8%, it is the best result, so that the system has high ability to discriminate between the normal and abnormal tissues. So the un-decimated discrete wavelet decomposition using symlet wavelet with the SGLD matrix lead to better classification results.

The proposed algorithm gave acceptable results compared with the ground truth given in the mini-MIAS database, Fig 4.23 and Fig 4.24 show the proposed algorithm applied in normal classes. Fig 4.25, Fig 4.26 and Fig 4.27 show the proposed algorithm applied in abnormal classes. The yellow color represents the fat region, green color for the glandular and connective tissue region, blue color for the dense tissue region, and the red one for abnormal region.

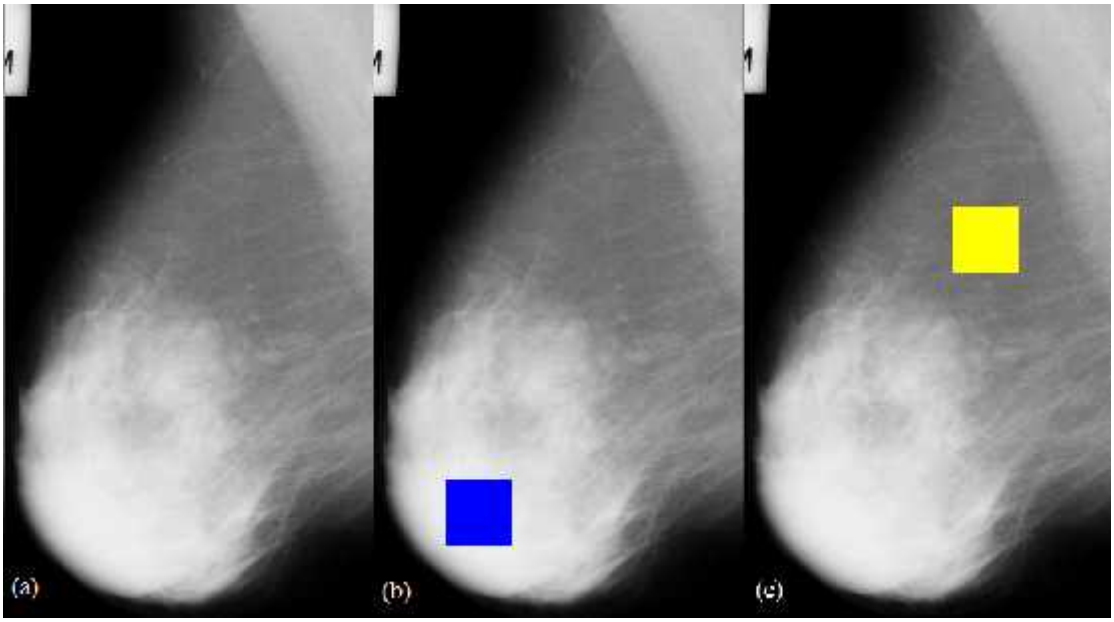

Fig 4.23: A normal mammogram diagnosed by the ground truth given in the mini-MIAS database (a) the original mammogram (b,c) mammogram with sub image (100×100) as detected by computer using the proposed algorithm on different normal regions, notice that (b) dense and(c) fat.

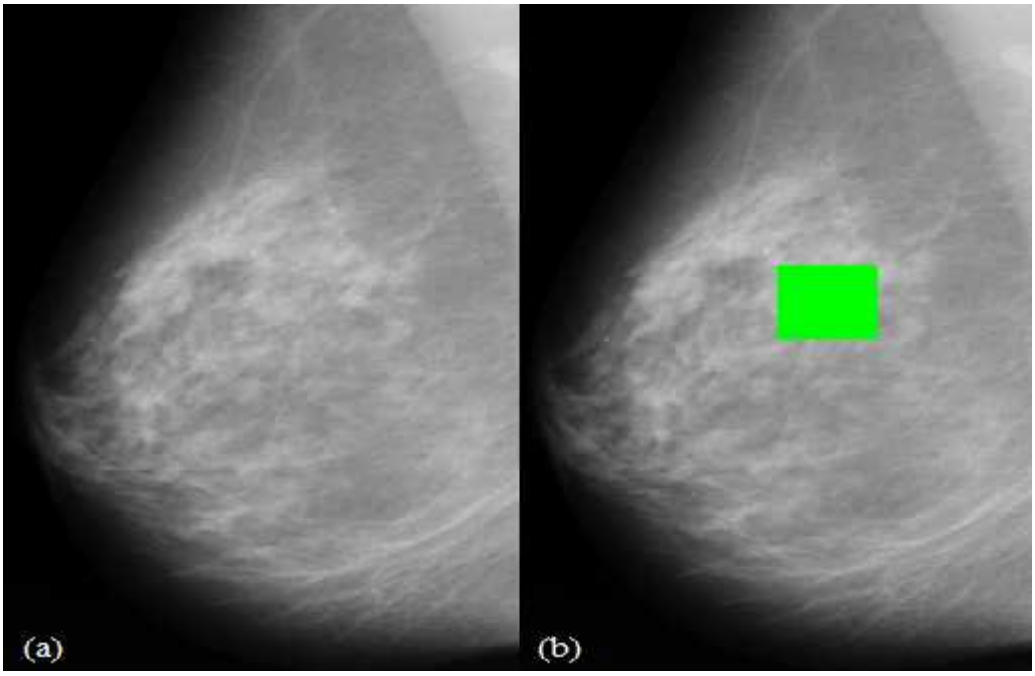

Fig 4.24: (a) the original mammogram (b) mammogram with sub image (100×100) as detected by computer using the proposed algorithm on the glandular region.

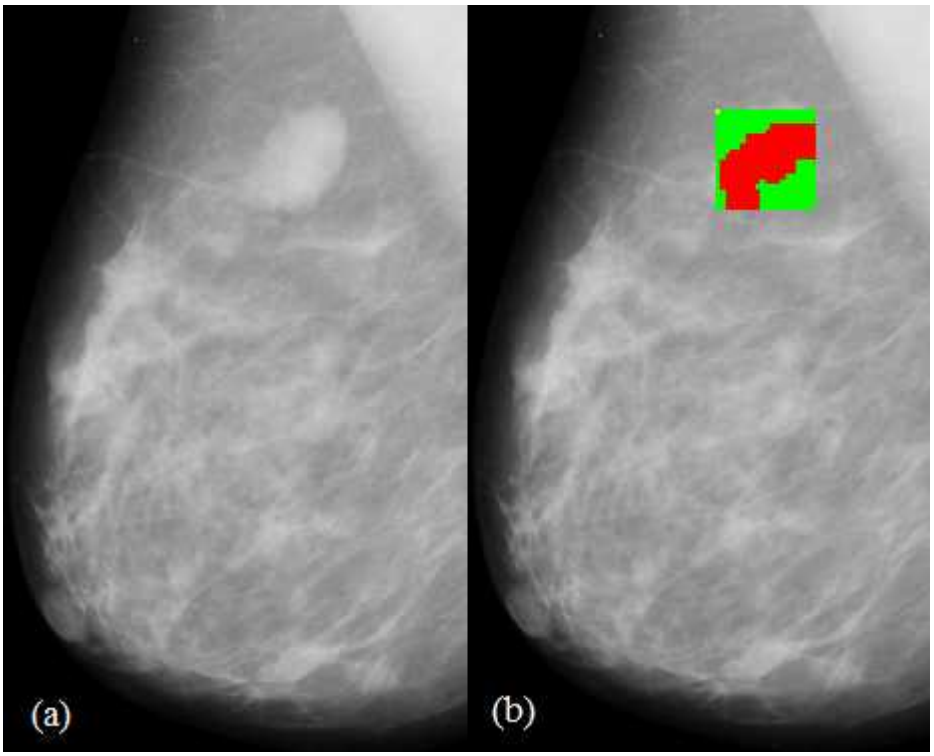

Fig 4.25: An abnormal mammogram diagnosed by the ground truth given in the mini-MIAS database (a) the abnormal original mammogram, (b) mammogram with sub image (100×100) as detected by the proposed algorithm on abnormal.

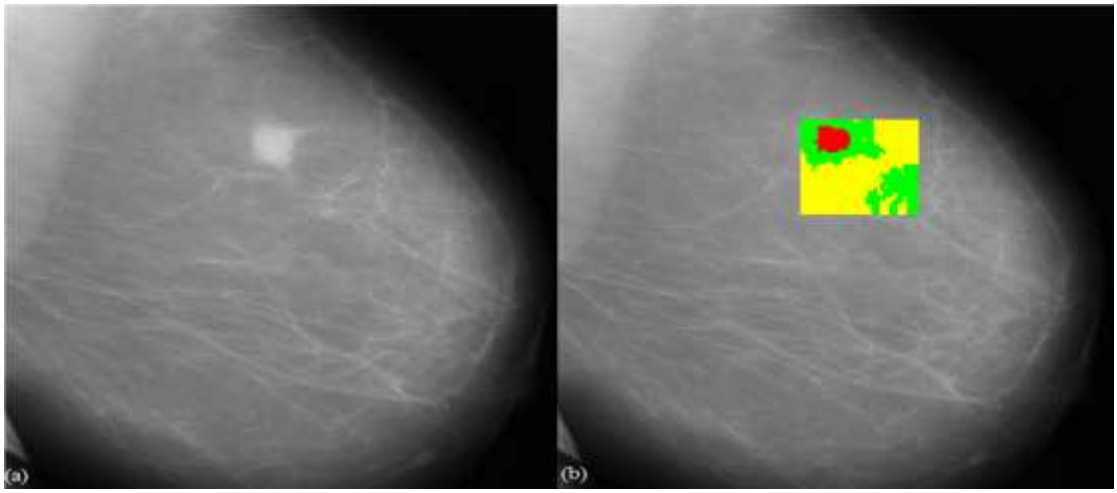

Fig 4.26: (a) An abnormal original mammogram, (b) mammogram with sub image (200×200) as detected by the proposed algorithm on abnormal.

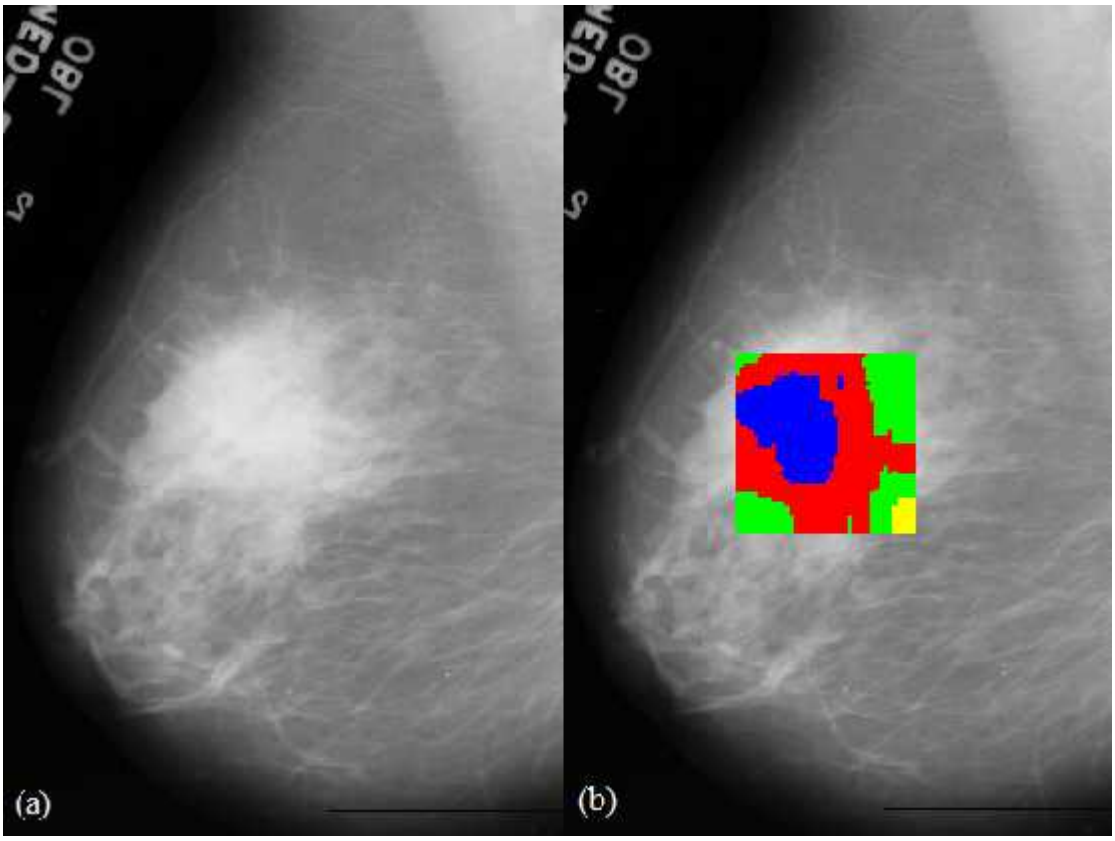

Fig 4.27: (a) An abnormal original mammogram, (b) mammogram with sub image (200×200) as detected by the proposed algorithm on abnormal.

The 200×200 window takes 47 to 53 minute in a computer with CPU Pentium (R) Dual Core T4500, with 2.30 GHz and 2GB RAM memory, to do the classification process, while the 100×100 takes10 minute, and 80×80 takes 5 minute. So the large window consume much time to do the classification process unlike the small one. But the 200×200 window takes 35 minute in a labtop DELL with processor core i7 Ram 8GB DDR3 hard disk 1TB. And it takes less time with Ram 16GB.

Chapter Five

Conclusion and Recommendations

5.1 Conclusion

The un-decimated discrete wavelet decomposition using the symlet wavelet as a mother function, combined with the Spatial Gray Level Dependency (SGLD) matrix was used in the proposed algorithm for the development of computer aided detection of breast tissues to help radiologists in the diagnosis of breast abnormality, because it achieved high accuracy (98.8%).

The identification of normal breast tissues in mammograms is an important step in identifying abnormal tissues. So this dissertation studied the effectiveness of using the wavelet decomposition technique and the SGLD matrix for classification of normal and abnormal breast tissues on digital mammograms. In this dissertation different sets of proposed combination techniques were used, in order to obtain the best accuracy in breast abnormality detection. The dissertation showed that the un-decimated discrete wavelet decomposition technique with the SGLD matrix achieved the best result. It achieved 98.8% accuracy (Table 4.12).

This dissertation proved that the wavelet decomposition technique using the symlet with orders four and eight (sym4, sym8) is efficient in classifying the breast tissues into normal (dense, glandular and fat) and abnormal tissue. It has been demonstrated that the approximation coefficients generated by the symlet (sym4, sym8) decomposition give better classification results. The wavelet decomposition technique alone is more efficiently in detecting the normal classes only, and the

accuracy decrease with the abnormal class, but the wavelet decomposition technique with the SGLD matrix is more efficiently in classifying all the classes, normal and abnormal ones (Table 4.12).

From the twelve Haralick's features that were used to optimize the extracted coefficients in the combination technique, the linear discriminant classifier found that the correlation (CO) feature is not effective to discriminate between the classes (Fig 4.16).

5.2 Recommendations

In the future work, further classification can be considered, identifying different types of lesions, particularly if they benign or malignant. Also this software can be considered with an isolated hardware design in order to be independent equipment for breast abnormality detection. This hardware must be implemented with high processor and Ram specification to reduce the time that consumes in the classification process. Also interfacing between mammography and the computer can be with designing of an expert system for real time mammogram image analysis. It can be implemented in local healthcare facilities in Sudan.

References

[1] Pelin Gorgel, Ahmet Sertbas, and Osman N. Ucan, ” Feature Extraction Based Wavelet Transform in Breast Cancer Diagnosis Using Fuzzy and Non Fuzzy Classification”, Department of Computer Engineering, Istanbul, Turkey, 2013.

[2] Rajashekar K.R Mtech, ”Detection and Classification of Tumors in a Digital Mammogram”, Manipal Institute of technology, India, 2012.

[3] S.Narasimhamurthy, et al. ”Methods towards the Classification of Clustered Microcalcification”, Department of Electronics and Communication Engineering, P.E.S. C.E, Karnataka, India, 2012.

[4] Mohamed M. M. Eltoukhy, Ibrahima FAYE, Brahim Belhaouari Samir, ” Breast Cancer Diagnosis Based on Texture Feature Extraction Using Curvelet Transform ”, Electrical and Electronic Engineering, Universiti Teknologi PETRONAS, 2006.

[5] Eliza Aghjekandi,” Microcalcification Detection in Mammography using Wavelet Transform and Statistical Parameters”

[6] Geoff Dougherty, ” Digital Image Processing for Medical Applications ’, California State University, Channel Islands, G Dougherty 2009.

[7] Isaac HBankman, ” Handbook of medical image processing and analysis ”, Elsevier Inc All rights reserved, 2009.

[8] Richard S. Snell, ”Clinical Anatomy By Regions”, Wolters Kluwer, © Lippincott Williams & Wilkins, United States of America, seventh edition 2004.

[9] Article breast image anatomy www.img.webmd.com

[10] Henry Gray, ”Anatomy of the Human Body”, New York: Bartleby, 2004.

[11] www.en.wikipedia.org/wiki/Breast

[12] Rod R. Seeley, Trent D. Stephens and Philip Tate, ” Anatomy and Physiology”, McGraw-Hill Science-Engineering-Math, 7th edition, 2004.

[13] Joseph Panno, ”CANCER: The Role of Genes, Lifestyle, and Environment”, © by Joseph Panno, Library of Congress Cataloging-in-Publication Data, New York, 2005.

[14] Female breast images, www.female breast.com

[15] Arthur C. Guyton and John E. Hall, ”Text book of Medical Physiology”, University of Mississippi Medical Center, Jackson, Mississippi, 11th edition, 2006.

[16] Célia Freitas da Cruz, ” Automatic Analysis of Mammography Images”, Engineering Faculty – Porto University, Porto, February 2011.

[17] Gunderman, R. B. "Essential radiology: clinical presentation, pathophysiology, imaging", Thieme, 2006.

[18] symptoms/understand_bc/what_is_bc www.breastcancer.org

[19] what-is-cancer www.nationalbreastcancer.org

[20] Rita Teixeira, ”Automatic analysis of mammography images: classification of breast density”, Faculdade de Engenharia da Universidade do Porto, Porto, 2013.

[21] Alvin Silverstein, Virginia Silverstein, and Laura Silverstein, ”Cancer:”, Library of congress cataloging in Publication, 2006.

[22] Exam and test descriptions www.cancer.org

[23] Sankar, D., and Thomas, ”A New Fast Fractal Modeling Approach for the Detection of Microcalcifications in Mammograms”, 2010.

[24] Chang et al., ”Microcalcification detection in 3-d breast ultrasound”, Annual International Conference of the IEEE Engineering in Medicine and Biology Society, 2005.

[25] Kavitha et al., ”A Comparative Study of Various Microcalcification Cluster Detection Methods in Digitized Mammograms”, International Workshop on Systems, Signals and Image Processing and 6th EURASIP Conference focused on Speech and Image Processing, Multimedia Communications and Services, 2007.

[26] Li, et al., ”Fractal modeling and segmentation for the enhancement of microcalcifications in digital mammograms”, IEEE Trans Med Imaging, 16, Nº6, 1997.

[27] Arnau, O., ”Automatic mass segmentation in mammographic images”, Universitat de Girona, Department of Electronics, Computer Science and Automatic Control, Girona, 2007.

[28] Bruce, L. M., & Adhami, R. R., ”Classifying Mammographic Mass Shapes Using the Wavelet Transform Modulus-Maxima Method”, IEEE Trans. Medical Imaging, 1999.

[29] Mini, M., & Thomas, T., ” A neural network method for mammogram analysis based on statistical features”, TENCON 2003, Conference on Convergent Technologies for Asia-Pacific Region, 2003.

[30] Bozek, J., & Dumic, E., ”Bilateral asymmetry detection in digital mammography using B-spline interpolation”, Systems, Signals and Image, 2009.

[31] Li, B., & Wang, X., ”The bilateral information asymmetry on insurance market”, Industrial Engineering and, (70772057), 750-752, 2009.

[32] Jatoi, I., & Kaufmann, M., ”Management of breast diseases”, Springer, 2010.

[33] Susan G. Komen, ” Facts for life: Types of Breast Cancer Tumors”, © Susan G. Komen® Item No KOMEED008900, 2014.

[34] symptoms/diagnosis/invasive www.breastcancer.org

[35] breast-cancer-types www.cancerquest.org

[36] Invasive ductal carcinoma www.nationalbreastcancer.org

[37] J Micheal Dixon, ”A B C of Breast Disease”, Western General Hospital, © Blackwell Publishing Ltd, 3rd edition, Edinburgh, 2006.

[38] Sivaramakrishna, R., & Gordon, R., ”Detection of Breast Cancer at a Smaller Size Can Reduce the Likelihood of Metastatic Spread: A Quantitative Analysis”, ACAD Radiology, Association of University Radiologists, Canada, 1997.

[39] www.radiologyinfo.org

[40] Ed. Joseph D. Bronzino, ” The Biomedical Engineering HandBook, Second Edition”, Boca Raton: CRC Press LLC, 2000.

[41] B. N. Prathibha, ”An Analysis on Mammograms using KDA in Multi Transform Domain”, National Engineering College, Kovilpatti, 2013.

[42] Oliver, et al., ” A Statistical Approach for Breast Density Segmentation”, J Digit Imaging, 23, No.5, 2010.

[43] Chagas, et al., ”An Application of Hough Transform to Identify Breast Cancer in Images”, VIPimage, 2007.

[44] Fatehia Garma, ”Detection of breast cancer cells”, Sudan University of Science and Technology, biomedical engineering department, Sudan, 2014.

[45] Breast anatomy www.yale.edu

[46] abnormal-mammogram www.conciergeradiologist.com

[47] Blanks, et al., ”A comparison of cancer detection rates achieved by breast cancer screening programmes by number of readers, for one and two view mammography: results from the UK National Health Service breast screening programme”, J Med Screen , 5, pp. 195-201, 1998.

[48] Astley, S., ”Computer-aided detection for screening mammography”, International Congress Series, 1256, pp. 927-932, 2003.

[49] Akay, M., ”Wiley Encyclopedia of Biomedical Engineering”, 1st edition, Wiley Interscince, 2006.

[50] Dong ping Tian, ”A Review on Image Feature Extraction and Representation Techniques”, Institute of Computer Software, Baoji University of Arts and Sciences, China, July 2013.

[51] stable/modules/feature extraction www.scikit-learn.org

[52] Feature extraction www.en.wikipedia.org

[53] A Nilk. Jain ,”fundamental of Digital Image Processing”,prentice Hall, Aparamount communicatons company, Englewood Clills, NewJersy, 1989.

[54] R. Haralick, K. Shanmugam, I. Dinstein, —Textural Features for Image Classification,‖ IEEE Trans. on Systems, Man and Cybernetics, vol. SMC-3, no. 6, pp. 610-621, 1973.

[55] D. Lee Fugal, ” Conceptual wavelets in digital signal processing - an in depth practical approach for the non-mathematician ”, © Space & Signals Technologies LLC, 2009.

[56] IEEEwave/IEEEwavelet www.amara.com

[57] Michel Misiti, et al., ”Wavelet Toolbox: for Use with MATLAB”, User’s Guide, Version 2.1, © Math Works Inc., 2001.

[58] JK Modi, “Wavelet Transforms and Applications”, University of Hyderabad, 2004.

[59] Nizar Ben Hamad, et al.” Mammographic Microcalcifications Detection using Discrete Wavelet Transform”, ISBS Rte La Soukra km, Tunisia, 2013.

[60] Juuso Olkkonen, ” Discrete Wavelet Transforms - Theory and Applications”, © InTech, India, 2011.

[61] Sheng Y., ”Wavelet Transform - The Transforms and Applications Handbook”, Second Edition, Ed. Alexander D. Poularikas Boca Raton, CRC Press LLC, 2000.

[62] Rafael C. Gonzalez, Richard E. Woods, Steven L. Eddins, ”Digital Image Processing using MATLAB”, Electrical and Comuter Engineering Department, University of Tennessee, UTK, 1997.

[63] James E. Fowler, ”The Redundant Discrete Wavelet Transform and Additive Noise”, IEEE Signal Processing Letters, vol. 12, pp. 629-632, September 2005.

[64] wa_discrete_wavelet_transform www.zone.ni.com

[65] Carissa Erickson, ”Automated Detection of Breast Cancer Using SAXS Data and Wavelet Features”, © Copyright Carissa Erickson, July 2005.

[66] S.S Sreeja Mole and Dr.L.Ganesan, ”Unsupervised Hybrid Classification for Texture Analysis Using Fixed and Optimal Window Size”, Department of CSE, Government College of Engineering, Tirunelveli, International Journal on Computer Science and Engineering, Vol. 02, No. 09, 2910-2915, 2010.

[67] Fritz Albregtsen, ”Statistical Texture Measures Computed from Gray Level Coocurrence Matrices”, Image Processing Laboratory, Department of Informatics, University of Oslo, November 5, 2008.

[68] Robert M. Haralick, www.realbiblecodes.com

[69] Robert M.Haralick, K.Shanmugan, and Irs Hak ”Textural Features for Image Classification”, The Institute of Electrical and Electronic Engineer, USA, 1973.

[70] S. Balakrishnama and A. Ganapathiraju, ”Linear Discriminant Analysis - A brief Tutorial, Institute for Signal and Information Processing, Department of Electrical and Computer Engineering, Mississippi State University, Mississippi State, Mississippi 39762.

[71] Daniel D Costa, et al., ”Classification of breast tissue in mammograms using efficient coding”, Laboratory of Biological Information Processing, Department of Electrical Engineering, Federal University of Maranhão, Brazil, 2011.
[72] M.R.M. Samulski, ”Classification of Breast Lesions in Digital Mammograms”, University Medical Center Nijmegen, Department of Radiology, June 2006.
[73] SPSS Tutorial, www.hmdc.edu/projectslspsstut.shtml.
[74] Chris Carroll, ” SPSS and surveys ”, ScHARR, University of Sheffield, 2006.
[75] Shruti Dalmiya, et al., ”Application of Wavelet based K-means Algorithm in Mammogram Segmentation”, International Journal of Computer Applications (0975 – 8887) Volume 52– No.15, August 2012.
[76] Ms. S. M. Salve and Prof. V. A. Chakkarwar, ”Classification of Mammographic images using Gabor Wavelet and Discrete Wavelet Transform”, International Journal of Advanced Research in Electronics and Communication Engineering (IJARECE), May 2013.
[77] Pelin Gorgel, et al., ”A Comparative Study of Breast Mass Classification based on Spherical Wavelet Transform using ANN and KNN Classifiers”, International Journal of Electronics, Mechanical, and Mechatronics Engineering, 2013.
[78] R.Ramani, et al., ”Breast Cancer Detection in Mammograms based on Clustering Techniques: A Survey”, International Journal of Computer Applications, January 2013.
[79] S. Mohan Kumar and G. Balakrishnan, ”Classification of Microcalcification in Digital Mammogram using Stochastic Neighbor Embedding and KNN Classifier”, International Conference on Emerging Technology Trends on Advanced Engineering Research (ICETT’12).
[80] Seyyid Ahmed Medjahed, et al., ”Breast Cancer Diagnosis by using k-Nearest Neighbor with Different Distances and Classification Rules”, International Journal of Computer Applications, January 2013.

[81] B. N. Prathibha, ”An Analysis on Mammograms using KDA in Multi Transform Domain”, National Engineering College, Kovilpatti, International Journal of Computer Applications (0975 – 8887) Volume 79 – No3, October 2013.

[82] Jihene Malek, et al., ” Automated Breast Cancer Diagnosis Based on GVF-Snake Segmentation, Wavelet Features Extraction and Fuzzy Classification”, Electronics and Micro-Electronic Laboratory (LEME), Faculty of Sciences of Monastir, Route de Kairouan, 5000 Monastir, Tunisia, 2008.

[83] Fatehia Garma et al., ”Detection of Breast Cancer Cells by Using Texture Analysis”, Sudan University of Science and Technology, Khartoum, Sudan, 2013.

[84] Mammographic Image Analysis Society www.wiau.man.ac.uk/services/MIAS/